Removal of Perfluoroalkyl Acids and Common Drinking Water Contaminants by Weak-Base Anion Exchange Resins

by

Christian Kassar

A Thesis Presented in Partial Fulfillment
of the Requirements for the Degree
Master of Science

Approved March 2022 by the
Graduate Supervisory Committee:

Treavor Boyer, Chair
Paul Westerhoff
Otakuye Conroy-Ben

ARIZONA STATE UNIVERSITY

May 2022

ABSTRACT

Although anion exchange resins (AERs) have been implemented for a wide range of aqueous contaminants including notorious perfluoroalkyl acids (PFAAs) that are of human health concern, the potential benefits and underlying chemistry of weak-base (WB) AERs are overlooked. To fill these key gaps in the literature, this research evaluated the removal and regeneration efficiency of WB-AER (IRA 67 and IRA 96) with strong-base (SB) AER as the baseline. Batch equilibrium tests were first conducted for the removal of nitrate, sulfate, 3-phenylpropionic acid, and six legacy PFAAs with contrasting properties at different solution pH using polyacrylic and polystyrene chloride-form AERs. In ambient (pH 7) and acidic (pH 4) solutions, the polymer composition was the controlling factor followed by the length of alkyl chain of the resin while AER basicity did not influence the selectivity for the selected contaminants. WB resin had higher capacity than SB analogs based on quantitative analysis using isotherm model parameters. Batch and column adsorption experiments showed significantly greater removal of PFAAs by polystyrene than polyacrylic AERs regardless of resin basicity, with the order of decreasing polyacrylic resin selectivity of PFOS >> PFHxS ≈ PFOA > PFBS > PFHxA ≈ PFBA. The removal performance of WB-AER was reversible, declining drastically at basic conditions and gradually regained once below the pK_a of the resin due to the pH-dependent nature of amine groups. This was not the case for IRA 96 (i.e., polystyrene) which exhibited high removal of PFAAs irrelevant of pH because of the nonpolar character of polystyrene matrix. The non-hydrophobic IRA 67 (i.e., polyacrylic) had a satisfactory regeneration using non-toxic salt-only solutions comprising 1% NaOH and 0.5% NaOH + 0.5% NaCl, while IRA 96 was only amenable

to brine/methanol regeneration. Important caveats on the validity of isotherm modeling in batch adsorption tests were discussed. Results for batch and column experiments using chloride-form and free-base form WB-AER, respectively, provide insights for industrial applications.

ACKNOWLEDGMENTS

I would like to express my deepest gratitude to my committee chair, Dr. Boyer for his cross-disciplinary mentorship and his unequivocal trust in my abilities. Without his guidance and resources unconfined to research, this work would not have been possible. I consider myself fortunate for being part of Dr. Boyer's research team through which I have received continuous exposure, support, and soft skills development.

I would like to thank my committee members Dr. Otakuye Conroy-Ben and Dr. Paul Westerhoff for their inputs throughout this journey. I would like to further offer my sincere appreciation to Dr. Westerhoff as well as his obliging research group, especially Zunhui Lin and Dr. Mahmut Ersan, who endowed me with the appropriate instrument and training required for sample analysis. I also express my profound appreciation for Charlie He for supplying groundwater and offering technical advice.

This work would not have been possible without the Strategic Environmental Research and Development Program (SERDP) grant ER18-1063. I am grateful to everyone involved in the project, specifically Anderson Ellis and Dr. Timothy Strathmann at the Colorado School of Mines who inspired me through their devotedness and passion for research.

I am truly grateful for all the sleepless nights my parents back in Lebanon had sacrificed and all the encouragements my brothers had proffered to support me during my time at ASU. Finally, I would like to express my most heartfelt and genuine thanks to my uncle John Matta, his wife Grace Matta, and their family for their unconditional kindness and warm hospitability while away from home and without whom this journey would not have been possible.

TABLE OF CONTENTS

Page

LIST OF TABLES

Table Page

LIST OF FIGURES

CHAPTER 1

INTRODUCTION

Anion exchange have successfully been implemented for raw drinking water treatment over its facile operability, cost-effectiveness, and selectivity of specific resin structures to a range of pollutants. While the efficiency of strong-base (SB) anion exchange resins (AERs) is well established, the chemistry of weak-base (WB) AERs is understudied despite their strong buffering capability (Hinrichs & Snoeyink, 1976; Zhang et al., 2014), ease of regeneration (Ateia, Alsbaiee, et al., 2019), and high capacity (Boyer, Fang, et al., 2021; Höll & Kirch, 1978). Few pilot studies were dedicated to WB-AER thus overlooking the practicability in treatment settings. For instance, WB-AERs are less prone to organic fouling (Dixit, Dutta, et al., 2021) and present greater chemical stability in oxidative environments and higher thermal resistance (Harland, 1994) than SB analogs, all of which increase resin longevity and are important considerations for operational costs.

Regardless of resin basicity, AER technology is commonly used for the removal of problematic aqueous contaminants that are partially or fully dissociated and/or possess a hydrophobic character. The removal efficiency of inorganics (e.g., Cl^-, SO_4^{2-}, NO^{3-}, ClO_4^-, arsenic; uranium (VI)) (Dron & Dodi, 2011; Foster et al., 2017; Gu et al., 2005; Hekmatzadeh et al., 2012; Hu et al., 2016; Song et al., 2012), NOM (Bolto et al., 2002; Edgar & Boyer, 2021; Graf et al., 2014; Ness & Boyer, 2017), and organic ionizable compounds (Kanazawa et al., 2004; Li & SenGupta, 1998, 2004; Rahmani & Mohseni, 2017; Subramonian & Clifford, 1988), especially trace emerging contaminants such as pharmaceuticals (Gustafson & Lirio, 1968; Landry & Boyer, 2013; Landry et al., 2015)

and per- and polyfluoroalkyl substances (PFAS) (Chularueangaksorn et al., 2013, 2014; Dietz et al., 2021; Dixit et al., 2019, 2020a, 2020b; Dixit, Barbeau, et al., 2021; Dixit, Dutta, et al., 2021; Franke et al., 2019; Laura del Moral et al., 2020; Woodard et al., 2017; Yao et al., 2014; Zaggia et al., 2016; Zeng et al., 2020), by strong-base (SB) anion exchange resins (AERs) has been documented in the literature to a substantially greater extent than WB-AER. Therefore, the performance of WB-AER is underestimated, an issue that stems from the lack of review articles consecrated to elucidate the convolution of resin-solute interactions. While the selectivity and removal efficiency of SB-AER is generally influenced by the mobile counterion form (Laura del Moral et al., 2020) and properties of the resin (Helfferich, 1995), like polymer matrix composition (Li & SenGupta, 1998) and functional group (Samatya et al., 2006), added complexity is observed for WB-AER since the resin also exhibits different behaviors in the absence of counter-ions (i.e., free-base) and across a range of solution pH.

PFAS, specifically the perfluoroalkyl acids (PFAAs) subgroup, are susceptible for WB-AER treatment given their low acid dissociation constant (pK_a) (< 1.0) and hydrophobic character (Park et al., 2020). These anthropogenic compounds along with over 3000 types of PFAS have dominated the industry for the past 60 years through a wide array of applications including surfactants, impervious textiles, stain-resistant coatings, adhesives, non-stick cookware, and fire-fighting foams for both military and non-military use and are thus widely discharged in drinking water matrices (Dixit, Dutta, et al., 2021; Gagliano et al., 2020; Xiao et al., 2012). Although an enforceable drinking water regulation for PFOA and PFOS was established by the USEPA at levels < 70ng/L, several perfluoroalkyl carboxylic acids (PFCAs) and perfluoroalkyl sulfonic acids

(PFSAs) (e.g, PFOA, PFOS, PFHxS, PFNA, PFDA, PFUnA) were detected in the serum blood of more than 99% of the US population at concerning amounts (Calafat et al., 2019; CDC, 2021; USEPA, 2019). These compounds have been recently raising concern internationally due to their exceptional resistance to biotic and abiotic degradation and are responsible for numerous chronic diseases in mammals (Abunada et al., 2020; Domingo & Nadal, 2019; Pontius, 2019). Typical PFAAs concentrations in U.S. groundwaters serving as a source for potable water vary from tens (Appleman et al., 2014) to over hundreds of ng/L (Quiñones & Snyder, 2009; Zeng et al., 2020). Even though the natural occurrence of high PFAAs concentrations (i.e., mg/L) in environmental water matrices is unlikely, levels exceeding several hundreds of µg/L could emanate from industrial and military applications, namely effluents generated from electroplating (Schuricht et al., 2017), semiconductor and electronics industries (Lin et al., 2009), and fire-fighting activities (Schultz et al., 2004).

Most studies comparing PFAS and other contaminant removal in terms of resin basicity have emphasized on the decreasing WB-AER performance with increasing solution pH while disregarding other underlying convenience for industrial applications. The pH-dependent nature of WB-AER imparts promising strategies for contaminant desorption using aqueous-only alkaline solutions (i.e., NaOH; NH_4OH; KOH) with low ecotoxicological risk compared to the conventional SB-AER chloride salt and/or organic co-solvent (e.g., methanol, ethanol) solutions, which require proper management and disposal. Subsequent PFAAs destruction through electro-oxidation in methanol or NaCl solution is discouraged due to the need for combustion inhibitor systems for safety concerns and the potential for perchlorate by-products release respectively, as opposed to

the formation of hydroxyl radicals which enhance PFAAs oxidation (Dixit, Dutta, et al., 2021; Laura del Moral et al., 2020; Liang et al., 2022; Schaefer et al., 2020; Yang et al., 2018; Zaggia et al., 2016). However, PFAAs desorption by hydroxide ions does not imply WB-AER regeneration, which is a common misconception for studies conducting one service cycle only (Conte et al., 2015; Deng et al., 2010; Gao et al., 2017; Shuang et al., 2012; Wang et al., 2019). Briefly, the basicity of AER is defined by the type of alkylamine functional group, where the SB-AER-exclusive quaternary ammonium functional group is permanently charged at practical pH (i.e., < 13) (Clifford & Weber, 1983; Dudley, 2012), whereas primary, secondary, and tertiary amines lose much of the ion-exchange (IX) capacity through deprotonation at approx. > pH 9 and are specific to WB-AER (Clifford & Weber, 1983; Helfferich, 1995; Miyazaki & Nakai, 2011). Only a limited amount of proton (H^+) could be removed from unbuffered test waters before reaching equilibrium at around the pK_a of tertiary amines, meaning the adsorption mechanism of WB-AER in the free-base form is restricted to π-π, n-π, and hydrogen bonds, van der Waals forces and other non-electrostatic interactions. Therefore, there is a need for a functionalization step succeeding contaminant desorption to unlock the full potential of WB-AER, especially in systems where pH control is not an option. This is possible with strong acids having high affinity for the free-base tertiary amine functional group (Höll & Kirch, 1978). In the presence of aqueous solution of acids such as HCl, H_2SO_4, and HNO_3, IX is activated by resin uptake of H^+ with the inorganic anion as the mobile counterion. Several studies successfully conditioned WB resin using concentrated NaOH and HCl solutions (Bolto et al., 2002; Clifford & Weber, 1983; Miyazaki & Nakai, 2011; Moldes et al., 2003; Sengupta & Clifford, 1986). As opposed to NaCl, HCl is

highly volatile and can be easily separated from the effluent. When chloride was the mobile counterion, WB-AER had three times higher sorption capacity for lactic acid compared to the resin in free-base form, which was explained to be due to the absence of electrostatic interactions in the latter form. WB-AER with macroporous (MP) structure swells up to 20% more with chloride as the mobile counterion (Harland, 1994) allowing for greater uptake of macromolecules (e.g., NOM) (Bolto et al., 2002).

Nonetheless, free-base WB-AERs have also shown essential properties with the most advantageous being the higher buffering capacity than other form AERs (Zhang et al., 2014), which is an essential quality for water desalination or point-of-use demineralization through a series of strong-acid cation/weak-base anion exchange resin beds (Harland, 1994; Helfferich, 1995; Höll & Kirch, 1978). WB-AER in its free-base form also offers a cost-effective alternative relative to its chloride counterpart since the resin is used without the added step of pretreatment. Considering research studies to date on PFAA removal and/or regeneration, only SB-AERs were tested in column-flow mode and only polyacrylic WB-AERs were tested for regeneration in batch mode (Deng et al., 2010; Du et al., 2015; Gao et al., 2017) with the exception of Conte et al. (2015) who evaluated the regeneration of polystyrene MN102 resin.

A large body of literature highlighted the potential for conflicting conclusions in estimating the adsorption efficiency and mechanism by misapplying isotherm models (Allen et al., 2003; Bolster & Hornberger, 2007; Dron & Dodi, 2011; Foo & Hameed, 2010; Haupert et al., 2021; Tran, You, Hosseini-Bandegharaei, et al., 2017). The factors that affect the quality of model fit to experimental data include the optimization technique, goodness-of-fit parameters, data transformation (i.e., linear, and nonlinear

forms), and experimental operating conditions, all of which alter the error distribution structure and lead to biased interpretations.

Previous experiments have proven WB-AER to have great potential for IX applications. This study was intended to fill remaining gaps in the literature pertaining to the mechanisms that govern contaminant removal by salt-form and free-form WB-AER. Hence, four commercially available WB and SB-AERs with analogous porosity and polymer structure were selected for the removal of relevant drinking water contaminants, including PFAAs, sulfate, nitrate, and NOM surrogate (i.e., 3-phenylpropionic acid) in batch adsorption experiments. The co-removal of six PFAAs was tested at source zone concentration, while nitrate, sulfate, and 3-phenylpropionic acid experiments were conducted separately and were chosen to represent a wide range of competitors for IX sites. A cross-cutting follow-up column study evaluated the ability of four resins, notably the free-base WB-AERs, to remove and desorb high concentrations of PFAAs (hundreds of μg/L) in impacted groundwater. Solutions comprising caustic, caustic/brine, and brine/organic solvent were used for regeneration.

The specific objectives of this research were to (1) assess the effect of solution pH and resin properties, considering resin basicity, polymer structure, and functional group, on the removal efficiency; (2) validate the influence of PFAAs properties, in term of carbon chain-length and terminal head group, on the selectivity sequence for each AER; (3) evaluate the reliability of different isotherm modeling techniques for single-solute ion-exchange systems; (4) discuss the underlying mechanisms and efficacies of chloride-form for various water pollutants; (5) investigate the viability of free-base WB-AER for

PFAAs removal from groundwater in column-mode; and (6) explore the regeneration capabilities of PFAAs-laden WB resins.

CHAPTER 2

MATERIALS AND METHODS

2.1. Batch Experiments

2.1.1. Anion Exchange Resins

Four anion exchange resins (AERs) were selected for batch equilibrium tests and their properties are listed in Table 2.1. Weak-base (WB) Amberlite® IRA 67 (WB/PA/G/dimethyl) and Amberlite® IRA 96 (WB/PS/MP/dimethyl) resins were obtained as free base. Strong-base (SB) Amberlite® IRA 458 (SB/PA/G/trimethyl) and Purolite A520E (SB/PS/MP/triethyl) were in the chloride form. To ensure that most ion-exchange sites were occupied with chloride (Cl^-), all AERs were pretreated with 10× more Cl^- than the exchange capacity of the resin then repeatedly washed with deionized (DI) water. Sodium chloride (NaCl) was used to treat SB AER while WB-AER were saturated with hydrochloric acid (HCl) to help with the protonation of tertiary amine. Basicity is determined by the degree of protonation of the resin functional groups which increases for C1 and C2 alkylamines as follows: tertiary (pKa ≈ 9.8 – 10.72) ≈ primary (pKa ≈ 10.62 – 10.63) < secondary (pKa ≈ 10.77 – 10.93) < quaternary (pKa > 13). When synthesized, these values differ for each type of resin (e.g., 6.8 – 11.1) in terms of degree of resin cross-linking, temperature, and porosity (Clifford & Weber, 1983; Gustafson et al., 1970). Resin density was determined by measuring 20 mL of wet undisturbed resin in a graduated cylinder. Dry density was further calculated as the ratio of dry mass to wet volume after oven-drying the resins at 55℃ for 24 h.

Table 2.1. Characteristics of anion exchange resins.

Resin	Basicity	Divinylbenzene matrix type/ Porosity	Functional group	Exchange capacity (eq/L)[a]	Exchange capacity (meq/g)[b]	pKa	Experiment	**Water content (%)**
IRA 67	WB	PS/G	Tertiary amine: Dimethyl[c]	1.6	4.557	9.0[f]	Batch + Column	56-64[h]
IRA 96	WB	PS/MP	Tertiary amine: Dimethyl[c]	1.25	3.285	6.4[f]	Batch + Column	57-63[h]
IRA 458	SB	PA/G	Type I: Trimethyl[d]	1.25	4.099	> 13[g]	Batch	57-64[i]
A520 E	SB	PS/MP	Type I: Triethyl[e]	0.9	2.439	> 13[g]	Batch + Column	50-56[i]
A860	SB	PA/MP	Type I: Trimethyl[d]	0.8	Not Measured	> 13[g]	Column	66-72[i]

Strong-Base (SB), Weak-Base (WB), Polyacrylic (PA), Polystyrene (PS), Gel (G), Macroporous (MP).

[a] Data obtained from the manufacturer.
[b] Determined experimentally.
[c] R-$(CH_3)_2HN^+$ (protonated form) or R-$(CH_3)_2N$ (anhydrous free-base form)
[d] R-$(CH_3)_3N^+$.
[e] R-$(CH_2CH_3)_3N^+$.
[f] (Miyazaki & Nakai, 2011).
[g] (Dudley, 2012).
[h] Chloride form
[i] Free-base form

2.1.2 Chemical analytes

Synthetic solutions in both single and multi-solute batch experiments were prepared by dissolving ≈2.14 meq/L (30 mg-N/L) of total analytes in DI water (resistivity >18.2 mΩ-cm). The solution pH was adjusted using 1 M HCl and NaOH. Single-solute experiments included sodium nitrate ($NaNO_3$, CAS# 7631-99-4, Fisher Scientific), 3-phenylpropionic acid (C_8H_9COOH, CAS# 501-52-0, Alfa Aesar), and sodium sulfate (Na_2SO_4, CAS# 7757-82-6, Fisher Scientific). The multi-solute synthetic solution consisted of six PFAS with varying fluorinated carbon (C-F) tail lengths and functional head group, each at an initial concentration of 80 μg/L to reflect typical amounts (i.e., tens of μg/L) in groundwater amenable to source zone contamination (Kärrman et al., 2011; McGuire et al., 2014). A previous study showed the maximum adsorbent capacity to be inconsistent when bottle-point methods for equilibrium tests varied (Millar et al., 2015). Therefore, sodium bicarbonate ($NaCO_3$, CAS# 1066-33-7, Sigma Aldrich) was added to the mixture to bring the final equivalent concentration of analytes ($C_{\sum X^-}$) to 2.14 meq/L to provide similar adsorbent-to-volume ratio between batch adsorption tests. In the order of decreasing number of carbons (C#), six PFAS (C#, acronym, form, purity, CAS#) purchased from Sigma-Aldrich were considered in this study: perfluorooctane sulfonate (C8, PFOS, aqueous, 40% in water, 1763-23-1), perfluorooctanoic acid (C8, PFOA, solid, 95%, 335-67-1), perfluorohexane sulfonate (C6, PFHxS, sodium salt, 98%, 3871-99-6), perfluorohexanoic acid (C6, PFHxA, aqueous, 97%, 307-24-4), perfluorobutane sulfonate (C4, PFBS, sodium salt, 98%, 29420-49-3) and perfluorobutanoic acid (C4, PFBA, aqueous, 98%, 375-22-4). Accounting for purity, a 1 L stock solution was prepared adding 32 mg of each PFAS in DI water and was further sonicated to achieve full dissolution. Solid-form PFAS (i.e.,

PFBS, PFHxS, and PFOA) were measured by weight, whereas density was used for the determination of volume for PFAS in the aqueous phase (i.e., PFBA, PFHxA, and PFOS). The combined PFAS solution was diluted 400 times for each batch experiment.

2.1.3. Adsorption experiments

Adsorption equilibrium tests were conducted in a benchtop orbital shaker (Thermo Scientific™ MaxQ™) for 24 h with dry resins in 125 mL amber glass bottles containing 100 mL of synthetic contaminant solution. While it has been shown that the majority of contaminant uptake by AER is exhibited within the first hour (Dixit, Dutta, et al., 2021; Landry & Boyer, 2013; Millar et al., 2015) or two (Graf et al., 2014) of the experiment, it is crucial to evaluate the equilibrium time through preliminary kinetic tests to avoid generating erroneous conclusions (Tran, You, Hosseini-Bandegharaei, et al., 2017). In this study, the time to reach equilibrium was selected based on commonly reported values for batch IX experiments comprising inorganic (Hekmatzadeh et al., 2012; Hekmatzadeh et al., 2013; Hu et al., 2016) or complex organic (Dudley, 2012; Gao et al., 2017; Landry et al., 2015; Laura del Moral et al., 2020) pollutants. The percent resin dose was defined as the ratio of resin dose (meq/L) to initial total concentration of contaminants (meq/L). Five percent resin doses (25%, 50%, 100%, 150% and 300%) were selected for this study. The adsorption isotherm experiments were carried out by keeping $C_{\sum X^-}$ constant at 2.14 meq/L and varying the resin mass. The contaminant solutions were prepared at three different solution pH (4, 7 and 10) prior to the batch equilibrium test. To investigate the influence of alkaline conditions on WB-AER removal efficiency, WB resins were put in contact with a highly basic solution (~ pH 11) for 24 h then carefully decanted. The basic test water at ~ pH 11.4 was subsequently added to the

resin and equilibrated for 24 h. This method was adopted for WB-AER to compensate for the deprotonation of amine group, constantly decreasing the pH in unbuffered test water (Gustafson et al., 1970). To simplify the comparison between AERs, the two different methods used to equilibrate WB and SB resins in basic conditions will be referred to as "pH 10" in this paper. All samples were tested in triplicate and the pH was measured before and after adsorption experiments. Control samples with no resin show losses of contaminant due to glass adsorption to be negligeable.

2.1.4. Data analysis

The equivalent concentration of each analyte in the resin phase (qe; meq/g) was calculated on a mass balance basis from Eq. (1).

$$q_e = \frac{(C_0 - C_e)}{m}\, v \qquad (1)$$

Where C_0 (meq/L) and C_e (meq/L) are the initial and equilibrium aqueous concentration of the target analyte respectively. The Removal efficiency for each percent resin dose was determined as the amount of contaminant removed divided by its initial amount in solution and was reported as percent removal (%). To account for additional chloride sites, stemming from resin pre-conditioning, the resin capacity was recalculated for all resins using 10× more NO_3^- and 10× more SO_4^{2-} than the manufacturer value. The highest exchange capacity for each AER was then used for determination of isotherm parameters and separation factors (see section 2.3). This recalculation was due to higher observed contaminant uptake and chloride release for low percent resin dose than the maximum theoretical resin capacity. Previous work reported polyacrylic strong-base resin to have capacity $\approx 220\%$ than the manufacturer value (Hu et al., 2016). Percent removal, q_e, and separation factors for each percent resin dose and analyte were computed as the

average of triplicate samples with error bars representing one standard deviation. Isotherm models, goodness-of-fit parameters, and binary exchange plots are discussed in detail later (see section 2.3.).

2.2. Column experiments

2.2.1. Continuous-flow adsorption

Continuous-flow column adsorption tests were carried out in triplicate by loading 12 mL of wet IRA 67, IRA 96, A520E and Purolite® A860 resins (see Table 2.1) into 250 mm long and 10 mm wide glass columns with one adjustable end (Diba Omnifit® EZ Chromatography, Cole-Parmer), PTFE filters on both ends of the column were replaced by a fine mesh to prevent PFAA contamination and pressure buildup. A860 (SB/PA/MP/trimethyl) was selected instead of IRA 458 (SB/PA/G/trimethyl) due to higher initial adsorption rate of large contaminants for resins with a more porous structure (Boyer, Fang, et al., 2021; Li & SenGupta, 2000). Packed resins were used as received and were continuously fed in up-flow configuration at 2.4 mL/min with PFAAs-spiked natural groundwater having the physicochemical characteristics illustrated in Table B1. Elevated PFAA concentrations (mg/L) were considered to ensure high adsorbed amounts therefore minimizing the volume of groundwater needed (Schaefer et al., 2019). Effluent samples were collected every ~280 bed volumes (BV) over a period of 2000 BV (~24 L) at an average empty bed contact time (EBCT) of 5 min.

2.2.2. Resin regeneration

Regeneration experiments were conducted in coflow mode (i.e., direction of regeneration is same as treatment) by first backwashing the columns with DI water (2 × flowrate, down-flow configuration, 3.2 BV), then circulating air (3 × flowrate, up-flow

configuration, 1 BV) to prevent clogging, and finally passing 120 mL of the regeneration solution and 80 mL of DI water ($1/2$ × flowrate, up-flow configuration, 16-17 BV). Each PFAA-laden AER was subjected to regeneration using two salt-only aqueous solutions and a mixture of brine and organic cosolvent to evaluate the extent of PFAA desorption in the presence/absence of an alcohol cosolvent. For WB-AER, the three solutions comprised 1% NaOH (w/w), 0.5% NaOH (w/w) + 0.5% NaCl (w/w), and 1% NaCl (w/w) + 70% methanol (v/v). For SB-AER, the same latter two solutions were used with 1% NaOH being substituted for a concentrated brine solution (10% NaCl w/w).

2.2.3. Data analysis

The mass of PFAA adsorbed onto the resin is described by Eq. (2).

$$M_{rem} = M_{adsorb} = \int_{V_0}^{V_n} (C_{inf} - C_{eff,i})\, dV = V_{AER} \times \sum_{i=1}^{n} (C_{inf,0} - C_{eff,i}) \times (BV_i - BV_{i-1}) \qquad (2)$$

Where subscript i represents the sample number and subscript n the total number of samples taken during column treatment. $C_{inf,0}$ and $C_{eff,i}$ are PFAA concentration (μg/L) measured in the influent and in the effluent sample i, respectively, BV_i is the number of bed volumes treated prior to sample i (i-1 = 0 denotes the start of the experiment), and V_{AER} is the volume of packed resin (12 mL). The mass of PFAA removed from groundwater (M_{rem}, μg) is the same as the mass adsorbed onto the resin (M_{adsorb}, μg). Removal data during column treatment was expressed as the mean normalized concentration (i.e., $C_{eff,i}/C_{inf,0}$) of triplicate samples. The Regeneration efficiency (%) was calculated as the mass of PFAA removed during adsorption divided by the amount recovered in the 200 mL regenerant mixture (120 mL regeneration solution + 80 mL DI water).

2.3. Analytical methods

Concentrations of Cl^-, nitrate (NO_3^-), sulfate (SO_4^{2-}) anions, and sodium (Na^+) cations were measured using ion chromatography (IC) (Dionex ICS 5000+, Sunnyvale, California) as described elsewhere (Edgar & Boyer, 2021). Cl^- concentration was determined to calculate the separation factor of AER in binary batch system (i.e., Cl/NO_3^-, Cl^-/3-PPA, Cl^-/SO_4^{2-}). Background Na^+ was measured as control for chemicals in the salt form. Single-analyte samples were passed through a 0.45 μm nylon membrane (NM) filter, while 0.45 μm cellulose acetate (CA) syringe filters were used for all samples containing PFAAs since CA exhibits the lowest PFAAs losses to the filter material in ultrapure and DOC rich matrices ($p < 0.05$) (Sörengård et al., 2020). Samples from each column test were collected and filtered separately using CA and NM syringe filter materials for PFAAs and select physicochemical analyses (e.g., DOC, pH, conductivity), respectively. All batch and column samples were then stored in conical polypropylene tubes with zero head space at 5°C. Dissolved organic carbon (DOC) and dissolved inorganic Carbon (DIC) were measured using a Total organic carbon analyzer (TOC-VCH, Shimadzu, Japan). Reported results are the averages of duplicates with relative percent difference below 10%. During each run, organic carbon standard (1000 ppm C, CAS# 1847-16, Ricca Chemical) and inorganic carbon standard (1000 ppm C, CAS# 1845-4, Ricca Chemical) were used periodically as checks (RPD <15%). 3-PPA samples were analyzed for DOC and UV absorbance at 254 nm using a UV-Visible Spectrophotometer (UV-2700, Shimadzu) and showed DOC measurements to be representative of the 3-PPA isolate. The calibration curve for UV254 analysis ($R^2 > 0.995$) was made from several concentrations of 3-PPA (30, 50, 100, 200, 250, and 400 mg/L) in DI water. A high-performance liquid chromatography (HPLC 1290 Infinity II,

Agilent Technologies) coupled to a triple quadruple mass spectrometer (LC/MS 6490, Agilent Technologies) was employed for PFAA analysis. 5µL samples are injected into a C18 analytical column (5 µm, 100 x 3 mm, 110 Å, Phenomenex Gemini) protected by a C18 guard column (4 x 2 mm, Phenomenex Gemini), which is replaced at intervals of 100 injections. To ensure the retention of short-chain PFAAs (i.e., PFBA, PFBS and PFHxA), Phenomenex C18 equipment were separated by two hydrophilic DIOL guard columns (6 µm, 4.6 x 12.5 mm, Agilent Technologies). A C18(2) delay column (5 µm, 30 x 3 mm, 100 Å, Luna) was used to enhance analyte separation and minimize contamination. The eluent consisted of 20 mM ammonium acetate (CAS# 631-61-8) in water (CAS# 7732-18-5), as the aqueous mobile phase, and methanol (CAS# 67-56-1), as the organic mobile phase. All eluent reagents were purchased from Fischer Scientific at Optima HPLC-grade. The mixture flow rate was maintained at 0.8 mL/min.

2.4. Adsorption Isotherms

Adsorption isotherms portray the dependence of analyte concentration in the resin phase (q_e) on the aqueous concentration (C_e) at equilibrium (Helfferich, 1995). Langmuir, Freundlich, Dubinin-Radushkivich (DR) and Dubinin-Astakhov (DA) models were chosen and determined using the nonlinear least-squares (NLS) regression method in Rstudio (Version 1.4.1717). Parameters were first obtained plotting linear forms of each isotherm model to initiate values for the NLS function. To assess model fits of experimental data, the correlation coefficient (R^2), the average relative error (ARE), the sum of squared errors (SSE), the root mean squared error (RMSE), and the chi-squared (χ^2) were calculated using the metrics RStudio package and the equations S1-S5 listed in Supplementary Information (SI). The R^2 and ARE were used to compare multiple equilibrium experiments for one

model. The SSE, RMSE and χ^2 were used to evaluate the goodness-of-fit of multiple isotherms for one equilibrium experiment. In the adsorption isotherm graphs, qe (mmol/g), the contaminant concentration in the resin phase, is plotted against Ce (mmol/L), the aqueous contaminant concentration, at equilibrium. Isotherm models are chosen to evaluate the model approach that best describes adsorption mechanism. These include thermodynamic, kinetic, and potential theory considerations with each isotherm model derived in terms of at least one approach (Foo & Hameed, 2010).

2.4.1. Langmuir isotherm model

The Langmuir isotherm (Eq. 3) implies that the adsorbent has limited number of sites with equal and constant adsorption energy and homogeneous structure (Chan et al., 2012). Aqueous contaminants have similar thermodynamic character (i.e., enthalpy, activation energy of adsorption), which suggests equal preference for accessible sites (Tran, You, Hosseini-Bandegharaei, et al., 2017). Once adsorbed, only a one-molecule layer can be formed on the adsorbent, with no lateral transport on the surface and interactions between adsorbates (Foo & Hameed, 2010).

$$q_e = \frac{q_0 K_L C_e}{1+K_L C_e} \tag{3}$$

Where q_0 (mmol/g) is the maximum adsorption capacity of the resin and K_L (L/mmol) is the Langmuir coefficient related to the affinity between the adsorbent and adsorbed species. Further useful parameters such as the dimensionless separation factor (R_L) (Eq. 4) and the change in Gibbs free energy (ΔG^0) (Eq. 5) are calculated as follows:

$$R_L = \frac{1}{1+K_L C_0} \tag{4}$$

$$\Delta G^0 = -RT \ln K_L \tag{5}$$

Where T (K) is the temperature (average of 275.41 K in this study), R is the ideal gas constant (8.314 J/K mol). The extent of isotherm favorability is portrayed by R_L, whereby values between 0 and 1 represents suitable fit while being unfavorable above 1 (Namasivayam & Ranganathan, 1995). Negative values of the thermodynamic parameter ΔG^0 (kJ/mol) suggest favorable and spontaneous adsorption of aqueous contaminants, otherwise unfavorable and nonspontaneous (Dron & Dodi, 2011). More than four expressions for the linearized Langmuir equation are available, each yielding different R^2 and fitted parameter values (Bolster & Hornberger, 2007). Type I (Hanes-Woolf) and Type II (Lineweaver-Burk) (Table A1) are the two most common linear forms of the Langmuir equation (Kumar & Sivanesan, 2005), thus the form with the highest R^2 was used to determine starting parameters for the NLS function.

2.4.2. Freundlich isotherm model

As opposed to the semi-empirical Langmuir model (Langmuir, 1916), the Freundlich isotherm is an empirical model (Eq. 6) (Freundlich, 1906), which assumes bilayer formation of solutes on the surface of the adsorbent, heterogeneous sites, and non-ideal systems. The isotherm suggests potential for unlimited adsorbent capacity, translated by its shape not exhibiting a plateau, with the thermodynamic approach not accounted for (Ahmed & Dhedan, 2012). Hence, the Freundlich model lacks the ability to describe saturation effects at high analyte concentration while not converging to the Henry's law at trace levels (Chan et al., 2012; Dron & Dodi, 2011; Foo & Hameed, 2010).

$$q_e = K_F C_e^{1/n} \tag{6}$$

Where K_F (mmol/g)/(mmol/L)$^{1/n}$ and 1/n (dimensionless) are the Freundlich constants representative of adsorption intensity and the extent of surface heterogeneity or selectivity

respectively. Complementary to the R_L parameter of the Langmuir model, 1/n was used to evaluate the adsorption nature, where adsorption is favorable, linear, and unfavorable for 1/n values below, equal, and above unity respectively (Tran, You, Hosseini-Bandegharaei, et al., 2017).

2.4.3. Dubinin-Radushkevich (DR) and Dubinin-Astakhov (DA) isotherm models

The DR and DA empirical models assume pore filling adsorption onto microporous solids (Dubinin, 1947) rather than the layer-by-layer mechanism of previous models (i.e., Langmuir and Freundlich) (Inglezakis, 2007). The Dubinin isotherms are based on the Polanyi potential theory of adsorption expressed in Eq. 7 by the temperature dependent Polanyi potential (ε) parameter.

$$\varepsilon = RT \ln(1 + \frac{1}{C_e}) \tag{7}$$

Where C_e (g/g) is the concentration of analyte at equilibrium. Here, the non-solubility-normalized ε highly relates to the negative value of the Langmuir thermodynamic change in free energy parameter (Eq. 5) (Inglezakis, 2007). The nonlinear DR and DA parameters are calculated by fitting equilibrium data to Eq. 8 and Eq. 9 respectively. of contaminants from the aqueous to the surface of the adsorbent

$$q_e = q_0 \, exp\left[-\left(\frac{\varepsilon}{E\sqrt{2}}\right)^2\right] \tag{8}$$

$$q_e = q_0 \, exp\left[-\left(\frac{\varepsilon}{E\sqrt{2}}\right)^{n_D}\right] \tag{9}$$

Where q_e and q_0 are the equilibrium contaminant concentration in the solid phase and the maximum adsorbent capacity (g/g) respectively. E is the adsorption energy (J/mol), defined as energy needed for the contaminant to partition between the aqueous and solid phases from infinity (Onyango et al., 2004; Özcan et al., 2005), and n_D is the

heterogeneity parameter (dimensionless). The magnitude of E indicates the type of adsorption (i.e., chemical or physical) and is typically useful for the removal of organic ionizable compounds (OICs) by AER (Fu et al., 2008; Milmile et al., 2011; Özcan et al., 2005; Tran, You, Hosseini-Bandegharaei, et al., 2017). For the DR isotherm $n_D = 2$ (i.e., non-ideal) while higher values ($n_D > 3$) impart homogeneous pore structure (Dron & Dodi, 2011; Inglezakis, 2007). Both isotherms were treated as two-parameter models, whereby E and q_0, and E and n_D were obtained through nonlinear regression for DR and DA isotherms respectively while q_0 was determined experimentally for the DA isotherm as recommended elsewhere (Dron & Dodi, 2011; Landry et al., 2015).

2.4.4. Redlich-Peterson (RP) isotherm model

The RP is a three-parameter empirical model able to predict ideal and non-ideal adsorption at a wide range of concentrations (Chen et al., 2014; Foo & Hameed, 2010). As shown in Eq. 10, based on the dimensionless parameter, α (0-1), and C_e values, the hybrid RP model converts to the Langmuir (Eq. 11), the Freundlich (Eq. 12), and the Henry's law (Eq. 13) equations.

$$q_e = \frac{K_{RP} C_e}{1 + b_{RP} C_e^{\alpha}} \tag{10}$$

$$q_e = \frac{K_{RP} C_e}{1 + b_{RP} C_e} = \frac{q_0 K_L C_e}{1 + K_L C_e} \tag{11}$$

$$q_e = \frac{K_{RP}}{b_{RP}} C_e{}^{1-\alpha} = K_F C_e^{1/n} \tag{12}$$

$$q_e = \frac{K_{RP} C_e}{1 + b_{RP}} = H_{YC} C_e \tag{13}$$

Where K_{RP} (L/mmol) and b_{RP} (L/mmol)$^{\alpha}$ are the RP constants, α (dimensionless) is the RP exponent, K_L and q_0 are the Langmuir constants, K_F and $1/n$ are the Freundlich constants, and H_{YC} is the dimensionless Henry's law constant. Briefly, the RP reduces to

the Langmuir equation (Eq. 11) when α approaches 1, where K_{RP} and b_{RP} equal $q_0 K_L$ and K_L respectively (Chen et al., 2014; Foo & Hameed, 2010); it reduces to the Freundlich equation (Eq. 12) at large contaminant concentration (Jossens et al., 1978; Radke & Prausnitz, 1972) where K_{RP}/b_{RP} equals K_F and $1-\alpha$ equals $1/n$; and is in accordance with the Henry's law (Eq. 13) whenever α is close to 0 (Howe et al., 2012). Considering the mathematical complexities of a three-parameter model, the linearized RP form (see Table A1 in SI) is to be solved by either minimizing the SSE or maximizing the R^2 error functions to initiate values for the nonlinear model parameters (Allen et al., 2003).

2.4.5. Goodness-of-fit measures

Mathematical error functions from current literature were explored to determine the best-fit model for ion-exchange systems. All the following equations (Eqs. 14-18) could both be applied to linear and nonlinear data except for chi-squared (χ^2) being specific to the nonlinear regression method (Tran, You, Hosseini-Bandegharaei, et al., 2017).

$$R^2 = 1 - \frac{\sum_{i=1}^{n}(Y-\hat{Y})^2}{\sum_{i=1}^{n}(Y-\overline{Y})^2} \tag{14}$$

$$ARE = \frac{100}{n}\sum_{i=1}^{n}\frac{|Y-\hat{Y}|}{Y} \tag{15}$$

$$SSE = \sum_{i=1}^{n}(Y-\hat{Y})^2 \tag{16}$$

$$RMSE = \sqrt{\frac{1}{n}\sum_{i=1}^{n}(Y-\hat{Y})^2} \tag{17}$$

$$\chi^2 = \sum_{i=1}^{n}\frac{(q_{e,meas}-q_{e,calc})^2}{q_{e,calc}} \tag{18}$$

Where Y, $\overline{Y}$, and $\hat{Y}$ are the ordinate data, mean of ordinate data, and the ordinate data achieved from the linear or the nonlinear of the model, respectively. Accordingly, for

nonlinear equilibrium adsorption models, Y, $\overline{Y}$ and $\hat{Y}$ are the measured ($q_{e,meas}$; meq/g), the mean of measured ($\overline{q_{e,meas}}$; meq/g), and the calculated ($q_{e,calc}$; meq/g) equivalent concentrations of contaminants in the resin phase, respectively.

The coefficient of determination R^2 (Eq. S1) is a widely used statistical measure that compares the variance of independent variables (i.e., $q_{e,meas}$ and $q_{e,calc}$) to the variance about the mean of dependent variables (i.e., $q_{e,meas}$ and $\overline{q_{e,meas}}$) (Foo & Hameed, 2010). Values closer to 1 indicate a better fit of a model to experimental data. The average relative error (ARE) (Eq. 15) reflects on the degree of bias in the predicted model results. Both these error functions are used to evaluate model fitting for all solute-resin pairs (Dron & Dodi, 2011; Hu et al., 2016; Landry et al., 2015). The SSE and RMSE reflect on the variance of independent variables and are good indicators of model fitting to experimental data where isotherms provide a better fit when SSE and RMSE values are closer to 0 (Kinniburgh, 1986). However, both these functions could only be used to compare the fit of different models to one equilibrium experiment as the values are not normalized (Dron & Dodi, 2011) and become more sensitive to variation at the highest end of the curve (i.e., high C_e values) (Allen et al., 2003). χ^2 are specific to nonlinear regression only, where high χ^2 values show an underestimation or an overestimation of the calculated values, while conforming to the experimental data when approaching 0 (Tran, You, Hosseini-Bandegharaei, et al., 2017).

CHAPTER 3

RESULTS AND DISCUSSION

3.1. Effect of resin properties on individual contaminant removal

IRA 458 (SB/PA/G/trimethyl), A520E (SB/PS/MP/triethyl), IRA 67 (WB/PA/G/dimethyl), and IRA 96 (WB/PS/MP/dimethyl) were tested to investigate the effect of resin characteristics for separate removal of nitrate, sulfate, and 3-PPA. Fig. 3.1 shows percentage removal of 3-phenylpropionic acid (3-PPA), nitrate, and sulfate at pH 4, 7, and 10 and different resin properties as a function of resin dose from 25% to 300%. The following trends are specific to pH 4 and pH 7 removal data. Table A2 in appendix A summarizes the impact of resin properties on contaminant selectivity based on the results of Fig. 3.1. The most important results in Fig. 3.1 are SB/PS/MP/triethyl removed 3-PPA to a greater extent than WB/PS/MP/dimethyl, whereas SB/PA/G/trimethyl and WB/PA/G/dimethyl exhibited similar removal ($\leq 10\%$ difference) of all contaminants at each condition except 3-PPA at pH 4, where SB/PA/G/trimethyl $>$ WB/PA/G/dimethyl. Briefly, the functional groups of the selected WB-AERs and Type I SB-AERs were dimethylamine R-$(CH_3)_2HN^+$ (IRA 67 and IRA 96) and trialkylamine respectively, with SB-AER groups further subdivided into triethyl R-$(CH_2CH_3)_3N^+$ (A520E) and trimethyl R-$(CH_3)_3N^+$ (IRA 458). For the same resin porosity and polymer composition, the AER becomes more hydrophobic as the alkyl chain-length increases (Helfferich, 1995; Zaggia et al., 2016), which explains the higher preference of organic 3-PPAs to ethylamine than methylamine type functional groups. However, the addition of one methyl group did not affect contaminant removal, suggesting the order of decreasing hydrophobicity as triethyl > trimethyl $\approx$ dimethyl. The higher observed removal of 3-PPA by dimethyl compared to

triethyl-functionalized PA resin at pH 4 was due to the WB-AER release of proton ions (H^+) in unbuffered solution. Additionally, 3-PPA removal at pH 4 was reduced by 15-38% compared to pH 7 for all AERs at maximum resin dose (i.e., 300%). Both trends are consistent with weaker electrostatic interactions between 3-PPA and resin functional groups. To elaborate, 3-PPA contains a carboxylic acid group with pKa of 4.66 ($K_a = 2.19 \times 10^{-5} \text{mol/L}$) at 25°C (Kortüm et al., 1960). Once below the pKa value, a slight decrease in pH significantly increases the portion of 3-PPA in its conjugate acid form, whereby 82% of 3-PPA is in its protonated form at pH 4. The former results conclusively isolate the influence of the AER functional group structure and resin basicity on resin performance at $\text{pH} \leq 7$, where contaminant removal varied with carbon chain-length while remaining the same after the WB-AER-specific tertiary amine group was substituted by a quaternary ammonium (i.e., characteristic of SB-AER) with similar branched alkyl group. Several studies compared resin basicity using the same PA AERs (i.e., IRA 458 and IRA 67) for the removal of charged organic dyes from aqueous solution and showed IRA 458 to have half (Wawrzkiewicz, 2011), seven (Greluk & Hubicki, 2011), and ten times (Greluk & Hubicki, 2010; Wawrzkiewicz & Hubicki, 2011) more maximum capacity (i.e., q_0) than IRA 67. A possible reason for these differences is the use of non-normalized data to compare between studies using different resin and contaminant concentration. In this work, resin dose (%) accounted for the capacity of the resin (see Section 2.3), which also corroborated AER selectivity for a contaminant. A previous study supported all the above-mentioned statements, whereby for the same resin properties using normalized resin concentrations (i.e., selectivity), resin functional groups that showed decreasing maximum capacity for PFOS were

triethylammonium > trimethylammonium ≈ dimethylamine (Schuricht et al., 2017). The trend of increasing removal with increase in alkyl chain-length was only valid for $C \leq 2$. Another study showed that WB/PA/dimethyl had higher anion exchange capacity (meq/g) and similar selectivity for various hydrophobic ionizable organic compounds (HIOCs) than SB/PA/trimethyl resin (Gustafson & Lirio, 1968). This both highlights the intrinsic benefit of AER with smaller (i.e, close-packed) functional groups (Boyer, Fang, et al., 2021) and further solidifies the advantage of normalized data.

At 100% dose (i.e., equal available ion exchange sites on equivalent basis), the nitrate selective A520E resin (i.e., SB/PS/MP/triethyl) showed significant removal of nitrate (87-89%) while other resins exhibited 59-77% removal. Nitrate and 3-PPA both followed the same trend for all resins (Fig. 3.1a, 3.1b). In terms of resin properties, the order of decreasing removal was SB/PS/MP/triethyl (87%, 66%, and 44%) > WB/PS/MP/dimethyl (77%, 59%, and 36%) > SB/PA/G/trimethyl (65%, 45%, and 26%) ≈ WB/PA/G/dimethyl (59%, 46%, and 18%) for nitrate at pH 7, 3-PPA at pH 7, and 3-PPA at pH 4, respectively. Before reaching a plateau (i.e., < 100% resin dose), sulfate removal at pH 4 and 7 (Fig. 3.1c) decreased as follows: WB/PA/G/dimethyl (46-48% and 88-89%) > SB/PA/G/trimethyl (46% and 82-83%) > WB/PS/MP/dimethyl (35-36%, 65-67%) ≈ SB/PS/MP/triethyl (36-39% and 64%). As a general rule, the affinity of the solute is highest for the resin with complementary polarity character. PS matrix of the AER is composed of a repeating (CH_2)-CH-(CH_2)-benzene unit making it more hydrophobic than PA-AER with benzene rings substituted by carbonyl groups. Due to the longer alkyl chains of ethyl than methyl groups, A520E (SB/PS/MP/triethyl) is slightly

more hydrophobic than IRA 96 (WB/PS/MP/dimethyl). The degree of resin hydrophilicity was defined by Sengupta and Clifford (1986) as the media's ability to absorb polar water molecules. As such, a hydrophobic resin will favorably interact with poorly hydrated contaminants and vice versa (Sengupta & Clifford, 1986). NO_3^- and SO_4^{2-} have symmetrical structures with trigonal planar and tetrahedral geometries, respectively, cancelling the combined effects of individual S-O and N-O bond dipoles. This is indicative of the low polarization of polyatomic nitrate and sulfate with no dipole moment. Despite the similar thickness of the hydration shell of sulfate (0.043 nm) and nitrate (0.044 nm), sulfate is 3.6 times more hydrated than nitrate (Marcus, 1991). The main contributors to the energy of hydration are coulombic ion-water interactions, thus divalent sulfate immobilizes water molecules within its hydration shell more effectively than monovalent nitrate (Marcus, 1991; Vchirawongkwin & Rode, 2007). 3-PPA has a highly hydrophobic moiety with a phenyl group attached to a long aliphatic chain. Hence, 3-PPA and nitrate had higher affinity for PS resins than PA resins and A520E (PS/triethyl) than IRA 96 (PS/dimethyl) whereas sulfate is preferred by PA resins. These trends are validated by ΔG^0 values for the adsorption of HIOCs (Landry et al., 2015; Li & SenGupta, 1998, 2004) and inorganic anions (Hu et al., 2016) on AERs with structures similar to the ones tested in this study. which agrees with previous research results with respect to removal efficiency (Hu et al., 2016).

At stoichiometric dose (i.e., 100%), all resins exhibited > 96% sulfate removal apart from SB/PS/MP/triethyl with ~88% removal. The order of increasing percent removal was 3-PPA < nitrate < sulfate for all resins except for SB/PS/MP/triethyl (i.e.,

A520E) being 3-PPA < sulfate ≈ nitrate. These trends support the preference of resins with closely spaced alkylamine groups for divalent over monovalent ions (Howe et al., 2012; Subramonian & Clifford, 1988). Considering that all four AERs in this study have similar overall volume of active sites (i.e., water content), the low exchange capacity of A520E insinuates greater effective distance between triethyl groups than less bulky methyl groups of remaining resin (Subramonian & Clifford, 1988). Divalent sulfate, with distant ionic charges, needs to access two binding sites simultaneously to satisfy electroneutrality which is more appropriate for the resin with densely packed functional groups. The effect of charge separation is well demonstrated in previous research, whereby the preference of sulfate over nitrate decreased with increasing length of carbons of resin functional groups (Samatya et al., 2006), the selectivity of IRA 458 with closely-spaced trimethyl was higher for divalent bichromate than IRA 900 with more spaced active sites (Sengupta & Clifford, 1986), and was even relevant for zeolites (i.e., cation exchangers) where an increase in the silica to alumina ratio increased the intramolecular distance between anionic sites, which provided lower uptake of divalent cations (Ames, 1965). Therefore, triethylamine decreased the performance of A520E for sulfate removal relative to methyl groups of remaining resins. It is worthy to note that, while not significantly noticeable in this study, IRA 96 (~89%) with dimethyl group exhibited higher removal than IRA 458 (~80%) with trimethyl group which could be attributed to site spacing. This was also observed in a study comparing methylamines with different basicity (i.e., primary, secondary, tertiary, and quaternary) (Clifford & Weber, 1983).

Removal efficiency is generally influenced by AER properties in terms of polymer composition, porosity, and functional group (Landry & Boyer, 2013; Li & SenGupta, 1998, 2004). However, MP and G resin vary in pore size distribution (50-100 nm vs. < 2nm), also reflected by the higher Brunauer-Emmett-Teller (BET) surface area of MP resin (Dudley, 2012), and surface morphology (large array of tiny microgels vs. homogeneous unit), both only affecting the predominance of intra-particle diffusion (pore vs. solid phase) of large solutes (Li & SenGupta, 2000). This suggests that, for equilibrium tests (i.e., $\geq$ 24 h) and relatively low molecular weight contaminants, sorption kinetics was not the limiting factor, which implied the irrelevance of comparing the removal of the selected contaminants based on porosity.

Evaluating the impact of solution pH, SB-AERs had similar removal results between pH 4, 7, and 10, for nitrate and sulfate and between pH 7 and 10 for 3-PPA. However, for WB-AER, removal efficiency significantly decreased when solution pH increased to 10. This is because the tertiary amine functional group is mostly in its conjugate base form when pH > pK_a. Additional discussion on this is given in the following section.

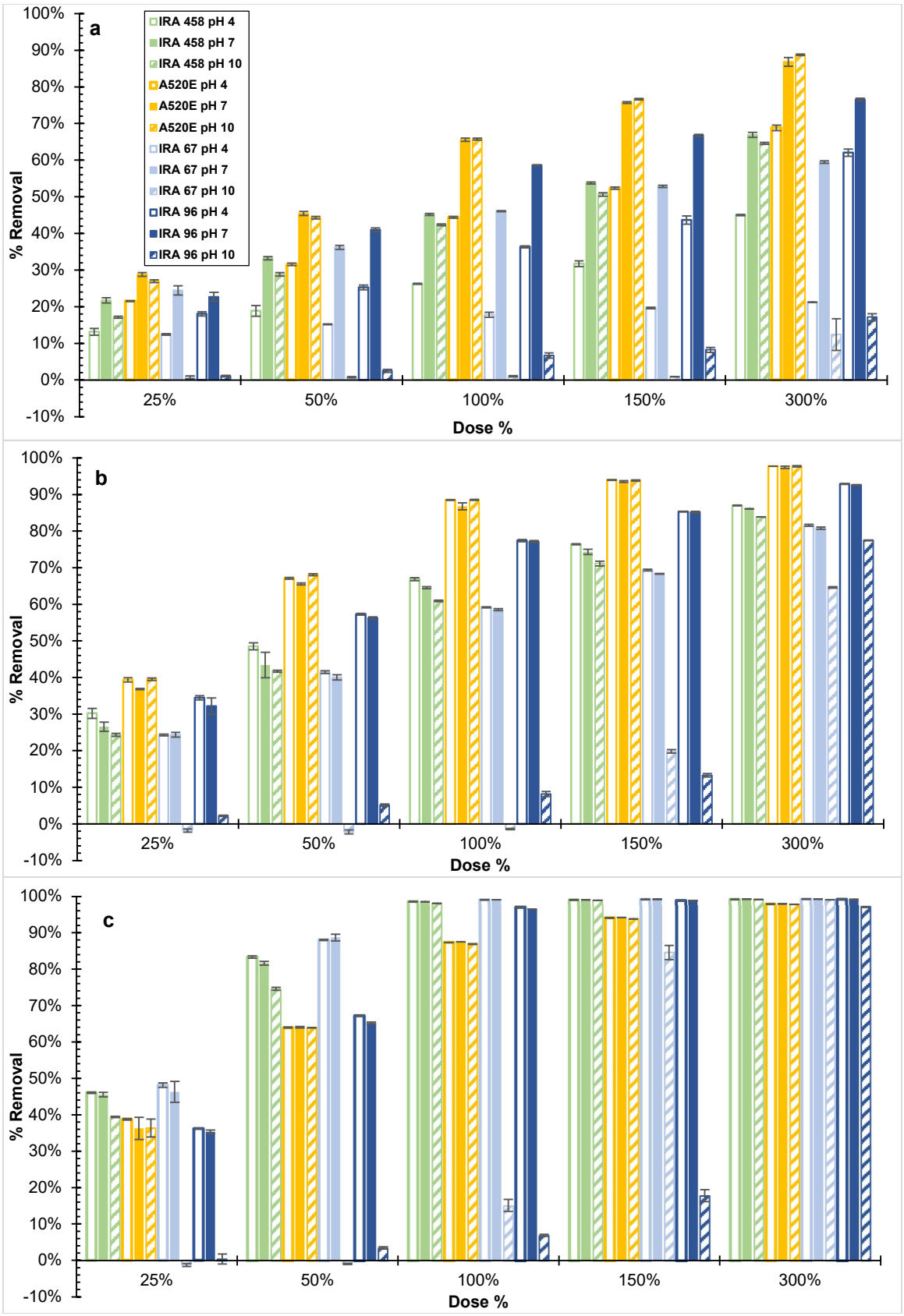
a
b
c
IRA 458 pH 4
IRA 458 pH 7
IRA 458 pH 10
A520E pH 4
A520E pH 7
A520E pH 10
IRA 67 pH 4
IRA 67 pH 7
IRA 67 pH 10
IRA 96 pH 4
IRA 96 pH 7
IRA 96 pH 10
% Removal
100%
90%
80%
70%
60%
50%
40%
30%
20%
10%
0%
-10%
25%
50%
100%
150%
300%
Dose %

Fig. 3.1. Removal of (a) 3-phenylpropionic acid, (b) nitrate, and (c) sulfate by ion-exchange at different solution pH (4, 7, and 10) in single-solute system. Initial contaminant concentration $C_0 \approx 2.14$ meq/L. Percent resin dose (Dose %) is the ratio of theoretical resin capacity to initial contaminant concentration on equivalent basis. Values for each pair of contaminant and resin are mean of triplicate with error bars showing one standard deviation.

3.2. Effect of solution pH

Fig. 3.2 shows the impact of solution pH on WB-AER removal efficiency. Pertaining to contaminants with equivalent concentration (i.e., ≈ 2.14 meq/L), WB-AERs showed less than 10% removal of 3-PPA (Figs. 3.2a and 3.2b), nitrate (Figs. 3.2c and 3.2d), sulfate (Figs. 3.2e and 3.2f), and bicarbonate (Figs. 3.2g and 3.2h) when pH > 11. When % dose >100%, contaminant removal increased with decreasing pH and increasing resin dose. At 300 % dose Both WB/PA/G/dimethyl (IRA 67) and WB/PS/MP/dimethyl (IRA 96) regained their sulfate removal efficiency to match their initial performance at pH 4 and pH 7 (Fig. 3.1c). At resin dose equal or lower than the stoichiometric dose (i.e., ≤ 100%), any amount of H^+ released from the resin was neutralized by excess OH^- ions in solution, which kept the pH unchanged. At a higher dose, OH^- was more than offset by H^+, thus significantly decreasing pH down to 6-8. Although the same trend was observed for PFAS removal by WB/PA/G/dimethyl, WB/PS/MP/dimethyl was not affected by solution pH and achieved > 88% removal at pH > 10. This strictly isolates the impact of highly basic conditions on the removal of all contaminants except for PFAS and is consistent with the decrease in resin performance with increasing deprotonated sites of

WB-AER. Miyazaki and Nakai (2011) estimated pKa = 9.3 for IRA 67 using the cesium (^{133}Cs) and hydrogen (^{1}H) nuclear magnetic resonance (NMR) method and pKa = 6.3 for IRA 96 using phosphorus (^{31}P) NMR. As the pH > pKa, most amine groups get protonated, which weakens ionic interactions (i.e., electrostatic) of the resin thus functioning as nonionic AER. In all cases, WB/PS/MP/dimethyl showed > 0 % removal even when pH >> pKa, which suggests that other interactions are influencing the IX process. Although the mechanism responsible for sulfate, nitrate, and bicarbonate removal at high pH is still not clear, it is suggested that the high hydrophobicity coupled with the porous structure of IRA 96 allow inorganic contaminants to diffuse within the resin pore and bind to remaining protonated resin sites through IX. PFAS and 3-PPA on the other hand are mainly removed by physisorption (e.g., hydrophobic interactions, van der Waals forces). Since the PFAS concentration ($\sum \text{PFAS} = 480\ \mu g/L$) was exceeded by resin doses (> 3000%), physisorption deemed sufficient to achieve high removal. This data does not rule out the possibility of either still having available protonated sites, or dissimilar amine groups with higher pK_a values (e.g., quaternary ammonium). Gel-type resins are generally regarded as more homogeneous and less porous than MP resins (Harland, 1994), which is consistent with both conjectures. In fact, multiple asymmetric peaks were detected over the ^{31}P NMR spectral range of IRA 96 evincing heterogeneity in amine functionalities of the resin structure (Miyazaki & Nakai, 2011). It was also observed that some WB-AERs had polyamines while advertised commercially as secondary or tertiary amines (Clifford & Weber, 1983). This non-uniformity arises from the difficulties of controlling the chloromethylation step during resin synthesis (Anderson, 1964). For the purpose of this study, having WB-AERs in the chloride form

was, to a small extent, a limitation. Previous research showed difficulties maintaining solution pH of unbuffered solutions for WB-AER batch adsorption experiments (Gustafson et al., 1970). In this study, WB-AERs were pretreated with HCl to ensure chloride saturation on the resin. When in contact with test water, H^+ tends to displace off the resin in response to a driving force (i.e., charge gradient and concentration gradient) thus significantly reducing the pH of the solution (Hinrichs & Snoeyink, 1976). The reason for this pretreatment method is due to WB-AER being highly selective for strong acids (e.g., HCl, HNO_3, H_2SO_4). To further elucidate, ion-exchange between WB resin and charged contaminants only occurs when a readily dissociating strong acid along with corresponding H^+ occupy IX sites (Helfferich, 1995), which precludes using free-base form WB-AERs in synthetic solutions with low ionic strength. The results in the literature showed similar pH-dependent behavior of WB-AER for inorganic (Awual et al., 2008; Kołodyńska, 2009, 2010), HOICs (Greluk & Hubicki, 2011; Gustafson & Lirio, 1968; Hinrichs & Snoeyink, 1976; Wawrzkiewicz, 2011; Wawrzkiewicz & Hubicki, 2011), and PFAS (Deng et al., 2010; Du et al., 2015; Gao et al., 2017; Wang et al., 2019; Yang et al., 2018) removal in batch conditions. All these results suggest the potential for WB-AER regeneration using NaOH and/or NaOH + salt only solutions with low ecotoxicological risk (Hinrichs & Snoeyink, 1976; Jackson & Bolto, 1990). Likewise, Ateia, Alsbaiee, et al. (2019) also highlighted the importance of the tertiary amine functionality of non-AER adsorbents, such as highly porous nanostructured polymers, due to the ease of regeneration.

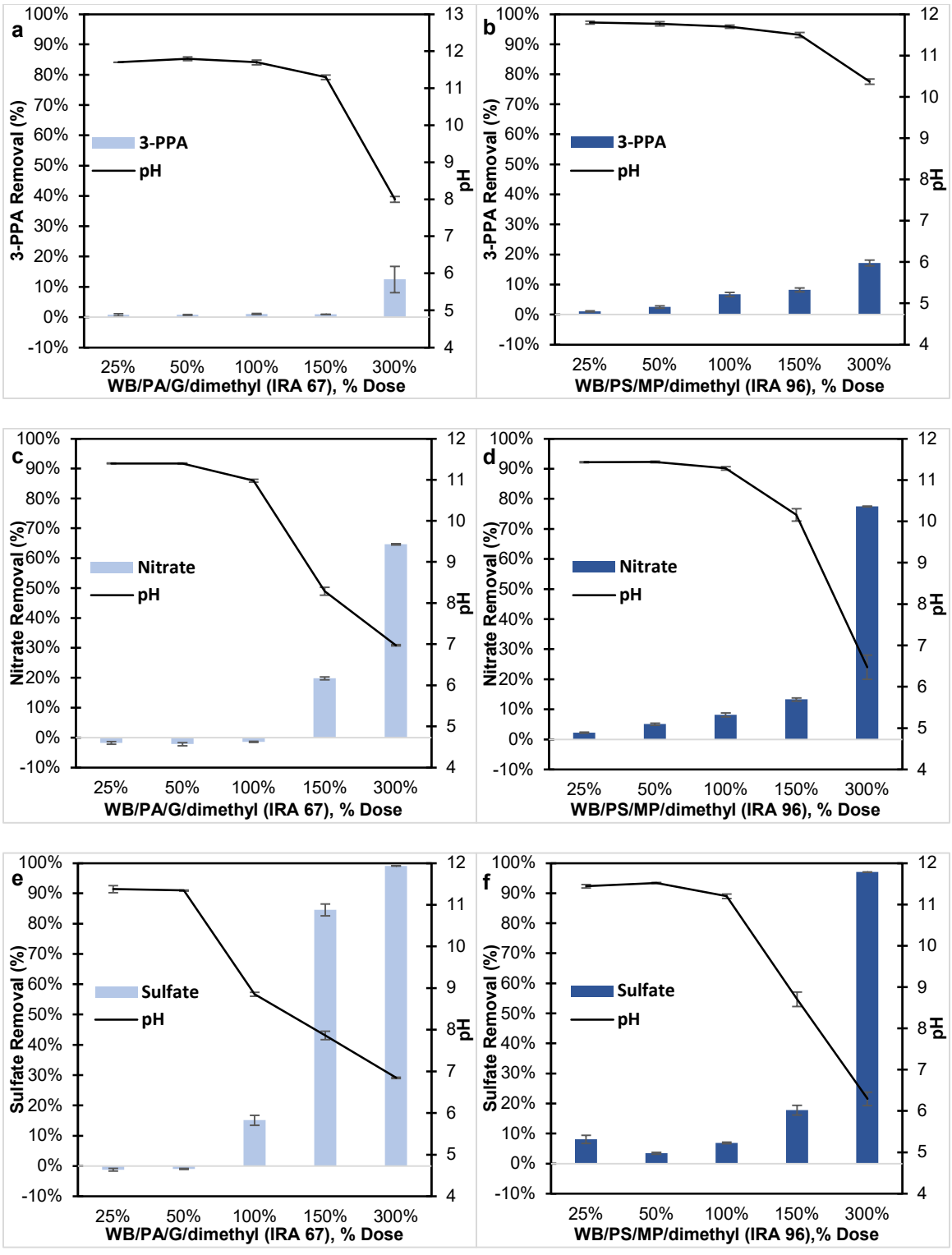
a
3-PPA Removal (%)
3-PPA
pH
WB/PA/G/dimethyl (IRA 67), % Dose
b
3-PPA Removal (%)
3-PPA
pH
WB/PS/MP/dimethyl (IRA 96), % Dose
c
Nitrate Removal (%)
Nitrate
pH
WB/PA/G/dimethyl (IRA 67), % Dose
d
Nitrate Removal (%)
Nitrate
pH
WB/PS/MP/dimethyl (IRA 96), % Dose
e
Sulfate Removal (%)
Sulfate
pH
WB/PA/G/dimethyl (IRA 67), % Dose
f
Sulfate Removal (%)
Sulfate
pH
WB/PS/MP/dimethyl (IRA 96),% Dose
25% 50% 100% 150% 300%

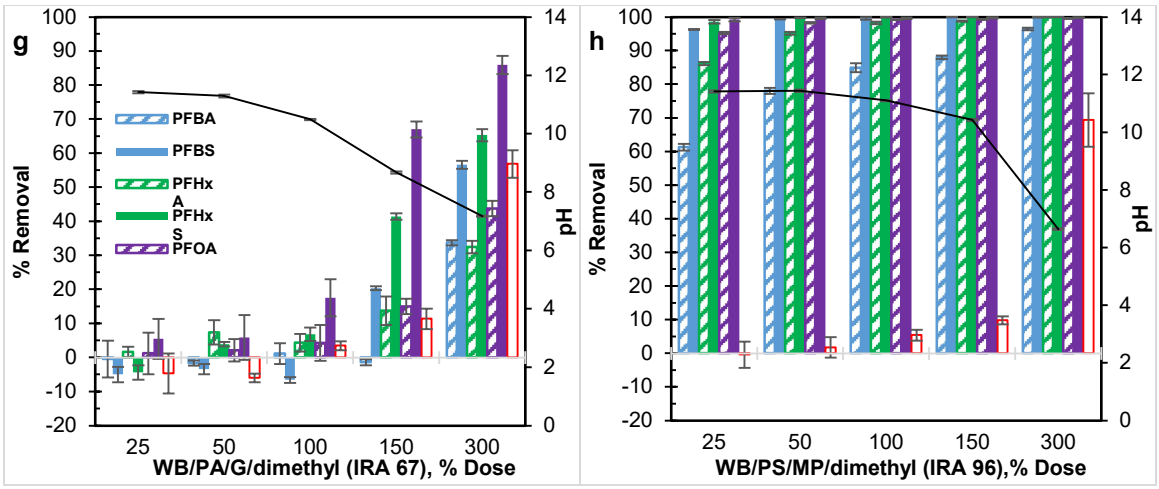

Fig. 3.2. Impact of solution pH on the removal by weak-base anion exchange resins of (a,b) 3-phenylpropionic acid, (c,d) nitrate, and (e,f) sulfate in single-solute system ($C_0 \approx 2.14$ meq/L) and (g,h) the six PFAS in the presence of sodium bicarbonate ($C_0 \approx 2.14$ meq/L) in multi-solute system. Initial concentration of each PFAS was $C_0 = 80$ µg/L ($\sum$PFAS $= 480$ µg/L). Resins were first equilibrated for 24 h at basic conditions (pH ≈ 11) then placed in test water at pH (a,b) 11.70, (c,d) 11.41, (e,f) 11.43, and (g,h) 11.40. Error bars show one standard deviation.

3.3. Competitive removal of six PFASs

Figs. 3.3, 3.4 and A1 show the effect of resin properties and solution pH on the co-removal of PFAS by AER at pH 4, 7, and 10, respectively. Comparing the removal efficiency in terms of resin basicity and solution pH, PFAS removal by WB-AER was similar to SB-AER with analogous resin polymer composition and porosity, and all AERs showed equal removal between pH 4 and pH 7. Although SB/PA/G/trimethyl, SB/PS/MP/triethyl, and WB/PS/MP/dimethyl resins maintained their performance with respect to PFAS removal, WB/PA/G/dimethyl had a considerable decrease in efficiency

at pH 10 (see Fig. A1). Since the pKa of selected PFASs varied from -3.33 to 1.07 (Maimaiti et al., 2018; Park et al., 2020), any change in removal efficiency was attributed to either the protonating state of amine group or the type of aqueous inorganic carbon species (i.e., carbonic acid, bicarbonate, and carbonate). Considering the low selectivity of bicarbonate species compared for AER compared to PFAS, the latter statement is not evident. As explained in the previous section, the PS polymer composition of WB/PS/MP/dimethyl imparts strong nonionic character to the resin thus showing similar PFAS removal between different solution pH, whereas for SB-AERs, this was attributed to quaternary ammonium functional groups always being protonated below pH 14 (Bolto et al., 2002). Several studies evaluated the impact of pH on PFAS uptake by SB-AER (Deng et al., 2010; Maimaiti et al., 2018; Wang et al., 2019; Yu et al., 2009) and WB-AER (Deng et al., 2010; Du et al., 2015; Maimaiti et al., 2018; Wang et al., 2019). As expected, PFAS removal decreased with increasing solution pH for WB-AER and was constant for SB-AER (Deng et al., 2010; Maimaiti et al., 2018). However, Yu et al. (2009) and Wang et al. (2019) have reported lower PFAS removal at higher pH for IRA 400 (SB/PS/MP/trimethyl). Some conjectured this to be due to the stronger hydrophobic character of PFAS, that outweighs electrostatic repulsion, stemmed from the more neutral surface potential of perfluorinated tail at lower pH (Du et al., 2014). Again, this is promising for the reuse of WB resin in conventional treatment settings. Effective PFAS desorption was previously achieved through the deprotonation of amine groups using 1% NaOH (~35%) (Gao et al., 2017), 0.04% NaOH (38 – 85%) (Du et al., 2015), 0.5% NaOH at 25 and 92°C (92%, 95%) (Wang et al., 2019), with an interesting regeneration result showing a decrease in desorption efficiency with increasing % NaOH as 50%

(0.04% NaOH) > 45% (0.4% NaOH) > 3% (4% NaOH). The main goal of using a base solution was to convert WB-AERs to the free-base form thus desorbing most PFAS. However, the current work highlights two key limitations for these regeneration results. The first is that most studies used NaOH to regenerate IRA 67 (WB/PA/G/dimethyl) while disregarding IRA 96 (WB/PS/MP/dimethyl) which showed high PFAS affinity even in its free-base form. The second caveat being the reusability of AER after desorption by NaOH. Once neutralized by OH^-, the WB-AER in its free-base form will exhibit less capacity for PFAS than other chloride form WB-AER (Moldes et al., 2003). Therefore, it is recommended that the tertiary amine be functionalized by chloride ions with an additional washing step using hydrochloric acid (HCl) as described elsewhere (Bolto et al., 2002; Moldes et al., 2003; Sengupta & Clifford, 1986).

The results in Fig. 3.3 clearly show increasing PFAS removal with increasing number of fluorinated carbons within each subgroup, and higher PFAS removal for PFSAs than PFCAs and for PS-AER than PA-AER. PFAS removal by SB-AER was extensively investigated within the literature with similar trends consistently observed (Laura del Moral et al., 2020; Maimaiti et al., 2018; Zaggia et al., 2016; Zeng et al., 2020). PFAS removal is governed by both electrostatic and non-electrostatic (i.e., London van der Waals, hydrophobic) interactions (Boyer, Fang, et al., 2021). A previous study estimated the total PFAS atomic charge using the density functional theory (DFT) method to highlight the more important electrostatic interactions between resin and PFSA relative to PFCA for PFAS with the same number of carbons. The most tangible difference was on the hydrophilic end showing the total charge of oxygen atoms of

carboxylates to be halved when compared to sulfonate analogues (Park et al., 2020). Non-electrostatic interactions are more noticeable with increasing hydrophobicity of the solute and the sorbent. As discussed earlier, hydrophobicity is greater for PS-AERs than PA-AERs, and ethyl than methyl functional groups. Building on the latter statement, SB/PS/MP/triethyl should remove PFAS to a greater extent than WB/PS/MP/dimethyl; nonetheless, this conclusion was not attained given the considerably high removal of both resins. However, this was confirmed elsewhere, whereby the change in removal efficiency between SB/PS/MP/triethyl and WB/PS/MP/trimethyl was hardly noticeable (Schuricht et al., 2017). Similar to the results of Fig. 3.1, PFAS removal was the same between SB/PA/G/trimethyl and WB/PA/G/dimethyl.

The effect of inorganic carbon on PFAS removal was not conclusively isolated. Under the tested conditions, inorganic carbon species are mostly in the in the neutral $CO_{2\,(aq)}/H_2CO_3$ form at pH 4 given the high henry's partitioning constant and pKa of HCO_3^- species being 0.83 and 6.3 at 25°C respectively (Howe et al., 2012). Hence, it can be inferred from Fig. 3.4 that the influence of inorganic carbon on PFAS removal was minimal. This was further supported in the literature, where less than 6% reduction in PFOA removal was shown when bicarbonate ions were added at 1 meq/L (Yang et al., 2018).

Regarding bicarbonate removal, the order of decreasing removal was WB/PA/G/dimethyl > WB/PS/MP/dimethyl > SB/PA/G/trimethyl > SB/PS/MP/triethyl. PA-AER is more selective of bicarbonate species than PS-AER owing to the hydrophilic

nature of PA resin matrix (Ness & Boyer, 2017). The main reason bicarbonate was removed to a greater extent by WB-AER than SB-AER analogues at pH 7 is similar to the one described for 3-PPA at pH 4 in section 3.1, where release of H^+ decreased the detected amount of bicarbonate in its neutral form. While the goal of this section does not include bicarbonate removal, it was further added for completeness.

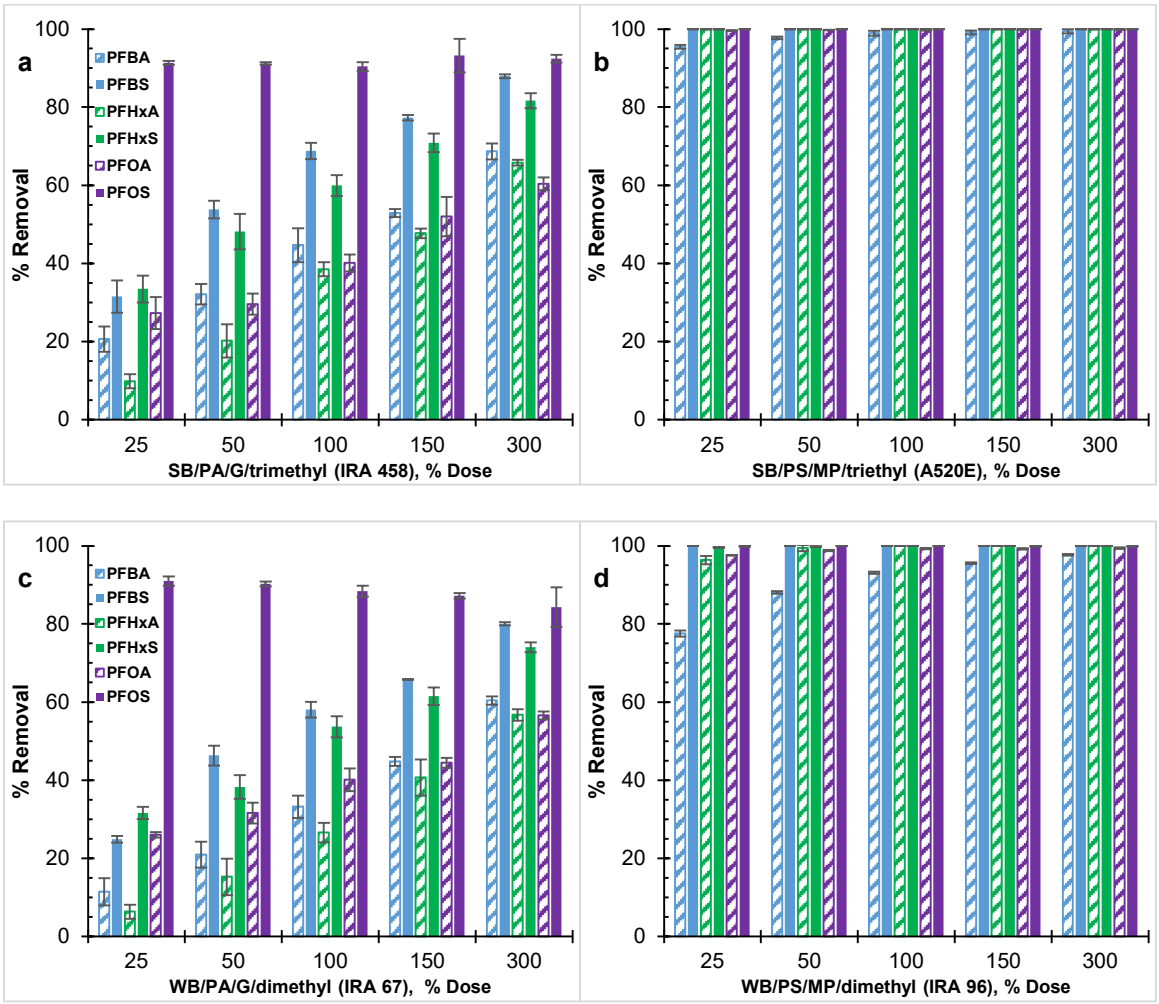

Fig. 3.3. Effect of resin polymer composition (PS vs PA) on perfluoroalkyl acids (PFAAs) removal by (a,c) polyacrylic, and (b,d) polystyrene strong-base and weak-base anion exchange resins at pH 4. Initial concentration of each PFAS was $C_0 = 80$ µg/L

($\sum$ PFAS = 480 µg/L). Bicarbonate ($pK_a = 6.3$) was mostly in the neutral $CO_{2(aq)}/H_2CO_3$ form at pH 4.

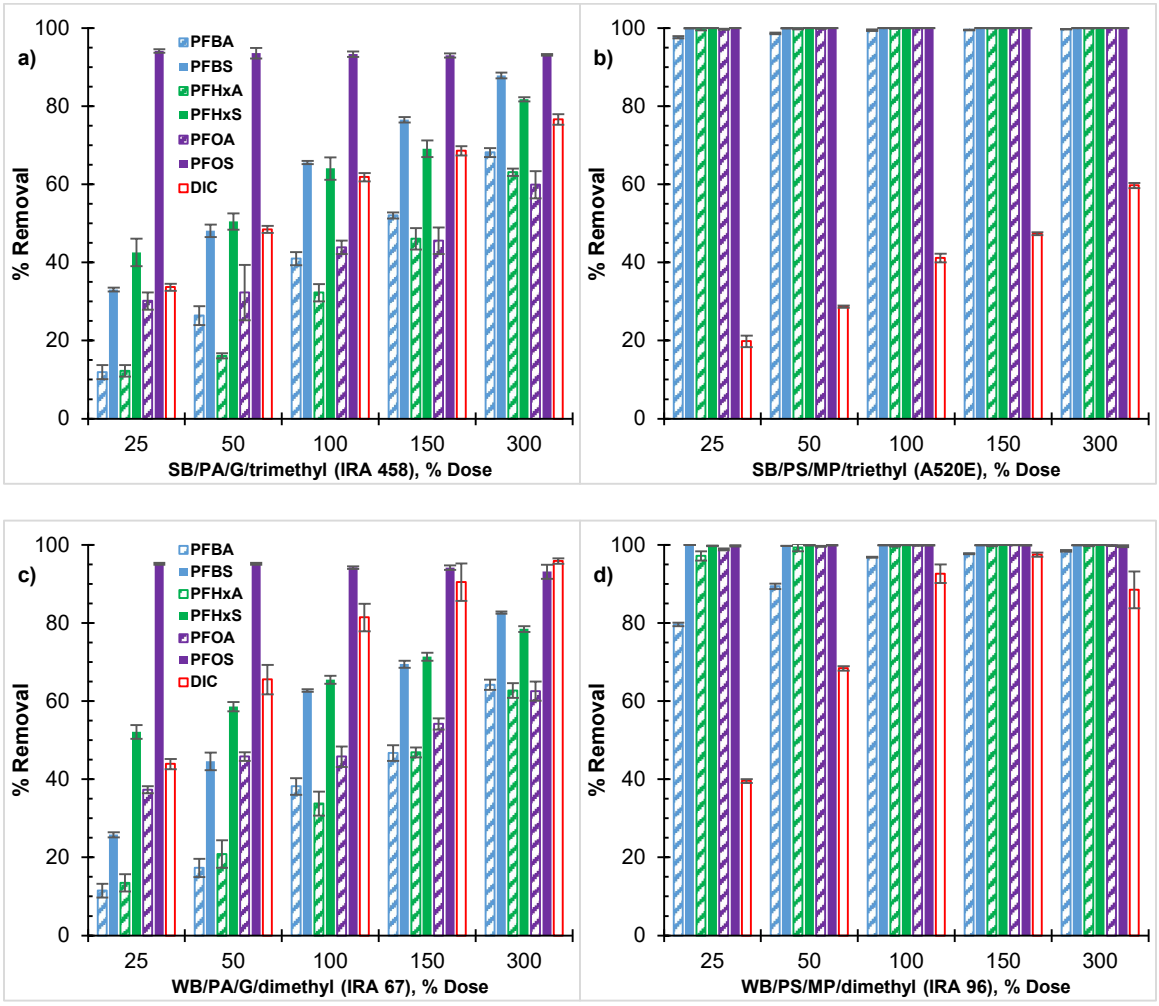

Fig. 3.4. Effect of resin polymer composition (PS vs. PA) on perfluoroalkyl acids (PFAAs) removal by (a,c) polyacrylic, and (b,d) polystyrene strong-base and weak-base anion exchange resins in the presence of sodium bicarbonate ($C_0 \approx 2.14$ meq/L) at pH 7. Initial concentration of each PFAS was $C_0 = 80$ µg/L ($\sum$ PFAS = 480 µg/L). DIC is dissolved organic carbon.

3.4. Sorption isotherms

3.4.1. Limitations of isotherm modeling for ion-exchange

The nonlinear and corresponding linear forms and plots of each isotherm model are summarized in Table A1 in Appendix A. To investigate the inaccuracies of the linearized curve-fitting method, the Langmuir isotherm parameters (K_L and q_0) and goodness-of-fit measures for the adsorption of sulfate and nitrate were calculated using the nonlinear and four different linear forms of the Langmuir model and are listed in Table A3 in Appendix A. When excluding A520E data, the Langmuir Type I form was a better fit than the Langmuir Type II form for the sulfate data as shown by the linear R^2 values of > 0.991 and 0.600-0.889 respectively, whereas Type II linearization provided the best fit to nitrate data (linear $R^2 > 0.995$) and A520E data for sulfate (linear $R^2 >$ 0.9937). The different outcomes were because Langmuir Type II fails to portray very high removal, which corroborates the strong affinity of AERs and the lower selectivity of A520E for sulfate. To elaborate, Bolster and Hornberger (2007) proved the Type II linearized form to be disadvantageous when q_e values approach zero since $1/q_e$ values become extremely sensitive to small variations of $1/C_e$ (x-axis). Also, the high linear R^2 values of the Langmuir Type I form, which suggest strong positive correlation between C_e/q_e and C_e, provide misleading deduction regarding adsorption mechanism given the interdependence of both variables. Considering all AERs at different solution pH, linear models fit to sulfate data that showed decreasing average linear R^2 values were Redlich-Peterson (RP) (0.9946) ≈ Langmuir Type I (0.9940) > DA (0.9475) > DR (0.8571) > Langmuir Type II (0.8370) > Freundlich (0.819) > Langmuir Type III = Langmuir Type IV (0.698). This creates possible misunderstanding, where adsorbates occupy a single

layer within resin walls when the Langmuir Type I or the RP linearization is accounted for, while following a pore filling mechanism otherwise (i.e., D-A). When comparing parameter estimation for Langmuir Type III vs. Type IV, lower K_L values were compensated by higher values of q_0, despite showing the same fit to all equilibrium data based on linear R^2. This was explained by both forms being associated to the same error distribution structure due to their identical x and y correlation (i.e., q_e/C_e and q_e). A study on the adsorption of safranin on activated carbon supported both statements with the order of decreasing R^2 values as RP > Langmuir Type I > Freundlich > Langmuir Type II > Langmuir Type III = Langmuir Type IV (Kumar & Sivanesan, 2005).

However, the results of this research showed that identifying the best-fit model cannot solely pertain to Linear R^2. Although the Langmuir Type I form exhibited a good fit to sulfate data (linear $R^2 > 0.9803$), values for the equilibrium constant, K_L, varied up to 30% (average ≈ 16%) compared to the nonlinear least-squares method. When the equilibrium contaminant concentration in the ion phase, q_e, was further calculated using the linearly estimated Langmuir parameters, all values for the nonlinear coefficient of determination (R^2) (see Eq. 14) decreased (nonlinear $R^2 > 0.8912$). Clearly, the axial settings of the Langmuir Type I form provided the lowest error distribution, thus maximizing linear R^2 while giving the impression of a favorable fit to experimental data. The strong correlation between the dependent variables of this linearized form was designated a “mathematical artifact” and could falsely represent the Langmuir model (El-Khaiary, 2008).

Following the logic of the previous paragraph, all linear data were transformed back to q_e and goodness-of-fit parameters were calculated to evaluate the difference in model fits between the nonlinear and the linearized forms of each isotherm model. The nonlinear R^2, SSE and RMSE improved for all the data while ARE was kept stable after transformation. The Langmuir model was the most impacted by nonlinear regression where SSE and RMSE values for the linearized equations exceeded the values for the nonlinear form by 2−1106% and 1−247%, respectively and nonlinear R^2 values improved from > 0.4290 to > 0.8993. The estimated parameter values for the linearized Langmuir equations varied from -169% − 62% compared to the nonlinear form, with the order of decreasing average deviation as Type II (33%) > Type IV (15%) > Type III (13%) > Type I (11%) given that observed extremes (i.e., -169% and + 62%) were for the Langmuir Type II form. However, the overall quality of the fit of all other models improved slightly (< 15%), which explained the non-significant difference between the adsorption parameters calculated by the linear and nonlinear methods (< 20%), except for extreme values (e.g., the DR maximum adsorbent capacity, q_0, for 3-PPA adsorption by IRA 67 at pH 4). An anion-exchange study for the removal of inorganic contaminants supported most assertions whereby Freundlich, DR, and DA were minimally affected by the modeling procedure and linear R^2 spuriously identified the linearized Langmuir model to be the best-fit model to equilibrium data, while nonlinear R^2 values and adsorption parameters values suggested otherwise (Dron & Dodi, 2011). Additionally, Langmuir isotherm model parameters and goodness-of-fit measures for all solute-resin pairs in this study converged to single values when using the nonlinear least-squares method regardless of initial nonunique values established from linear plots. In general, χ^2

values were all < 0.9 showing very small bias between measured and predicted NLS data. All these results suggest that while the differences between isotherm parameter values after optimization were not relevant enough to alter the interpretation of adsorption mechanisms, the nonlinearization process presented various advantages. For instance, the NLS function showed a unified error distribution structure, which eliminated biases in the estimation of model fitting parameters, whereas the linearly transformed plots were conditioned by the distortion of their error structures instead of their ability to describe the theory behind each model. The main goal of the NLS fitting process was to reduce SSE closest to 0, which implicitly decreased the RMSE (Bolster & Hornberger, 2007). Hence, it further optimized the results and corrected abnormal values, especially the ones derived from linear plots that showed extreme sensitivity to concentration ranges (i.e., Langmuir Type II). Error functions such as R^2, ARE, SSE, RMSE, χ^2 provided a meaningful comparison for model fitting. SSE and RMSE were good indicators to identify the best-fit model within each AER-solute system only, while remaining functions were used to evaluate the fitting degree of various isotherm models for all IX systems. This was because R^2, ARE and χ^2 were normalized by the concentration in the resin phase, q_e (i.e., dimensionless) (see Eqs. 14–18).

Several other studies highlighted the inherent superiority of the nonlinear least-squares over the linear regression but laid out additional suggestions to refine the estimation of adsorption isotherm parameters (Dron & Dodi, 2011; El-Khaiary, 2008; Foo & Hameed, 2010; Parimal et al., 2010; Tran, You, Hosseini-Bandegharaei, et al., 2017). As opposed to the linearized models, the nonlinear regression integrates an

objective function to minimize the error distribution between measured and modeled data (Bolster & Hornberger, 2007). These functions include SSE, ARE, R^2, Hybrid fractional error function (HYBRID), Marquardt's percent standard deviation (MPSD), etc. (Foo & Hameed, 2010). A study showed the NLS function, which relies on the minimization of SSE, to be less accurate as aqueous concentrations of analytes increased and further suggested using the HYBRID error function for adsorption equilibrium experiments. Other studies proposed associating a weighting factor (w_i) to objective functions, such as dividing the experimental adsorption data by the measurement variance (i.e., $1/\sigma^2$), to provide a more accurate model calibration during nonlinear regression (Bolster & Hornberger, 2007; Kinniburgh, 1986). Furthermore, the proper use of goodness-of-fit parameters is crucial for modeling of adsorption isotherms and could lead to false conclusions otherwise. Tran and coworkers (Tran, Wang, et al., 2017; Tran, You, & Chao, 2017a, 2017b; Tran, You, Hosseini-Bandegharaei, et al., 2017) emphasized several times on the importance of χ^2 and nonlinear R^2 (see Eq. 14 and Eq. 18) to identify the optimum isotherm and evaluate the effectiveness of a nonlinear minimization technique. Parimal et al. (2010), and Dron and Dodi (2011) recommended that all adsorption data be transformed to a single form (i.e., linear and nonlinear) before testing the constancy of an error function. One study showed the adsorption onto activated carbon to be explained by Langmuir and Freundlich models to the same extent when different nonlinear error functions were optimized, which implied concurrent monolayer and bilayer adsorption. To avoid conflicting conclusions, the authors proved that adding a validation step using a coefficient of non-determination, K^2, to be useful (Kumar et al., 2008).

Lastly, possible errors in the estimation of DR and DA parameters could lead to contradicting concepts. The mean free energy (E) of DR and DA models imparts useful information about the type of adsorption, whereby ion exchange occurs when the magnitude of E is between 8 and 16 kJ/mol (Helfferich, 1995) while corresponding to physical adsorption when below 8 kJ/mol (Mahramanlioglu et al., 2002). However, the inconsistency in estimating E has caused confusion when used to compare different adsorption experiments (Tran, 2017), possibly due to incorrect expressions of Polanyi potential (ε) in the DR and DA equations (Eqs. 7-9) (Fu et al., 2008). For instance, past publications considered either mass concentration, mg/L (Dron & Dodi, 2011; Foo & Hameed, 2010) (Onyango et al., 2004) et al., 2004), g/L (Mahramanlioglu et al., 2002), and g/g (Inglezakis, 2007), or molar concentration, mmol/L (Landry et al., 2015), and mol/L (Özcan et al., 2005), for C_e. Therefore, to prevent inaccurate conclusions regarding the type of adsorption, created from different ε values, it is advisable that DA and DR parameters be calculated on a mass basis to account for contaminant properties (i.e., molecular weight) and weight units (i.e, mg or g) be specified.

3.4.2. Ion-exchange behavior in single-solute systems

Isotherm shape, goodness-of-fit, and model parameters are good indicators of AER capacity, selectivity, and affinity for each contaminant (Sohn & Kim, 2005). Figs. 3.5-3.7, and Figs. A2-A4 show experimental adsorption data fit to the Langmuir, Freundlich, Dubinin-Radushkevich (DR), Dubinin-Astakhov (DA), and Redlich-Peterson (RP) models using the nonlinear least-squares (NLS) regression method to evaluate adsorption behavior.; the isotherm parameters are tabulated in Tables A3-A8 in Appendix

A. The following analysis excludes data for WB-AER at pH 10 given the dissimilarity between batch equilibrium methods. Experimental data showed favorable adsorption for sulfate and nitrate regardless of solution pH and AER due to the concave shape. The curvature was more pronounced for sulfate than nitrate as shown by the sharp slope, which implies higher uptake of sulfate at low resin dose. The adsorption of 3-PPA was favorable for PS AER (i.e., SB/PS/MP/triethyl and WB/PS/MP/dimethyl) at pH 7 while unfavorable for PA AER (i.e, SB/PA/G/trimethyl and WB/PA/G/dimethyl) at pH 7 and for all AERs at pH 4 as depicted by the convex shape. The linear shape of PA AER (i.e., SB/PA/G/trimethyl and WB/PA/G/dimethyl) for nitrate together with the absence of a plateau showed non-saturation even at low resin amounts, suggesting lower AER selectivity for nitrate. Dimensionless selectivity factor (R_L) and 1/n, calculated from the Langmuir and Freundlich models respectively, confirmed the conjectures on adsorption behavior, where values below unity were observed for nitrate and sulfate while the highest values were for PA AER adsorption of nitrate, with 1/n and R_L values ranging from 0.73-0.89 and 0.52-0.79, respectively.

In terms of nonlinear R^2 and ARE values, the order of decreasing two-parameter model fit to sulfate equilibrium data was DA ≈ DR >> Langmuir > Freundlich, while nitrate equilibrium data was equally well fit by all isotherm models ($R^2 > 0.96$; ARE < 10%), both indicating that IX of sulfate and to a lesser extent nitrate were potentially described by pore filling mechanism. The same trend was observed for the IX of various counterion/solute systems, involving Cl^-, NO_3^-, HCO_3^-, SO_4^{2-}, and OH^-, and further suggested that the IX process for inorganic compounds was attributed to intraparticle

diffusion rather than the layer-by-layer mechanism (Dron & Dodi, 2011). The RP model exhibited a suitable fit to all IX data ($R^2 \geq 0.9$). Values of α (0.29 – 0.92) for IX systems involving WB/PS/MP/triethyl indicated that adsorption by A520E does not agree with the theory behind the Langmuir model (i.e., true for α = 1), which suggests non-homogeneous and irreversible adsorption of contaminants with the potential for lateral migration along non-polar planes of the resin (Foo & Hameed, 2010). In most AER/analyte/pH systems, n_D values for the DA model (Table A8) were the lowest for A520E further supporting the previous postulation on the heterogeneity of the resin micropore structure (Dron & Dodi, 2011; Inglezakis, 2007).

Regardless of the goodness of model fit to sulfate equilibrium data, the magnitude of selectivity (1/n, R_L) and thermodynamic (ΔG^0, E) model parameters all agreed on the selectivity sequence for each resin, where selectivity increased with decreasing R_L, 1/n, ΔG^0 and increasing E_{DR} and E_{DA} values. SB/PS/MP/triethyl (1/n = 0.37 – 0.41, R_L = 0.089 – 0.106, ΔG^0 = -5.12 - -5.59 kJ/mol, E_{DR} = 7.70 – 8.05 kJ/mol, E_{DA} = 8.10 – 8.11 kJ/mol) had a significantly lower selectivity for sulfate compared to WB/PA/G/dimethyl, SB/PA/G/trimethyl, and WB/PS/MP/dimethyl (1/n = 0.22 – 0.26, R_L = 0.015 – 0.019, ΔG^0 = -5.12 - -5.59 kJ/mol, E_{DR} = 10.44 – 11.25 kJ/mol, E_{DA} = 11.49 – 12.05 kJ/mol), which showed equally high selectivity. Although previous research and removal results in Fig. 3.1c had already demonstrated increasing sulfate adsorption with increasing resin polarity and decreasing spacing of functional groups (Hu et al., 2016), the model data in this work are complementary suggesting that the spacing of alkyl groups has a much larger impact than polymer composition of AER. The latter assertion regarding resin

spacing was proven valid for both inorganic (Clifford & Weber, 1983) and organic (Subramonian & Clifford, 1988) divalent anions, whereas the preference of resin with polar character does not appertain to sulfonic HIOCs being favorably selected by polystyrene AERs (Landry et al., 2015; Laura del Moral et al., 2020; Li & SenGupta, 2004). PFAS-impacted groundwaters are typically also rich with competing inorganic compounds such as nitrates, bicarbonates, sulfates, and chlorides (Dietz et al., 2021; Maimaiti et al., 2018; Zaggia et al., 2016). While the latter three anions do not pose high ecotoxicological risk or adverse health effects on humans, sulfates are known competitors for IX sites (Song et al., 2012) and were shown to reduce the resin capacity for hazardous nitrates (Hekmatzadeh et al., 2012), but most importantly for highly selective PFAAs such as PFOA (Yang et al., 2018), PFHxS (Maimaiti et al., 2018) and PFOS (Deng et al., 2010) and evidently for short-chain PFAAs (Zeng et al., 2020). This is an important caveat for the applicability of WB-AER because it could potentially preclude using sulfate-selective tertiary amine groups for the treatment of groundwater intended for human consumption. However, the order of decreasing maximum resin capacity (q_0, mmol/g) for sulfate, based on the Langmuir and DR models at pH 4 and 7, was WB/PA/G/dimethyl (Langmuir, 2.23 – 2.25; DR, 2.83 – 2.91) > SB/PA/G/trimethyl (Langmuir, 1.92 – 1.93; DR, 2.48 – 2.51) > WB/PS/MP/dimethyl (Langmuir, 1.50 – 1.52; DR, 1.82 – 1.86 mmol/L) > SB/PS/MP/triethyl (Langmuir, 1.03 – 0.96; DR, 1.24 – 1.34 mmol/L), with the same trend being observed for 3-PPA and nitrate. The estimation of the maximum capacity parameter (q_0) is dependent on the solution condition (e.g., initial contaminant concentration, resin dose, water matrix), competing anions (Hekmatzadeh et al., 2012), and experimental procedure for batch adsorption tests (Millar et al., 2015), all

of which make comparison between studies difficult but could provide other helpful insights on resin properties. That said, WB-AER showed higher capacity for all contaminants than SB analogs, primarily due to the smaller tertiary amine functional groups compared to quaternary ammonium functional groups (Boyer, Fang, et al., 2021). The lower calculated capacity of SB/PS/MP/triethyl relative to WB/PS/MP/diethyl could also be attributed to an increase in alkyl chain-length (Samatya et al., 2006; Sengupta & Clifford, 1986). An interesting result is the higher calculated capacity of IRA 96 (175%) and IRA 67 (280%) resin for lactic acid when both WB-AERs, initially obtained as free-base form, were converted to the chloride form using concentrated HCl solution (Moldes et al., 2003), which is similar to the methodology used in this study. Helfferich (1995) stated that WB resins in their various forms (e.g., chloride, sulfate, bicarbonate) differ in terms of volume, weight, etc. The author further recommended that future studies calculate resin capacities, especially WB-AERs that are not in the free-base form, using an expression which considers degree of resin swelling, dry or wet resin density, and the atomic weight of the counterion. The greater buffering potential and the higher IX capacity of WB-AER, together with the inherent selectivity of a methylated PA resin for sulfate are of the utmost importance for water softening applications. For instance, the semiconductor industry uses highly soluble sulfate-based organic chemicals for chip manufacturing and was shown to discharge abnormally high levels of PFOS (i.e., hundreds μg/L) (Lin et al., 2009). This presumes reverse osmosis and nanofiltration for PFAS treatment in sulfate-rich waters, which is problematic due to the pH-independent deposition of calcium sulfate ($CaSO_4$) and barium sulfate ($BaSO_4$) (MacAdam & Jarvis,

2015). Therefore, a screening step using the WB/PA/G/dimethyl resin is recommended to increase membrane longevity.

Figs. A5-A7 show binary exchange plots for chloride-form AER in single-solute systems. With the addition of chloride, the general order of decreasing selectivity for each AER at pH 4 and 7 were as follows:

- SB/PA/G/trimethyl $SO_4^{2-} > NO_3^- \approx Cl^- >$ 3-PPA (pH 7) > 3-PPA (pH 4)
- SB/PS/MP/triethyl $NO_3^- > SO_4^{2-} >$ 3-PPA (pH 7) $\approx Cl^- >$ 3-PPA (pH 4)
- WB/PA/G/dimethyl $SO_4^{2-} > NO_3^- \approx Cl^- >$ 3-PPA (pH 7) > 3-PPA (pH 4)
- WB/PS/MP/dimethyl $NO_3^- \approx SO_4^{2-} >$ 3-PPA (pH 7) > Cl^- > 3-PPA (pH 4)

The results agree with isotherm models (Figs. 3.5-3.7 and A2-A4) and removal data (Fig. 3.1). However, higher chloride release than contaminant uptake was observed for WB-AER which precludes comparison between AER.

Looking collectively at isotherm and binary exchange plots (Figs. 3.5-3.7 and A2-A7) and corresponding data (Tables A4-A8), all plots were insignificantly different and model parameters showed relative difference values < 10% between pH 4 and pH 7, which suggest no impact of solution chemistry on resin selectivity and capacity at pH $\leq$ 7. This is especially important for WB-AER because it broadens its applicability to various drinking water contaminants. For instance, a past study showed that despite the monovalent form of the triprotic arsenic acid (H_3AsO_4) below pH 4.6, the tertiary amine group of WB-AER exhibited higher capacity than the quaternary ammonium of SB-AER and maintained its greater selectivity toward arsenate species in the presence of

equimolar chloride in acidic conditions (Awual et al., 2008). This was due to the strong preference of WB-AER for dissociated acids (Helfferich, 1995).

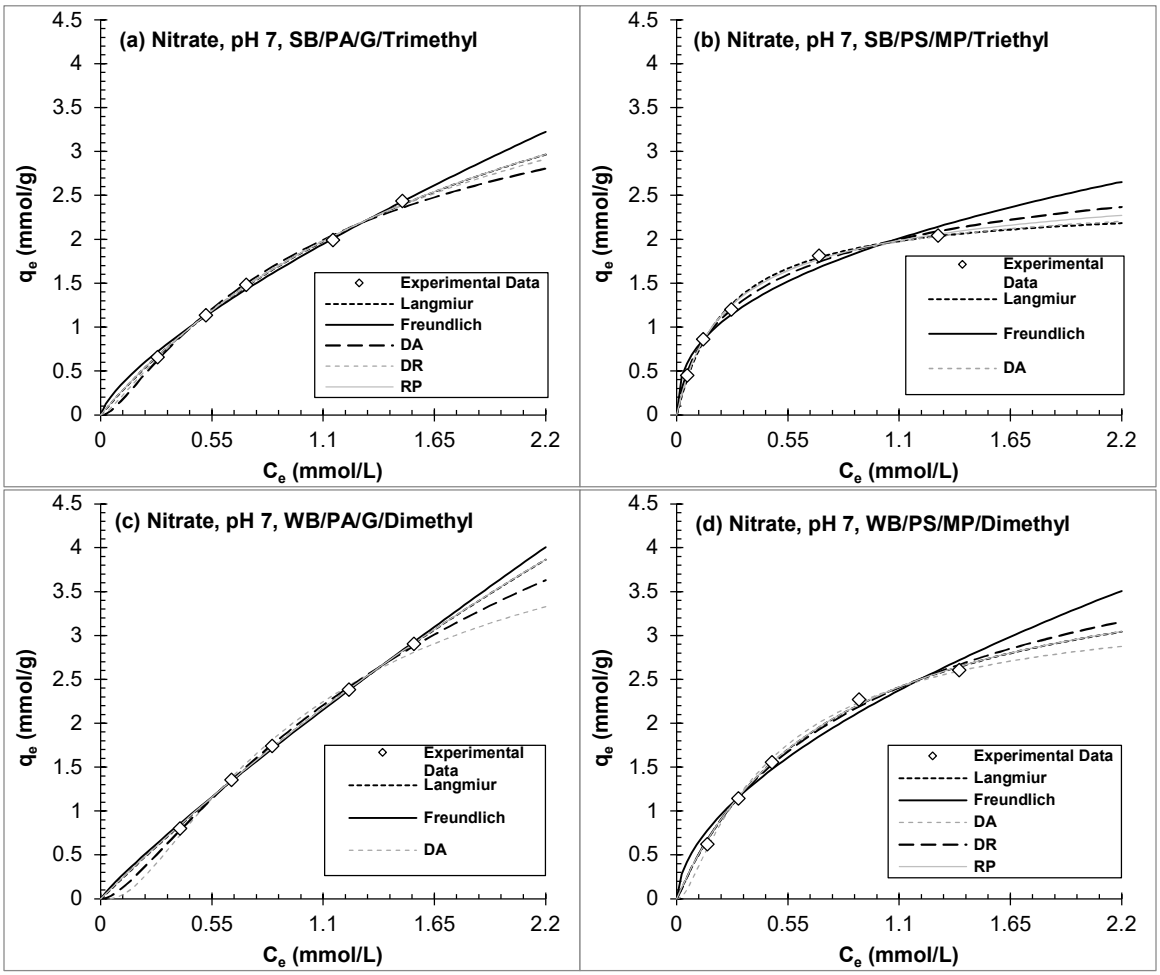

Fig. 3.5. Equilibrium adsorption isotherms of nitrate onto (a,c) polyacrylic and (b,d) polystyrene anion exchange resins at pH 7.

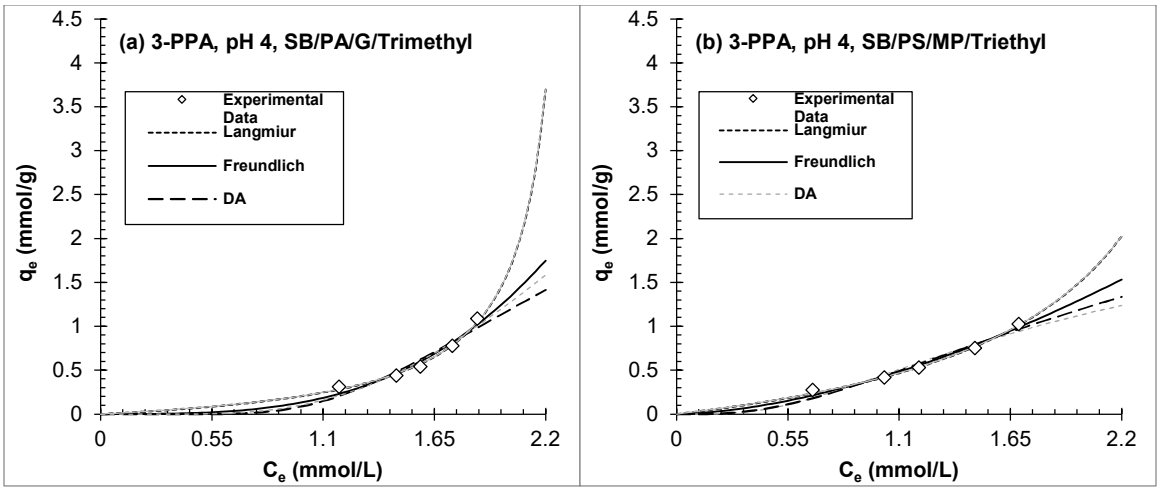
(a) 3-PPA, pH 4, SB/PA/G/Trimethyl
Experimental Data
Langmiur
Freundlich
DA
q_e (mmol/g)
C_e (mmol/L)
0
0.55
1.1
1.65
2.2
0.5
1
1.5
2
2.5
3
3.5
4
4.5

(b) 3-PPA, pH 4, SB/PS/MP/Triethyl
Experimental Data
Langmiur
Freundlich
DA
q_e (mmol/g)
C_e (mmol/L)
0
0.55
1.1
1.65
2.2
0.5
1
1.5
2
2.5
3
3.5
4
4.5

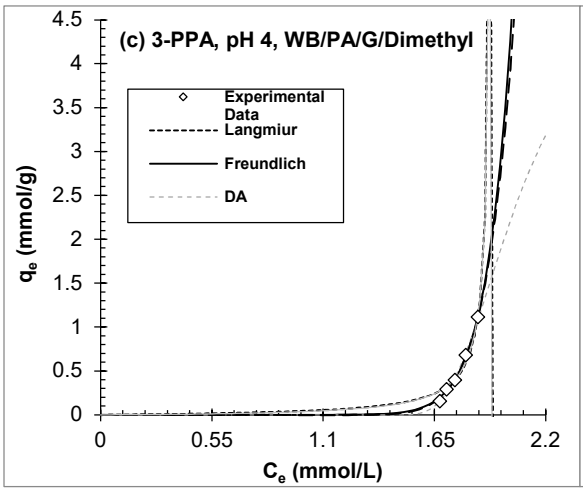
(c) 3-PPA, pH 4, WB/PA/G/Dimethyl
Experimental Data
Langmiur
Freundlich
DA
q_e (mmol/g)
C_e (mmol/L)
0
0.55
1.1
1.65
2.2
0.5
1
1.5
2
2.5
3
3.5
4
4.5

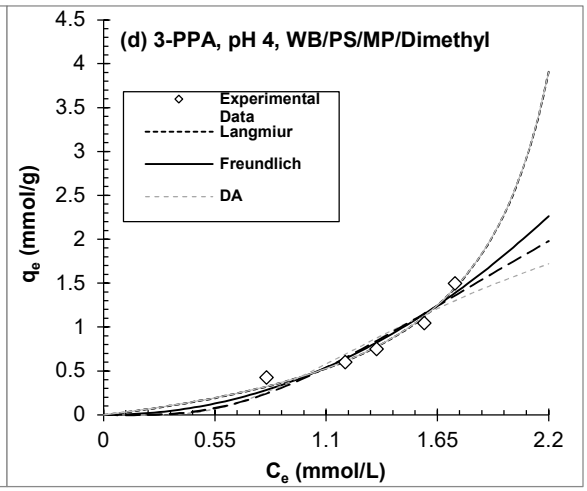
(d) 3-PPA, pH 4, WB/PS/MP/Dimethyl
Experimental Data
Langmiur
Freundlich
DA
q_e (mmol/g)
C_e (mmol/L)
0
0.55
1.1
1.65
2.2
0.5
1
1.5
2
2.5
3
3.5
4
4.5

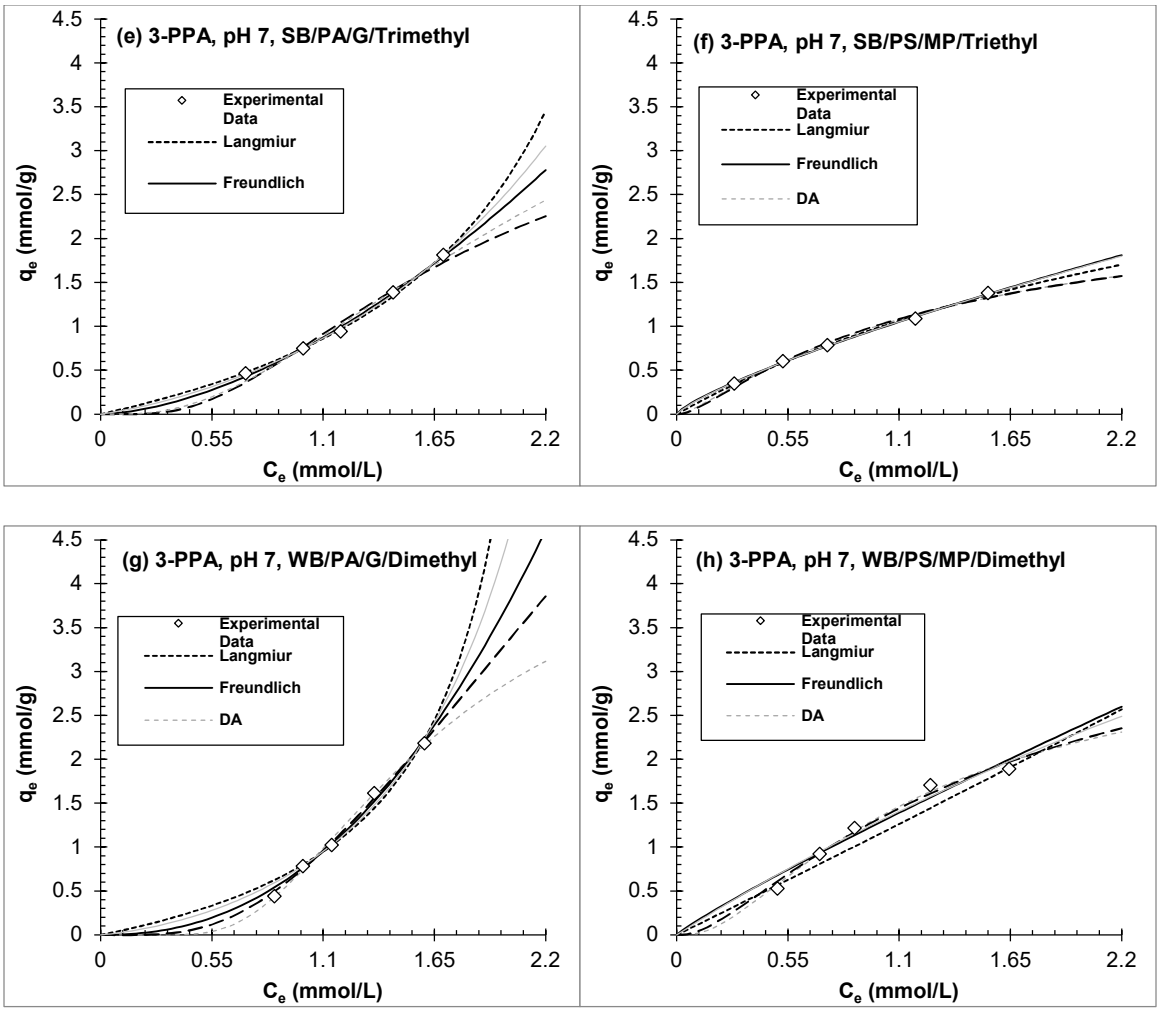

Fig. 3.6. Equilibrium adsorption isotherms of 3-phenylpropionic acid (3-PPA) onto polyacrylic (left panels) and polystyrene (right panels) anion exchange resins at (a-d) pH 4 and (e-h) pH 7.

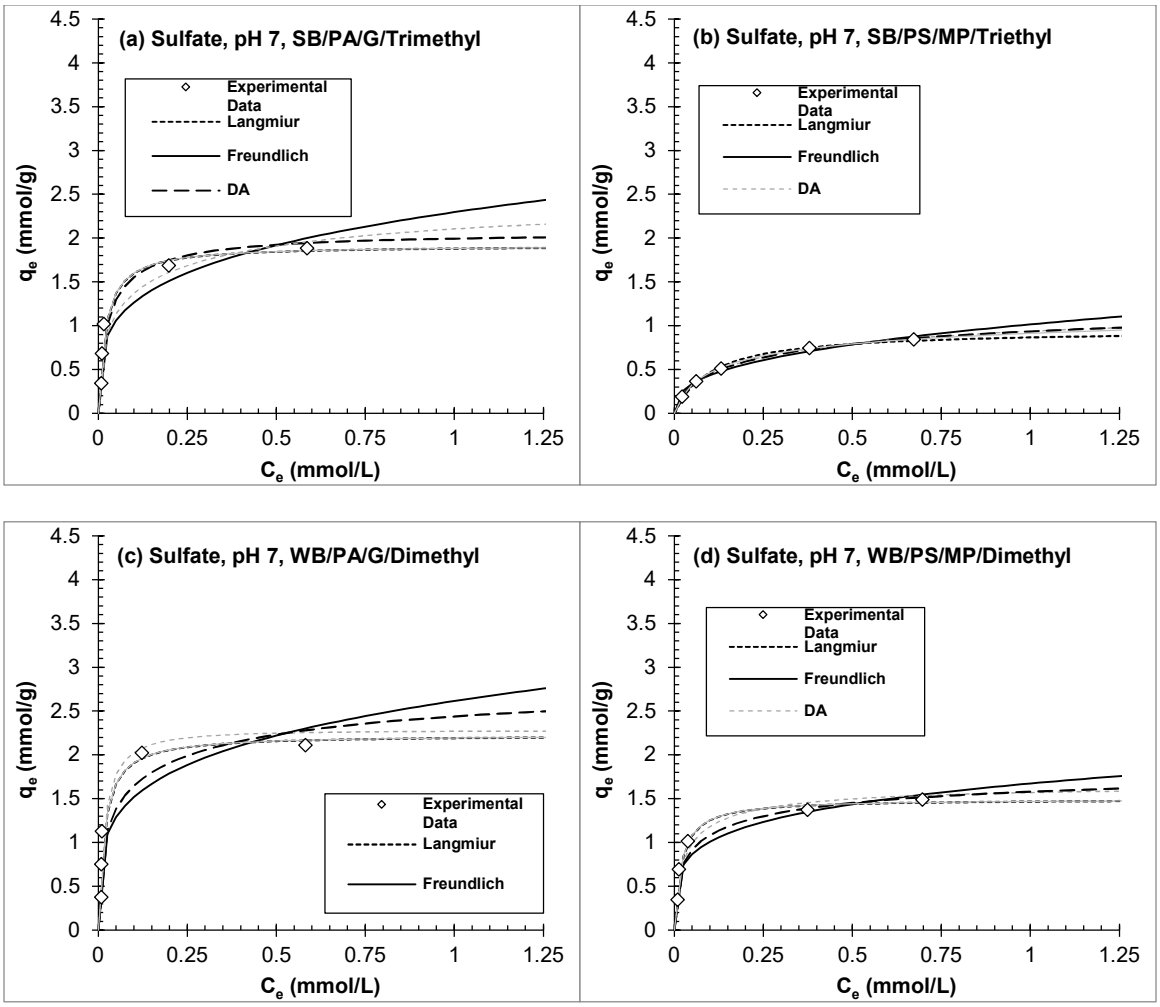

Fig. 3.7. Equilibrium adsorption isotherms of sulfate onto (a,c) polyacrylic and (b,d) polystyrene anion exchange resins at pH 7.

3.5. Mechanisms of ion-exchange

Fig. 3.8 shows possible interactions between HOIC (3-PPA) and AER. These include electrostatic interactions, hydrophobic interactions, London-van der Waals forces, hydrogen bonding, n-π bonding, π-π bonding (Tran, You, Hosseini-Bandegharaei, et al., 2017). The main mechanisms are discussed in the following:

Electrostatic interactions (1) are the basis of IX. The literature describes PFAAs uptake as strong ionic bonds occurring between the dissociated sulfonic and carboxylic acid head group of PFSAs and PFCAs with positively charged nitrogen of amine groups. The strong electronegativity of fluorine atoms of PFAAs molecules also generates additional ionic interactions with the resin (Du et al., 2014). However, these are several folds weaker than main ionic bonds as indicated by DFT (Park et al., 2020) and molecular orbital theory (Erkoç & Erkoç, 2001) calculations showing that the total negative charge of oxygen dwarfed that of individual fluorine atoms.

Hydrophobic interactions and van der Waals forces are the dominant physical mechanisms for most adsorbents including AER. Hydrophobicity is described as the ability of a chemical structure to repel water molecules. Aromatic structures and bonds such as C-F of PFAAs confer high oleophobic (i.e., high Log K_{ow}) and hydrophobic properties, which in turn decrease the solubility of aqueous contaminants (Du et al., 2015). It has been shown that van der Waals forces contributed to the removal of most pharmaceuticals and were even stronger than electrostatic interactions for certain HIOCs (Landry et al., 2015). Being less relevant for PFAAs, C-F bonds with low polarizability produce weak but cumulative induced-induced dipole interactions (i.e., van der Waals) and potentially form molecular bilayers (i.e., micelle) on the resin, especially when at high enough concentration (Ateia, Alsbaiee, et al., 2019). These types of interactions are absent in the case of polar PA AERs as previously demonstrated by a one-to-one ratio of PFAS removal to chloride release of the A860 resin on an equivalent basis (Dixit et al., 2020a).

π-π bonding (2) occurs between the aromatic rings of 3-PPA and PS polymer structure of AER. One study suggested that π-π bonding occurred between acid orange 7, an HIOC with similar structure to 3-PPA, and IRA 67 resin (Greluk & Hubicki, 2011). However, the benzene rings of acrylic acid-divinylbenzene-based WB-AER, as seen elsewhere, (Miyazaki & Nakai, 2011) are surrounded by lengthy aliphatic compounds that inhibit potential π-π bonds. This precludes the possibility of HOIC adsorption on PA resin.

Hydrogen bonding (H-bond) is a particular type of dipole-dipole interactions and was not shown in Fig. 3.8 due to the absence of carbonyl groups in the SB/PS/MP/triethyl structure. H-bonding typically occurs between oxygen atoms acting both as proton donors (hydroxyl group) and proton acceptors (carbonyl group). Free-form amine groups of WB-AERs have also shown to act as proton acceptors for undissociated acid groups of macromolecules (i.e., dyes, NOM) (Bolto et al., 2002; Greluk & Hubicki, 2011). These are of great value for the removal of organics with multiple undissociated -NH, -COOH, and -OH functional groups (e.g., histidine, diclofenac, paracetamol) (Landry & Boyer, 2013; Landry et al., 2015).

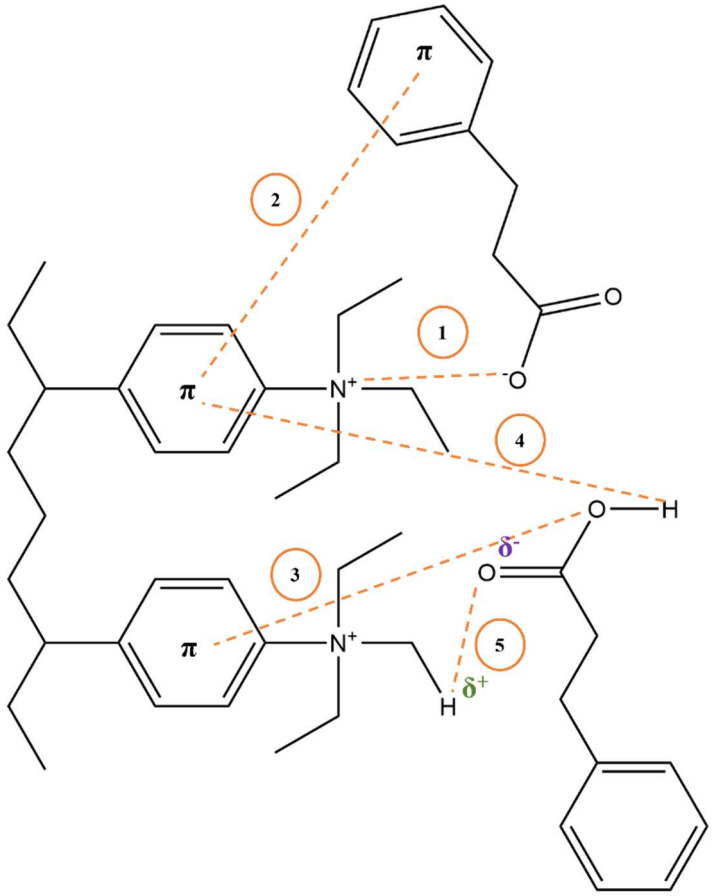

Fig. 3.8. Different interactions between dissociated (top) or protonated (bottom) 3-phenylpropionic (3-PPA) molecules and triethyl quaternary ammonium of A520E. Dashed lines indicate (1) electrostatic interactions (for pH > pKa), (2) π-π lateral bonds between carbon atoms of polar benzene rings, (3) n-π bonds between oxygen donor atoms of 3-PPA and benzene rings, (4) Yoshida hydrogen bonds between benzene rings of resin matrix and hydroxyl group of protonated 3-PPA (for pH < pKa), and (5) dipole-dipole bonds between positively and negatively charged H and O atoms respectively (Tran, You, Hosseini-Bandegharaei, et al., 2017) (Tran, You, & Chao, 2017a). The numbers given to each interaction represent corresponding magnitude in reverse order (i.e., 1 being the strongest).

CHAPTER 4

PRELIMINARY STUDY

4.1. Column-mode adsorption study

4.1.1. Effect of resin basicity

Fig. 4.1 and Fig. B1 illustrate the performance of WB and SB resins, respectively, for the removal of six short-chain (i.e., PFBA, PFHxS, and PFHxA) and long-chain (i.e., PFHxS, PFOA, and PFOS) PFAAs from groundwater. Comparing the results of WB/PA/G/dimethyl and SB/PA/MP/trimethyl (Fig. 4.1a and Fig. B1a) with WB/PS/MP/dimethyl and SB/PS/MP/triethyl (Fig. 4.1b and Fig. B1b) highlights the greater impact of resin polymer structure than other major resin properties (i.e., basicity, porosity, and functional groups) on PFAA removal. Most importantly, the similar removal achieved by SB and WB resin with analogous polymer composition insinuates the successful operability of WB-AER in its free-base form. Fig. 4.2 shows the pH of groundwater after being contacted with WB resin, where high pH values were measured at the early stages of operation (< 200 BV) due to the release of hydroxide (OH^-) ions and approached the initial groundwater pH thereupon. The more basic groundwater effluent of IRA 67 than IRA 96 is consistent with increasing estimated pK_a values for their protonated forms. This trend is helpful to understand the chemistry of weakly basic tertiary amine group in the free-base form, which was well elucidated by previous researchers (Greluk & Hubicki, 2011; Harland, 1994; Höll & Kirch, 1978) and described as follows:

$$\overline{R \equiv (CH_3)_2} + H_2O \rightleftarrows \overline{R \equiv N(CH_3)_2H^+.OH^-} \quad (19)$$

$$\overline{R \equiv N(CH_3)_2H^+.OH^-} + HCl \rightarrow \overline{R \equiv (CH_3)_2H^+.Cl^-} + H_2O \quad (20)$$

$$\overline{R \equiv N(CH_3)_2H^+.OH^-} + X^- \rightleftarrows \overline{R \equiv (CH_3)_2H^+.X^-} + OH^- \quad (21)$$

Where reversible reactions are strongly favored in the direction of two-headed arrows (↞) and the presence and absence of overbars indicate molecules in the resin and aqueous phase, respectively. Upon solvation, the anhydrous $\overline{R \equiv (CH_3)_2}$ amine gets immediately protonated with OH^- as the counterion through weak dissociation of water (Eq. 19). For effective ion-exchange to occur, OH^- ions need to be neutralized (Eq. 20) or displaced (Eq. 21) by either introducing strong acids or high concentrations of competing anions to account for the strong preference of tertiary amines for hydroxide ions (OH^-). Hence, the use of strong acids such as HCl, H_2SO_4, or dilute HNO_3 to functionalize and convert the resins to the desired form (Bolto et al., 2002; Höll & Kirch, 1978; Moldes et al., 2003). Note that while Eqs. 19-21 are useful for understanding the underlying chemistry of free form WB-AERs, Harland (1994) recommends representing tertiary amines as initially deionized (i.e., anhydrous form). All the above-stated findings suggest the potential to replace chloride-form SB-AER with free-base form WB-AER for column treatment of natural waters (e.g., groundwater, surface water, wastewater). The following explanation strongly depends on the buffering capacity of the feed where pH and pKa are those of the natural water in contact with WB resins and of their tertiary amine moieties, respectively. In column adsorption systems the water is continuously replaced flushing out excess OH^- ions ($pH >> pK_a$), which results in a new driving force ($pH < pK_a$) after each BV treated. However, this is not possible in batch studies due to the presence of competing OH^- once equilibrium is reached ($pH > pK_a$). This is of outmost importance for a multistage water deionization system consisting typically of alternating strong-acid and weak-base ion-exchange columns, whereby uptake of aqueous inorganic cations and

anions is accompanied by a neutralization reaction between released H^+ and OH^- to form pure water (Harland, 1994; Helfferich, 1995; Höll & Kirch, 1978). Clark et al. (2022) interestingly combined free-base IRA 67 with a zinc (Zn^{2+}) form cation exchange resin in a mixed bed to enhance the recovery of total ammonia (i.e., NH_3 and NH_{4+}) from hydrolyzed urine, where IRA 67 (pKa = 9) acted as a pH buffer to bias the formation of neutral ammonia (pKa = 9.25) and prevent the elution of the NH_3-selective Zn^{2+}.

It is not graphically evident (Fig. 4.1 and Fig. B1) that for the same resin polymer, WB resins had greater capacity for PFAAs than SB counterparts. Nonetheless, for the same volume of packed resins and based on PFAAs removal on mass (w; μg) and equivalent (eq; μeq) basis (Eq. 2), the total amounts on the resins are in the relation of w; eq (SB/PA/MP/Trimethyl) = 1.29 w; 1.32 eq (WB/PA/G/Dimethyl) = 2.30 w; 2.72 eq (SB/PS/MP/Triethyl) = 2.75 w; 3.20 eq (WB/PS/MP/Dimethyl), which insinuates greater inherent capacity of tertiary amines than quaternary ammonium (Boyer, Fang, et al., 2021).

4.1.2. PFAAs removal Efficiency

Both WB/PA/G/dimethyl (IRA 67) and SB/PA/MP/trimethyl (A860) resin treated ≤ 290 BV before exhibiting a significant decrease in removal efficiency for all PFAAs except PFOS as indicated by an early steep slope followed by a plateau (see Fig. 4.1a and Fig. B1a). The high adsorption of PFOS is associated to unfavorable interactions with water molecules rather than favorable interactions with PA resin. Fig. B2 shows the corresponding preference in a different format, where PFOS represented only 18-20% of

the total PFAAs equivalent concentration in the influent, whereas occupied 48% and 60% of the total PFAAs sites on the WB/PA (Fig. B2a) and SB/PA resin (Fig. B2b), respectively. It has been previously elucidated that for highly hydrophobic IOCs, partitioning out of water to the resin phase is energetically favored (i.e., $\Delta G^0 < 0$, $\Delta H^0 > 0$, and $T\Delta S^0 > 0$) for all polymer matrix composition (Li & SenGupta, 1998). While PFOS and PFOA have the same number of carbons, PFSAs have longer alkyl chains with one carbon not residing in the functional acid moiety as opposed to PFCAs. The more hydrophobic character of PFOS compared to remaining PFAAs is further justified by physicochemical properties such as lower water solubility (570 vs. ≥ 3400 mg/L), higher Log D_{OW} (3.05 vs. ≤ 1.58), and higher M_W (500.13 vs. ≤ 414.07 g/mol) (Brooke et al., 2004; Park et al., 2020; Yu et al., 2009). This trend was observed elsewhere for the same polyacrylic A860 resin where the highest removal ($C/C_0 < 0.25$) in batch equilibrium tests (Fang et al., 2021; Laura del Moral et al., 2020) and the lowest breakthrough ($C/C_0 < 0.20$) in column adsorption (Dietz et al., 2021) was for PFOS. Therefore, the two-step uptake of PFOS by PA resin can be viewed as migration to the surface of the resin by repelling water molecules followed by electrostatic interactions with the resin. Some suggested that micelle formation could also play an important role in the adsorption at the mg/L, especially for PA resin (Fang et al., 2021; Schuricht et al., 2017). However, Dixit et al. (2019) proved stoichiometrically (i.e., chloride release = PFOS removal) that the highly polar A860 will only remove PFOS via ion-exchange when below 10 mg/L.

Other evident results of Fig. 4.1 show significantly higher PFAAs removal by PS than PA resins due to the stronger interplay between electrostatic and van der Waals

attraction forces for PS-AERs with aromatic rings than PA-AERs with more polar open-chain carbonyl structure (Landry & Boyer, 2013; Laura del Moral et al., 2020; Li & SenGupta, 1998, 2004). Two recent studies involving the SB-AERs that were used in this experiment (i.e., A520E and A860) portrayed the same impact of polymer composition on PFAAs removal (Fang et al., 2021). PFAAs that showed decreasing affinity for PA-AER based on lower breakthrough curves (i.e., decreasing C/C_0) were PFOS >> PFHxS ≈ PFOA > PFBS > PFHxA ≈ PFBA which is consistent with decreasing octanol-water partition coefficient at pH 7 (Log D_{OW}) (Park et al., 2020; Zeng et al., 2020) and the increasing preference of PA resin for more hydrophobic organic compounds (Rahmani & Mohseni, 2017). For the same carbon chain-length, PFSAs were removed to a greater extent than PFCAs given the more hydrophobic nature (Du et al., 2014) and more pronounced electrostatic interactions (Park et al., 2020) of sulfonates compared with carboxylate homologs. All these trends are supported by the batch experiments in this work and the work of other researchers (Du et al., 2015; Franke et al., 2019; Laura del Moral et al., 2020; Maimaiti et al., 2018; McCleaf et al., 2017; Park et al., 2020; Zaggia et al., 2016). Conversely, Ateia, Arifuzzaman, et al. (2019) displayed higher removal of PFSAs regardless of carbon chain-length with Park et al. (2020) further showing adsorption onto MIEX resin to be remarkably more sensitive to the total negative atomic charge than Log Dow values of PFAAs. This pattern was also maintained for the IX removal of non-fluorinated organic ions, whereby the selectivity coefficients of PS were higher than PA AERs and the affinity of aromatic HOICs having the same polar functional group increased with increasing Log D_{ow}, while the selectivity of monosulfonate ions was greater than monocarboxylate ions inconsistent with the Log D_{ow}

values (Kanazawa et al., 2004). Electrostatic potential and hydrophobicity are indissociable factors in adsorption and should be perceived as complementary rather than strictly additive. For instance, low polarity would majorly contribute to a first-stage migration of PFAAs from water onto a more thermodynamically stable solid state (i.e., surface of adsorbent) and the anionic character would in turn bolster the selectivity to secure active sites on the resin.

In the case of PA AERs, as shown in Fig. 4.1a and Fig. B1a, breakthrough (i.e., constant C/C_0) took place at the very early stages of the experiment (< 500 BV) for all PFAAs except PFOS. PFOA, PFHxS, and PFBS exhibited a plateau in adsorption without ever meeting the influent concentration (C_0). Key reasons for this are the aforementioned higher affinity of less polar PFAAs to PA resins and more importantly the higher initial concentration in groundwater (see Table B1), which initiates a driving force (i.e., concentration gradient) for diffusion. Both these elements were highlighted by Du et al. (2015) with adsorbed amounts of PFCAs on IRA 67 as: PFOA (C8) >> PFHpA (C7) > PFHxA (C6). Kinetic models portrayed the IX removal of PFAAs as a multi-stage process with intraparticle diffusion being the predominant and rate-limiting step, followed by diffusion through the boundary layer of the resin (McCleaf et al., 2017; Wang et al., 2019; Yu et al., 2009), meaning that sites occupied by long-chain PFAAs block the pores for shorter-chain counterparts. Since the data is not indicative of PFBA and/or PFHxA desorption, which should otherwise resemble the competitive exchange curves portrayed by Gu et al. (2004), PFOA, PFHxS, and PFBS are supposedly displacing less selective anions, most likely inorganic compounds (e.g., SO_4^{2-}, Cl^-, NO_3^-).

The column exchange curves of Zeng et al. (2020) were identical to this study but no clear reasons for the observed plateau in adsorption were reported.

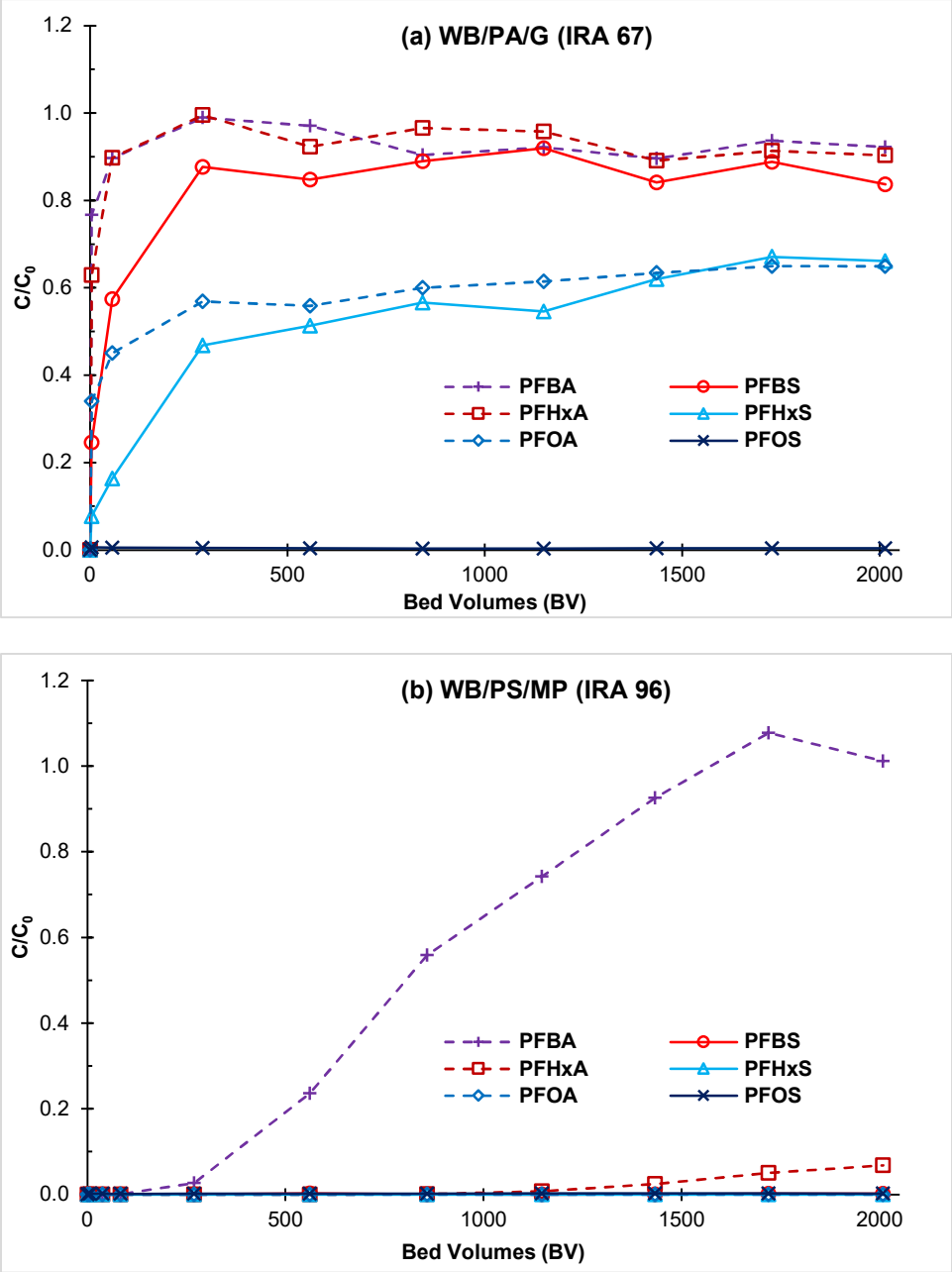

Fig. 4.1. Efficiency of weak-base (a) polyacrylic/gel and (b) polystyrene/macroporous anion exchange resins for PFAAs removal in impacted groundwater. Each data point

represents the average of triplicate column experiments with same operating conditions. Initial concentrations of individual and total PFAAs given in Table B1.

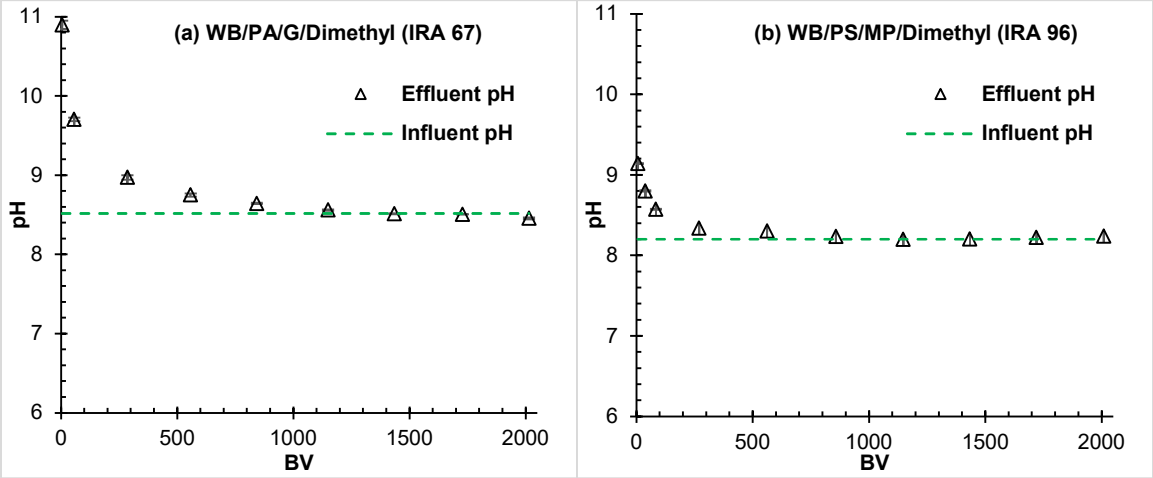

Fig. 4.2. Dissociation effect of free-base tertiary amine groups of (a) IRA 67 (pK_a = 9.0) and (b) IRA 96 (pK_a = 6.4) WB-AERs on groundwater pH. Dashed green lines represent initial groundwater pH, triangles represent the pH measured in effluent immediately after collecting each sample with error bars denoting of in the free-base form dissociation WB resin

4.2. Column-mode regeneration study

Fig. 4.3 shows the efficiency of 1% NaOH (w/w), 0.5% NaOH + 0.5% NaCl (w/w), and 1% NaCl (w/w) + 70% methanol (v/v) regeneration solutions at desorbing PFAAs from spent WB IRA 67 and IRA 96 resins. For salt aqueous solutions (i.e., NaOH and NaOH/NaCl), only PFBA desorbed > 5% from the PS resin, whereas PFAAs recovery ranged from ~10% to 57% for PA resin except for PFOS. On the other hand, the NaCl/methanol mixture had an effective desorption of the six PFAAs (> 43%) from the IRA 96 resin (i.e., polystyrene). For IRA 67 (i.e., polyacrylic), the addition of methanol did not impact the recovery of short-chain PFAAs, but increased markedly for PFHxS

(from ~ 52% to 93%), for PFOA (from ~47% to 85%), and PFOS (from ~4% to 34%) when NaCl/methanol was substituted for salt aqueous reagents. These results indicate satisfactory regeneration efficiency of PA resin using NaOH to deprotonate the amino-groups of the weak-base resins. However, it is evident that the presence of highly hydrophobic contaminants such as long-chain PFAAs and/or AERs with nonpolar character such as PS resin requires a concentrated solution of organic solvent. Only one study tested the regeneration of WB/PS resin and showed no desorption of PFOA (~ 0%) using NH_4Cl and/or NH_4OH as opposed to ~20% and ~ 95% recovery when methanol and NH_4OH/methanol were employed, respectively (Conte et al., 2015). This suggests that while the nonpolar character of polystyrene derivatives is more important than the neutralization of tertiary amine, both electrostatic and non-electrostatic forces of attraction cannot be decoupled thus a mixture of alkaline and organic solvent is recommended for optimal regeneration efficiency of IRA 96.

Among all PFAAs, PFOS desorbed the least (< 5%) for both resins using salt-only solutions, which is consistent with the lower solubility of PFOS in aqueous solutions with higher ionic strength (Brooke et al., 2004; Yu et al., 2008). By salting-out and adhering physically to the surface of the resin, van der Waals forces get more pronounced, which implies the need for organic cosolvent. Gao et al. (2017) and Deng et al. (2010) showed the same trend whereby PFOS recovery from IRA 67 was lower in NaOH solutions than NaOH/methanol mixtures but further demonstrated that 100% methanol alone cannot desorb PFOS (< 5%).

Figs. B2 shows the equivalence distribution of PFAAs in different regeneration eluates of IRA 67, IRA 96, A860, and A520E. Comparing the composition of each regeneration eluate in terms of PFAAs properties and resin polymer composition agrees with previous assertions on selectivity. For PS resins, the PFAAs composition in 1% NaOH, 0.5% NaOH + 0.5% NaCl, and 10% NaCl regeneration solutions (i.e., salt-only) were 62 – 88% PFBA and 69 – 99% PFCAs, which is consistent with increasing desorption with decreasing polarizability of PFAAs (i.e., less fluorinated carbons) and for carboxylates having weaker negative inductive effect than sulfonates. Although PFOS occupied 48% and 61% of the WB and SB polyacrylic resin sites respectively, it amounted to less than 8% of the total PFAAs in salt-only eluates. All the above-mentioned discrepancies were less noticeable using 1% NaCl + 70% methanol. These findings were true regardless of resin basicity, which further support the greater impact of polymer composition on selective regeneration of PFAA than resin basicity. Nonetheless, the low recovery of short-chain PFAAs from WB/PA compared to SB/PA suggests that a portion of PFBA, PFBS, and PFHxA might have desorbed throughout the DI backwashing process.

Fig. B2 compares for each PFAA, the amount recovered in one type of regeneration solution relative to the amount recovered in all three solutions of a single PA resin. Regarding WB/PA, the efficiency of NaOH (~35-40%) and NaOH/NaCl (~34-36%) were slightly better than the NaCl/methanol mixture (~29-32%) for short-chain PFAAs and decreased to small extent for PFOA and PFHxS (~ 24-29% for salt-only vs. ~47-48% for NaCl/methanol). Conversely for SB/PA, 10% NaCl and 0.5% NaOH +

0.5% NaCl were only effective at desorbing PFBA and PFHxA while being significantly less effective for long-chain PFAAs (≤ 11%) relative to the regeneration solution comprising 1% NaCl + 70% methanol (≥ 84%). This insinuates the potential to further enhance salt-only solutions for the regeneration of WB/PA resin while maintaining reduced environmental impact (i.e., solvent-less). A thorough life cycle assessment (LCA) for the treatment of AER regeneration eluates showed that although fully recycling salt-only solutions of NaCl/NaOH contributed to greater carcinogenicity than NaCl/methanol, the overall environmental impact of regeneration solutions comprising chloride/hydroxide salts was the same regardless of the co-ion used (e.g., Na^+, NH_4^+, K^+) (Boyer, Ellis, et al., 2021). For example, Conte et al. (2015) and Zaggia et al. (2016) proposed using ammonium co-ion (e.g., NH_4OH) due to higher solubility of PFAS-NH_4^+ than PFAS-K^+ or PFAS-Na^+. In addition, WB-AER could be regenerated with only 1.3-1.5 × the total IX sites (Dorfner, 2011), which allows the use of dilute solutions of NH_4OH or NH_4Cl/NH_4OH, down to 0.05% w/w (pH > 12), and still be enough to deprotonate the resin.

For completion, the measurements of nitrate, sulfate and UV254 in the regeneration eluates of WB resins are illustrated in Fig. B3 in Appendix B. The data shows that for WB/PA resin, the salt-only solutions were ~60% and ~130% more effective at desorbing inorganic nitrates and sulfates than the organic solvent mixture, respectively (see Fig. B3a and b). In the case of WB/PS, recovery values measured for nitrates and UV254 were greater using the solvent mixture while the relatively more

hydrophilic sulfates desorbed to a lesser extent (see Fig. B3d-f). This is important to further validate the understanding of WB/PA and PS.

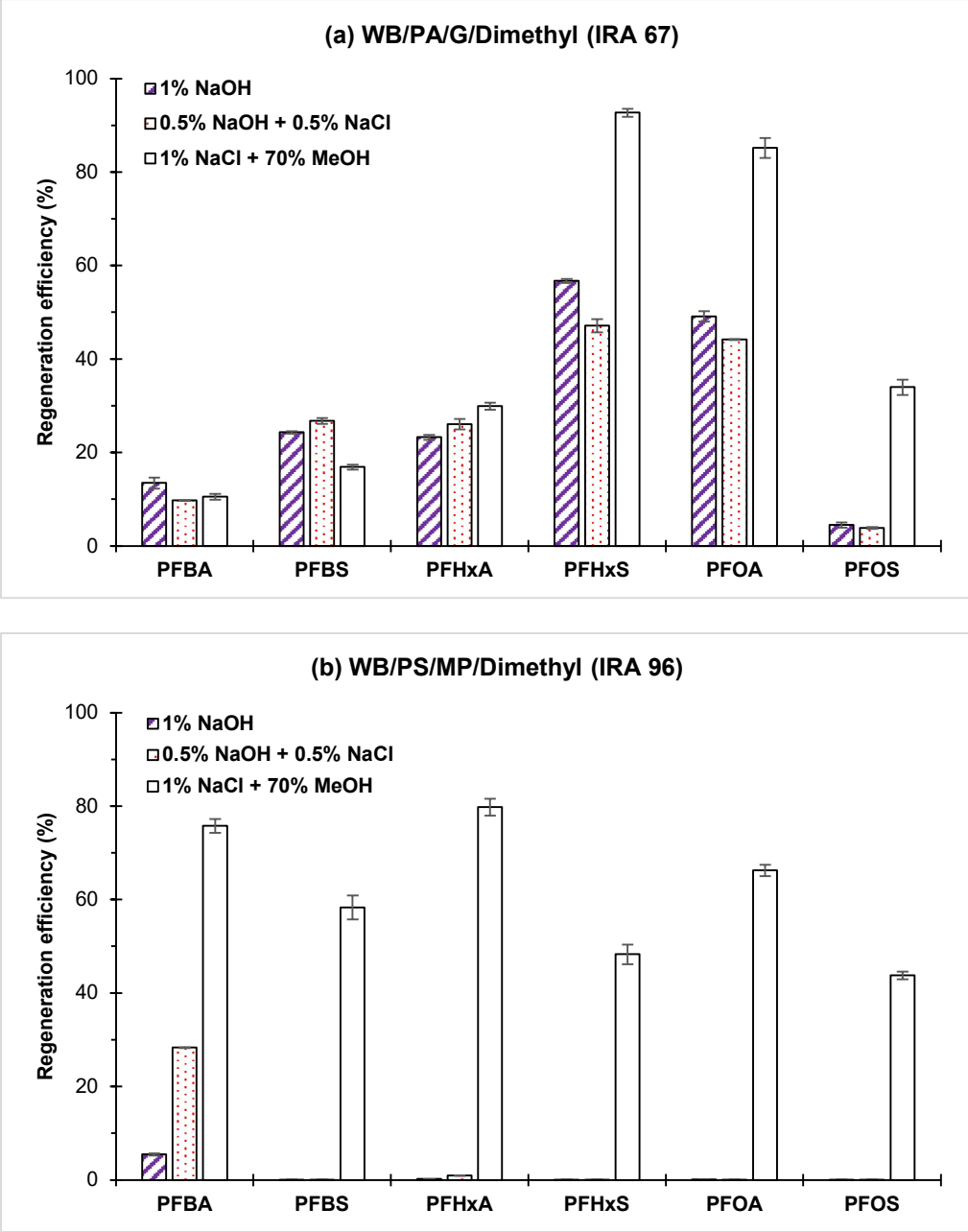

Fig. 4.3. Column regeneration of PFAAs-laden (a) polyacrylic and (b) polystyrene weak-base resins. Reported values are amounts of PFAAs recovered during regeneration

normalized by the total adsorbed amounts during treatment and are expressed in percent (%) with error bars representing one standard deviation of triplicate measurements.

CHAPTER 5

CONCLUSIONS

- At natural pH, chloride-form WB-AER had higher capacity and similar selectivity than chloride-form SB-AER with analogous properties (i.e., polymer composition, porosity, functional group) as indicated by isotherm parameters in single-analyte system (i.e., nitrate, sulfate, and 3-phenylpropionic acid) and normalized removal data for all contaminants. The effectiveness of chloride-form WB-AER demonstrates the potential to substitute conventional chloride-form SB-AER in batch reactors and that pretreatment schemes using hydrochloric acid (HCl) were successful.
- When resin dose significantly exceeded the concentration of six legacy PFAAs (i.e., PFBA, PFBS, PFHxA, PFHxS, PFOA, and PFOS) present as a mixture, removal by polyacrylic resin increased with increasing PFAAs carbon chain-length, resin dose, and was greater for PFAAs with sulfonic head group compared to carboxylic analogs. Regardless of resin amount, the near complete removal of PFOS by polyacrylic AERs and of all PFAAs by polystyrene AERs were linked to the strong tendency of PFOS to repel water molecules and to the combination of electrostatic and non-electrostatic interactions enhanced by the hydrophobic character of polystyrene resin, respectively. The presence of relatively high concentrations of bicarbonate ions (≈ 2.14meq/L) showed no impact on PFAAs removal.
- At high pH (i.e., > 10) WB polyacrylic/gel and polystyrene/macroporous resin had low, to no removal of nitrate, 3-phenylpropionic acid, and sulfate due to the

deprotonation of amine group, which implies the potential for regeneration of WB resin using salt-only alkaline solutions with low ecotoxicological risk (e.g., NaOH, NH_4OH; $NaHCO_3$). However, the complete removal of relatively low PFAAs concentration by polystyrene/macroporous resin was maintained, suggesting that PFAAs adsorption was either solely governed by hydrophobic interactions or that a fraction of ion-exchange sites was not converted to its free-base form. Further research should explore the trade-offs in both PFAAs removal by WB/polystyrene and regeneration by WB/polyacrylic AERs.

- The estimation of isotherm constants for the two-parameter Freundlich, Dubinin-Radushkevich (DR), and Dubinin-Astakhov (DA) models showed no significant difference between the regression methods (i.e., linear and nonlinear) used to fit adsorption data in single-analyte system. Conversely, selectivity and capacity parameter values determined from four linearized Langmuir versions were biased while the nonlinear least-squares method provided unique values. Relying on goodness-of-fit measures only to gain insight on adsorption mechanism could be misleading as two isotherms with conflicting theories (e.g., Langmuir, Freundlich) might fit equilibrium data the same extent depending on the operating conditions. Therefore, qualitative rather than quantitative analysis should be considered to identify potential trends and three-parameter hybrid models such as Redlich-Peterson (RP) should be employed given the wider range of applicability offered by additional variables.
- In column experiments for the treatment of PFAAs-spiked groundwater, the free-base form WB resin had similar selectivity and higher capacity for PFAAs than

SB-AER with same polymer composition. This result not only suggests WB-AER as a viable alternative to conventional SB-AER but also offers a more cost-effective and sustainable option of neglecting the added step of resin pretreatment (e.g., HCl, NaCl, H_2SO_4) in continuous-flow mode. Because of the hypothesized high overall chemical stability, buffering capabilities, and capacity of the tertiary amine functional group in its free-base form, long-term pilot scale studies are needed in order to evaluate the durability of commercially available WB-AERs.

- The individual influence of the hydrophobic and electrostatic characters of PFAAs on the adsorption affinity were not conclusively differentiable given their additive nature and were instead interpreted as complementary in this study. A thorough multiple linear regression analysis would be helpful to synthesize resins for optimal removal and/or regeneration.
- WB/polystyrene exhibited significantly higher removal of PFAAs from groundwater than WB/polyacrylic resin as indicated by column breakthrough curves. However, subsequent desorption from PFAAs-laden WB resin using solvent-free regeneration solutions comprising 1% NaOH or 0.5% NaOH + 0.5% NaCl was only possible for the polyacrylic type. This poses an inevitable trade-off between performance and reusability of WB resins. Since the electrostatic and the hydrophobic character of polystyrene resin could not be decoupled with salt-only aqueous regenerants. The shift in research should focus on optimizing the formulation of caustic or caustic/brine solutions for the regeneration of WB/polystyrene AER.

REFERENCES

Abunada, Z., Alazaiza, M. Y. D., & Bashir, M. J. K. (2020). An Overview of Per- and Polyfluoroalkyl Substances (PFAS) in the Environment: Source, Fate, Risk and Regulations. *Water*, *12*(12), 3590. https://www.mdpi.com/2073-4441/12/12/3590

Ahmed, M. J., & Dhedan, S. K. (2012). Equilibrium isotherms and kinetics modeling of methylene blue adsorption on agricultural wastes-based activated carbons. *Fluid Phase Equilibria*, *317*, 9-14. https://doi.org/https://doi.org/10.1016/j.fluid.2011.12.026

Allen, S. J., Gan, Q., Matthews, R., & Johnson, P. A. (2003). Comparison of optimised isotherm models for basic dye adsorption by kudzu. *Bioresource Technology*, *88*(2), 143-152. https://doi.org/https://doi.org/10.1016/S0960-8524(02)00281-X

Ames, L. L. (1965). Zeolite cation selectivity. *The Canadian Mineralogist*, *8*(3), 325-333.

Anderson, R. E. (1964). A contour map of anion exchange resin properties. *Industrial & Engineering Chemistry Product Research and Development*, *3*(2), 85-89.

Appleman, T. D., Higgins, C. P., Quiñones, O., Vanderford, B. J., Kolstad, C., Zeigler-Holady, J. C., & Dickenson, E. R. V. (2014). Treatment of poly- and perfluoroalkyl substances in U.S. full-scale water treatment systems. *Water Research*, *51*, 246-255. https://doi.org/https://doi.org/10.1016/j.watres.2013.10.067

Ateia, M., Alsbaiee, A., Karanfil, T., & Dichtel, W. (2019). Efficient PFAS Removal by Amine-Functionalized Sorbents: Critical Review of the Current Literature. *Environmental Science & Technology Letters*, *6*(12), 688-695. https://doi.org/10.1021/acs.estlett.9b00659

Ateia, M., Arifuzzaman, M., Pellizzeri, S., Attia, M. F., Tharayil, N., Anker, J. N., & Karanfil, T. (2019). Cationic polymer for selective removal of GenX and short-chain PFAS from surface waters and wastewaters at ng/L levels. *Water Research*, *163*, 114874. https://doi.org/https://doi.org/10.1016/j.watres.2019.114874

Awual, M. R., Urata, S., Jyo, A., Tamada, M., & Katakai, A. (2008). Arsenate removal from water by a weak-base anion exchange fibrous adsorbent. *Water Research*, *42*(3), 689-696. https://doi.org/https://doi.org/10.1016/j.watres.2007.08.020

Bolster, C. H., & Hornberger, G. M. (2007). On the Use of Linearized Langmuir Equations. *Soil Science Society of America Journal*, *71*(6), 1796-1806. https://doi.org/https://doi.org/10.2136/sssaj2006.0304

Bolto, B., Dixon, D., Eldridge, R., King, S., & Linge, K. (2002). Removal of natural organic matter by ion exchange. *Water Research*, *36*(20), 5057-5065. https://doi.org/https://doi.org/10.1016/S0043-1354(02)00231-2

Boyer, T. H., Ellis, A., Fang, Y., Schaefer, C. E., Higgins, C. P., & Strathmann, T. J. (2021). Life cycle environmental impacts of regeneration options for anion exchange resin remediation of PFAS impacted water. *Water Research*, *207*, 117798. https://doi.org/https://doi.org/10.1016/j.watres.2021.117798

Boyer, T. H., Fang, Y., Ellis, A., Dietz, R., Choi, Y. J., Schaefer, C. E., Higgins, C. P., & Strathmann, T. J. (2021). Anion exchange resin removal of per- and polyfluoroalkyl substances (PFAS) from impacted water: A critical review. *Water Research*, *200*, 117244. https://doi.org/https://doi.org/10.1016/j.watres.2021.117244

Brooke, D., Footitt, A., & Nwaogu, T. (2004). Environmental risk evaluation report: Perfluorooctanesulphonate (PFOS).

Calafat, A. M., Kato, K., Hubbard, K., Jia, T., Botelho, J. C., & Wong, L.-Y. (2019). Legacy and alternative per- and polyfluoroalkyl substances in the U.S. general population: Paired serum-urine data from the 2013–2014 National Health and Nutrition Examination Survey. *Environment international*, *131*, 105048. https://doi.org/https://doi.org/10.1016/j.envint.2019.105048

Chan, L. S., Cheung, W. H., Allen, S. J., & McKay, G. (2012). Error Analysis of Adsorption Isotherm Models for Acid Dyes onto Bamboo Derived Activated Carbon. *Chinese Journal of Chemical Engineering*, *20*(3), 535-542. https://doi.org/https://doi.org/10.1016/S1004-9541(11)60216-4

Chen, R., Yang, Q., Zhong, Y., Li, X., Liu, Y., Li, X.-M., Du, W.-X., & Zeng, G.-M. (2014). Sorption of trace levels of bromate by macroporous strong base anion exchange resin: Influencing factors, equilibrium isotherms and thermodynamic studies. *Desalination*, *344*, 306-312. https://doi.org/https://doi.org/10.1016/j.desal.2014.04.001

Chularueangaksorn, P., Tanaka, S., Fujii, S., & Kunacheva, C. (2013). Regeneration and reusability of anion exchange resin used in perfluorooctane sulfonate removal by batch experiments [https://doi.org/10.1002/app.39169]. *Journal of Applied Polymer Science*, *130*(2), 884-890. https://doi.org/https://doi.org/10.1002/app.39169

Chularueangaksorn, P., Tanaka, S., Fujii, S., & Kunacheva, C. (2014). Batch and column adsorption of perfluorooctane sulfonate on anion exchange resins and granular activated carbon [https://doi.org/10.1002/app.39782]. *Journal of Applied Polymer Science*, *131*(3). https://doi.org/https://doi.org/10.1002/app.39782

Clark, B., Gilles, G., & Tarpeh, W. A. (2022). Resin-Mediated pH Control of Metal-Loaded Ligand Exchangers for Selective Nitrogen Recovery from Wastewaters. *ACS Applied Materials & Interfaces*. https://doi.org/10.1021/acsami.1c22316

Clifford, D., & Weber, W. J. (1983). The determinants of divalent/monovalent selectivity in anion exchangers. *Reactive Polymers, Ion Exchangers, Sorbents*, *1*(2), 77-89. https://doi.org/https://doi.org/10.1016/0167-6989(83)90040-5

Conte, L., Falletti, L., Zaggia, A., & Milan, M. (2015). Polyfluorinated Organic Micropollutants Removal from Water by Ion Exchange and Adsorption. *Chemical Engineering Transactions*, *43*, 2257-2262.

Deng, S., Yu, Q., Huang, J., & Yu, G. (2010). Removal of perfluorooctane sulfonate from wastewater by anion exchange resins: Effects of resin properties and solution chemistry. *Water Research*, *44*(18), 5188-5195. https://doi.org/https://doi.org/10.1016/j.watres.2010.06.038

Dietz, R., Kassar, C., & Boyer, T. H. (2021). Regeneration efficiency of strong-base anion exchange resin for perfluoroalkyl and polyfluoroalkyl substances [https://doi.org/10.1002/aws2.1259]. *AWWA Water Science*, *3*(6), e1259. https://doi.org/https://doi.org/10.1002/aws2.1259

Dixit, F., Barbeau, B., Mostafavi, S. G., & Mohseni, M. (2019). PFOA and PFOS removal by ion exchange for water reuse and drinking applications: role of organic matter characteristics. *Environmental Science: Water Research & Technology*, *5*(10), 1782-1795.

Dixit, F., Barbeau, B., Mostafavi, S. G., & Mohseni, M. (2020a). Efficient removal of GenX (HFPO-DA) and other perfluorinated ether acids from drinking and recycled waters using anion exchange resins. *Journal of Hazardous Materials*, *384*, 121261. https://doi.org/https://doi.org/10.1016/j.jhazmat.2019.121261

Dixit, F., Barbeau, B., Mostafavi, S. G., & Mohseni, M. (2020b). Removal of legacy PFAS and other fluorotelomers: Optimized regeneration strategies in DOM-rich waters. *Water Research*, *183*, 116098. https://doi.org/https://doi.org/10.1016/j.watres.2020.116098

Dixit, F., Barbeau, B., Mostafavi, S. G., & Mohseni, M. (2021). PFAS and DOM removal using an organic scavenger and PFAS-specific resin: Trade-off between regeneration and faster kinetics. *Science of The Total Environment*, *754*, 142107. https://doi.org/https://doi.org/10.1016/j.scitotenv.2020.142107

Dixit, F., Dutta, R., Barbeau, B., Berube, P., & Mohseni, M. (2021). PFAS removal by ion exchange resins: A review. *Chemosphere*, *272*, 129777. https://doi.org/https://doi.org/10.1016/j.chemosphere.2021.129777

Domingo, J. L., & Nadal, M. (2019). Human exposure to per- and polyfluoroalkyl substances (PFAS) through drinking water: A review of the recent scientific literature. *Environmental Research*, *177*, 108648. https://doi.org/https://doi.org/10.1016/j.envres.2019.108648

Dorfner, K. (2011). *Ion Exchangers*. De Gruyter. https://books.google.com/books?id=wFpP7mbfhrMC

Dron, J., & Dodi, A. (2011). Comparison of adsorption equilibrium models for the study of CL−, NO3− and SO42− removal from aqueous solutions by an anion exchange resin. *Journal of Hazardous Materials*, *190*(1), 300-307. https://doi.org/https://doi.org/10.1016/j.jhazmat.2011.03.049

Du, Z., Deng, S., Bei, Y., Huang, Q., Wang, B., Huang, J., & Yu, G. (2014). Adsorption behavior and mechanism of perfluorinated compounds on various adsorbents—A review. *Journal of Hazardous Materials*, *274*, 443-454. https://doi.org/https://doi.org/10.1016/j.jhazmat.2014.04.038

Du, Z., Deng, S., Chen, Y., Wang, B., Huang, J., Wang, Y., & Yu, G. (2015). Removal of perfluorinated carboxylates from washing wastewater of perfluorooctanesulfonyl fluoride using activated carbons and resins. *Journal of Hazardous Materials*, *286*, 136-143. https://doi.org/https://doi.org/10.1016/j.jhazmat.2014.12.037

Dubinin, M. (1947). The equation of the characteristic curve of activated charcoal. Dokl. Akad. Nauk. SSSR.,

Dudley, L.-A. (2012). Removal of Perfluorinated Compounds by Powdered Activated Carbon, Superfine Powder Activated Carbon, and Anion Exchange Resin.

Edgar, M., & Boyer, T. H. (2021). Removal of natural organic matter by ion exchange: Comparing regenerated and non-regenerated columns. *Water Research*, *189*, 116661. https://doi.org/https://doi.org/10.1016/j.watres.2020.116661

El-Khaiary, M. I. (2008). Least-squares regression of adsorption equilibrium data: Comparing the options. *Journal of Hazardous Materials*, *158*(1), 73-87. https://doi.org/https://doi.org/10.1016/j.jhazmat.2008.01.052

Erkoç, Ş., & Erkoç, F. (2001). Structural and electronic properties of PFOS and LiPFOS. *Journal of Molecular Structure: THEOCHEM*, *549*(3), 289-293. https://doi.org/https://doi.org/10.1016/S0166-1280(01)00553-X

Fang, Y., Ellis, A., Choi, Y. J., Boyer, T. H., Higgins, C. P., Schaefer, C. E., & Strathmann, T. J. (2021). Removal of Per- and Polyfluoroalkyl Substances (PFASs) in Aqueous Film-Forming Foam (AFFF) Using Ion-Exchange and Nonionic Resins. *Environmental Science & Technology*, *55*(8), 5001-5011. https://doi.org/10.1021/acs.est.1c00769

Foo, K. Y., & Hameed, B. H. (2010). Insights into the modeling of adsorption isotherm systems. *Chemical Engineering Journal*, *156*(1), 2-10. https://doi.org/https://doi.org/10.1016/j.cej.2009.09.013

Foster, J. T. T., Hu, Y., & Boyer, T. H. (2017). Affinity of potassium-form cation exchange resin for alkaline earth and transition metals. *Separation and Purification Technology*, *175*, 229-237. https://doi.org/https://doi.org/10.1016/j.seppur.2016.11.034

Franke, V., McCleaf, P., Lindegren, K., & Ahrens, L. (2019). Efficient removal of per- and polyfluoroalkyl substances (PFASs) in drinking water treatment: nanofiltration combined with active carbon or anion exchange. *Environmental Science: Water Research & Technology*, *5*(11), 1836-1843. https://doi.org/10.1039/c9ew00286c

Freundlich, H. (1906). Over the adsorption in solution. *J. Phys. chem*, *57*(385471), 1100-1107.

Fu, L., Wang, J., Lu, H., Su, Y., & Ren, A. (2008). Comment on "The removal of phenolic compounds from aqueous solutions by organophilic bentonite". *Journal of Hazardous Materials*, *151*(2), 851-854. https://doi.org/https://doi.org/10.1016/j.jhazmat.2007.11.090

Gagliano, E., Sgroi, M., Falciglia, P. P., Vagliasindi, F. G. A., & Roccaro, P. (2020). Removal of poly- and perfluoroalkyl substances (PFAS) from water by adsorption: Role of PFAS chain length, effect of organic matter and challenges in adsorbent regeneration. *Water Research*, *171*, 115381. https://doi.org/https://doi.org/10.1016/j.watres.2019.115381

Gao, Y., Deng, S., Du, Z., Liu, K., & Yu, G. (2017). Adsorptive removal of emerging polyfluoroalky substances F-53B and PFOS by anion-exchange resin: A comparative study. *Journal of Hazardous Materials*, *323*, 550-557. https://doi.org/https://doi.org/10.1016/j.jhazmat.2016.04.069

Graf, K. C., Cornwell, D. A., & Boyer, T. H. (2014). Removal of dissolved organic carbon from surface water by anion exchange and adsorption: Bench-scale testing to simulate a two-stage countercurrent process. *Separation and Purification Technology*, *122*, 523-532. https://doi.org/https://doi.org/10.1016/j.seppur.2013.12.012

Greluk, M., & Hubicki, Z. (2010). Kinetics, isotherm and thermodynamic studies of Reactive Black 5 removal by acid acrylic resins. *Chemical Engineering Journal*, *162*(3), 919-926. https://doi.org/https://doi.org/10.1016/j.cej.2010.06.043

Greluk, M., & Hubicki, Z. (2011). Comparison of the gel anion exchangers for removal of Acid Orange 7 from aqueous solution. *Chemical Engineering Journal*, *170*(1), 184-193. https://doi.org/https://doi.org/10.1016/j.cej.2011.03.052

Gu, B., Ku, Y.-K., & Brown, G. M. (2005). Sorption and Desorption of Perchlorate and U(VI) by Strong-Base Anion-Exchange Resins. *Environmental Science & Technology*, *39*(3), 901-907. https://doi.org/10.1021/es049121f

Gu, B., Ku, Y.-K., & Jardine, P. M. (2004). Sorption and Binary Exchange of Nitrate, Sulfate, and Uranium on an Anion-Exchange Resin. *Environmental Science & Technology*, *38*(11), 3184-3188. https://doi.org/10.1021/es034902m

Gustafson, R., Fillius, H., & Kunin, R. (1970). Basicities of weak base ion exchange resins. *Industrial & Engineering Chemistry Fundamentals*, *9*(2), 221-229.

Gustafson, R. L., & Lirio, J. A. (1968). Adsorption of organic ions by anion exchange resins. *Industrial & Engineering Chemistry Product Research and Development*, *7*(2), 116-120.

Harland, C. E. (1994). *Ion exchange: theory and practice* (Vol. 6). Royal society of Chemistry.

Haupert, L. M., Pressman, J. G., Speth, T. F., & Wahman, D. G. (2021). Avoiding pitfalls when modeling removal of per- and polyfluoroalkyl substances by anion exchange [https://doi.org/10.1002/aws2.1222]. *AWWA Water Science*, *3*(2), e1222. https://doi.org/https://doi.org/10.1002/aws2.1222

Hekmatzadeh, A. A., Karimi-Jashani, A., Talebbeydokhti, N., & Kløve, B. (2012). Modeling of nitrate removal for ion exchange resin in batch and fixed bed experiments. *Desalination*, *284*, 22-31. https://doi.org/https://doi.org/10.1016/j.desal.2011.08.033

Hekmatzadeh, A. A., Karimi-Jashni, A., Talebbeydokhti, N., & Kløve, B. (2013). Adsorption kinetics of nitrate ions on ion exchange resin. *Desalination*, *326*, 125-134. https://doi.org/https://doi.org/10.1016/j.desal.2013.07.017

Helfferich, F. G. (1995). *Ion exchange*. Courier Corporation.

Hinrichs, R. L., & Snoeyink, V. L. (1976). Sorption of benzenesulfonates by weak base anion exchange resins. *Water Research*, *10*(1), 79-87. https://doi.org/https://doi.org/10.1016/0043-1354(76)90161-5

Höll, W., & Kirch, R. (1978). Regeneration of weak base ion exchange resins. *Desalination*, *26*(2), 153-162. https://doi.org/https://doi.org/10.1016/S0011-9164(00)82197-9

Howe, K. J., Hand, D. W., Crittenden, J. C., Trussell, R. R., & Tchobanoglous, G. (2012). *Principles of water treatment*. John Wiley & Sons.

Hu, Y., Foster, J., & Boyer, T. H. (2016). Selectivity of bicarbonate-form anion exchange for drinking water contaminants: Influence of resin properties. *Separation and Purification Technology*, *163*, 128-139. https://doi.org/https://doi.org/10.1016/j.seppur.2016.02.030

Inglezakis, V. J. (2007). Solubility-normalized Dubinin–Astakhov adsorption isotherm for ion-exchange systems. *Microporous and Mesoporous Materials*, *103*(1), 72-81. https://doi.org/https://doi.org/10.1016/j.micromeso.2007.01.039

Jackson, M. B., & Bolto, B. A. (1990). Effect of ion-exchange resin structure on nitrate selectivity. *Reactive Polymers*, *12*(3), 277-290. https://doi.org/https://doi.org/10.1016/0923-1137(90)90078-I

Jossens, L., Prausnitz, J. M., Fritz, W., Schlünder, E. U., & Myers, A. L. (1978). Thermodynamics of multi-solute adsorption from dilute aqueous solutions. *Chemical Engineering Science*, *33*(8), 1097-1106. https://doi.org/https://doi.org/10.1016/0009-2509(78)85015-5

Kanazawa, N., Urano, K., Kokado, N., & Urushigawa, Y. (2004). Exchange characteristics of monocarboxylic acids and monosulfonic acids onto anion-exchange resins. *Journal of Colloid and Interface Science*, *271*(1), 20-27. https://doi.org/https://doi.org/10.1016/j.jcis.2003.11.008

Kärrman, A., Elgh-Dalgren, K., Lafossas, C., & Møskeland, T. (2011). Environmental levels and distribution of structural isomers of perfluoroalkyl acids after aqueous fire-fighting foam (AFFF) contamination. *Environmental Chemistry*, *8*(4), 372-380. https://doi.org/https://doi.org/10.1071/EN10145

Kinniburgh, D. G. (1986). General purpose adsorption isotherms. *Environmental Science & Technology*, *20*(9), 895-904.

Kołodyńska, D. (2009). Polyacrylate anion exchangers in sorption of heavy metal ions with the biodegradable complexing agent. *Chemical Engineering Journal*, *150*(2), 280-288. https://doi.org/https://doi.org/10.1016/j.cej.2008.12.027

Kołodyńska, D. (2010). Cu(II), Zn(II), Ni(II), and Cd(II) Complexes with HEDP Removal from Industrial Effluents on Different Ion Exchangers. *Industrial & Engineering Chemistry Research*, *49*(5), 2388-2400. https://doi.org/10.1021/ie9014414

Kortüm, G., Vogel, W., & Andrussow, K. (1960). Disssociation constants of organic acids in aqueous solution. *Pure and Applied Chemistry*, *1*(2-3), 187-536. https://doi.org/doi:10.1351/pac196001020187

Kumar, K. V., Porkodi, K., & Rocha, F. (2008). Isotherms and thermodynamics by linear and non-linear regression analysis for the sorption of methylene blue onto activated carbon: Comparison of various error functions. *Journal of Hazardous Materials*, *151*(2), 794-804. https://doi.org/https://doi.org/10.1016/j.jhazmat.2007.06.056

Kumar, K. V., & Sivanesan, S. (2005). Comparison of linear and non-linear method in estimating the sorption isotherm parameters for safranin onto activated carbon. *Journal of Hazardous Materials*, *123*(1), 288-292. https://doi.org/https://doi.org/10.1016/j.jhazmat.2005.03.040

Landry, K. A., & Boyer, T. H. (2013). Diclofenac removal in urine using strong-base anion exchange polymer resins. *Water Research*, *47*(17), 6432-6444. https://doi.org/https://doi.org/10.1016/j.watres.2013.08.015

Landry, K. A., Sun, P., Huang, C.-H., & Boyer, T. H. (2015). Ion-exchange selectivity of diclofenac, ibuprofen, ketoprofen, and naproxen in ureolyzed human urine. *Water Research*, *68*, 510-521. https://doi.org/https://doi.org/10.1016/j.watres.2014.09.056

Langmuir, I. (1916). The constitution and fundamental properties of solids and liquids. Part I. Solids. *Journal of the American chemical society*, *38*(11), 2221-2295.

Laura del Moral, L., Choi, Y. J., & Boyer, T. H. (2020). Comparative removal of Suwannee River natural organic matter and perfluoroalkyl acids by anion exchange: Impact of polymer composition and mobile counterion. *Water Research*, *178*, 115846. https://doi.org/https://doi.org/10.1016/j.watres.2020.115846

Li, P., & SenGupta, A. K. (1998). Genesis of Selectivity and Reversibility for Sorption of Synthetic Aromatic Anions onto Polymeric Sorbents. *Environmental Science & Technology*, *32*(23), 3756-3766. https://doi.org/10.1021/es980628y

Li, P., & SenGupta, A. K. (2000). Intraparticle diffusion during selective ion exchange with a macroporous exchanger. *Reactive and Functional Polymers*, *44*(3), 273-287.

Li, P., & SenGupta, A. K. (2004). Sorption of hydrophobic ionizable organic compounds (HIOCs) onto polymeric ion exchangers. *Reactive and Functional Polymers*, *60*, 27-39. https://doi.org/https://doi.org/10.1016/j.reactfunctpolym.2004.02.008

Liang, S., Mora, R., Huang, Q., Casson, R., Wang, Y., Woodard, S., & Anderson, H. (2022). Field demonstration of coupling ion-exchange resin with electrochemical oxidation for enhanced treatment of per- and polyfluoroalkyl substances (PFAS) in groundwater. *Chemical Engineering Journal Advances*, *9*, 100216. https://doi.org/https://doi.org/10.1016/j.ceja.2021.100216

Lin, A. Y.-C., Panchangam, S. C., & Lo, C.-C. (2009). The impact of semiconductor, electronics and optoelectronic industries on downstream perfluorinated chemical contamination in Taiwanese rivers. *Environmental Pollution*, *157*(4), 1365-1372. https://doi.org/https://doi.org/10.1016/j.envpol.2008.11.033

MacAdam, J., & Jarvis, P. (2015). Chapter 1 - Water-Formed Scales and Deposits: Types, Characteristics, and Relevant Industries. In Z. Amjad & K. D. Demadis (Eds.), *Mineral Scales and Deposits* (pp. 3-23). Elsevier. https://doi.org/https://doi.org/10.1016/B978-0-444-63228-9.00001-2

Mahramanlioglu, M., Kizilcikli, I., & Bicer, I. O. (2002). Adsorption of fluoride from aqueous solution by acid treated spent bleaching earth. *Journal of Fluorine Chemistry*, *115*(1), 41-47. https://doi.org/https://doi.org/10.1016/S0022-1139(02)00003-9

Maimaiti, A., Deng, S., Meng, P., Wang, W., Wang, B., Huang, J., Wang, Y., & Yu, G. (2018). Competitive adsorption of perfluoroalkyl substances on anion exchange resins in simulated AFFF-impacted groundwater. *Chemical Engineering Journal*, *348*, 494-502. https://doi.org/https://doi.org/10.1016/j.cej.2018.05.006

Marcus, Y. (1991). Thermodynamics of solvation of ions. Part 5.—Gibbs free energy of hydration at 298.15 K. *Journal of the Chemical Society, Faraday Transactions*, *87*(18), 2995-2999.

McCleaf, P., Englund, S., Östlund, A., Lindegren, K., Wiberg, K., & Ahrens, L. (2017). Removal efficiency of multiple poly- and perfluoroalkyl substances (PFASs) in drinking water using granular activated carbon (GAC) and anion exchange (AE) column tests. *Water Research*, *120*, 77-87. https://doi.org/https://doi.org/10.1016/j.watres.2017.04.057

McGuire, M. E., Schaefer, C., Richards, T., Backe, W. J., Field, J. A., Houtz, E., Sedlak, D. L., Guelfo, J. L., Wunsch, A., & Higgins, C. P. (2014). Evidence of Remediation-Induced Alteration of Subsurface Poly- and Perfluoroalkyl Substance Distribution at a Former Firefighter Training Area. *Environmental Science & Technology*, *48*(12), 6644-6652. https://doi.org/10.1021/es5006187

Millar, G. J., Couperthwaite, S. J., & Leung, C. W. (2015). An examination of isotherm generation: Impact of bottle-point method upon potassium ion exchange with strong acid cation resin. *Separation and Purification Technology*, *141*, 366-377. https://doi.org/https://doi.org/10.1016/j.seppur.2014.12.024

Milmile, S. N., Pande, J. V., Karmakar, S., Bansiwal, A., Chakrabarti, T., & Biniwale, R. B. (2011). Equilibrium isotherm and kinetic modeling of the adsorption of nitrates by anion exchange Indion NSSR resin. *Desalination*, *276*(1), 38-44. https://doi.org/https://doi.org/10.1016/j.desal.2011.03.015

Miyazaki, Y., & Nakai, M. (2011). Protonation and ion exchange equilibria of weak base anion-exchange resins. *Talanta*, *85*(4), 1798-1804. https://doi.org/https://doi.org/10.1016/j.talanta.2011.07.010

Moldes, A. B., Alonso, J. L., & Parajó, J. C. (2003). Recovery of lactic acid from simultaneous saccharification and fermentation media using anion exchange resins. *Bioprocess and Biosystems Engineering*, *25*(6), 357-363. https://doi.org/10.1007/s00449-002-0316-7

Namasivayam, C., & Ranganathan, K. (1995). Removal of Cd(II) from wastewater by adsorption on "waste" Fe(III)Cr(III) hydroxide. *Water Research*, *29*(7), 1737-1744. https://doi.org/https://doi.org/10.1016/0043-1354(94)00320-7

Ness, A., & Boyer, T. H. (2017). Pilot-Scale Evaluation of Bicarbonate-Form Anion Exchange for DOC Removal in Small Systems [https://doi.org/10.5942/jawwa.2017.109.0124]. *Journal AWWA*, *109*(12), 13-26. https://doi.org/https://doi.org/10.5942/jawwa.2017.109.0124

Onyango, M. S., Kojima, Y., Aoyi, O., Bernardo, E. C., & Matsuda, H. (2004). Adsorption equilibrium modeling and solution chemistry dependence of fluoride removal from water by trivalent-cation-exchanged zeolite F-9. *Journal of Colloid and Interface Science*, *279*(2), 341-350. https://doi.org/https://doi.org/10.1016/j.jcis.2004.06.038

Özcan, A., Özcan, A. S., Tunali, S., Akar, T., & Kiran, I. (2005). Determination of the equilibrium, kinetic and thermodynamic parameters of adsorption of copper(II) ions onto seeds of Capsicum annuum. *Journal of Hazardous Materials*, *124*(1), 200-208. https://doi.org/https://doi.org/10.1016/j.jhazmat.2005.05.007

Parimal, S., Prasad, M., & Bhaskar, U. (2010). Prediction of Equillibrium Sorption Isotherm: Comparison of Linear and Nonlinear Methods. *Industrial & Engineering Chemistry Research*, *49*(6), 2882-2888. https://doi.org/10.1021/ie9013343

Park, M., Daniels, K. D., Wu, S., Ziska, A. D., & Snyder, S. A. (2020). Magnetic ion-exchange (MIEX) resin for perfluorinated alkylsubstance (PFAS) removal in groundwater: Roles of atomic charges for adsorption. *Water Research*, *181*, 115897. https://doi.org/https://doi.org/10.1016/j.watres.2020.115897

Pontius, F. (2019). Regulation of Perfluorooctanoic Acid (PFOA) and Perfluorooctane Sulfonic Acid (PFOS) in Drinking Water: A Comprehensive Review. *Water*, *11*(10). https://doi.org/10.3390/w11102003

Prevention, C. f. D. C. a. (2021). Fourth National Report on Human Exposure to Environmental Chemicals, Updated Tables, March 2021. *US Department of Health and Human Services, Centers for Disease Control and Prevention (CDC)*. https://www.cdc.gov/exposurereport/pdf/FourthReport_UpdatedTables_Volume4_Mar2021-508.pdf

Quiñones, O., & Snyder, S. A. (2009). Occurrence of Perfluoroalkyl Carboxylates and Sulfonates in Drinking Water Utilities and Related Waters from the United States. *Environmental Science & Technology*, *43*(24), 9089-9095. https://doi.org/10.1021/es9024707

Radke, C., & Prausnitz, J. (1972). Adsorption of organic solutes from dilute aqueous solution of activated carbon. *Industrial & Engineering Chemistry Fundamentals*, *11*(4), 445-451.

Rahmani, S., & Mohseni, M. (2017). The role of hydrophobic properties in ion exchange removal of organic compounds from water [https://doi.org/10.1002/cjce.22823]. *The Canadian Journal of Chemical Engineering*, *95*(8), 1449-1455. https://doi.org/https://doi.org/10.1002/cjce.22823

Samatya, S., Kabay, N., Yüksel, Ü., Arda, M., & Yüksel, M. (2006). Removal of nitrate from aqueous solution by nitrate selective ion exchange resins. *Reactive and Functional Polymers*, *66*(11), 1206-1214. https://doi.org/https://doi.org/10.1016/j.reactfunctpolym.2006.03.009

Schaefer, C. E., Nguyen, D., Ho, P., Im, J., & LeBlanc, A. (2019). Assessing Rapid Small-Scale Column Tests for Treatment of Perfluoroalkyl Acids by Anion Exchange Resin. *Industrial & Engineering Chemistry Research*, *58*(22), 9701-9706. https://doi.org/10.1021/acs.iecr.9b00858

Schaefer, C. E., Tran, D., Fang, Y., Choi, Y. J., Higgins, C. P., & Strathmann, T. J. (2020). Electrochemical treatment of poly-and perfluoroalkyl substances in brines. *Environmental Science: Water Research & Technology*, *6*(10), 2704-2712.

Schultz, M. M., Barofsky, D. F., & Field, J. A. (2004). Quantitative Determination of Fluorotelomer Sulfonates in Groundwater by LC MS/MS. *Environmental Science & Technology*, *38*(6), 1828-1835. https://doi.org/10.1021/es035031j

Schuricht, F., Borovinskaya, E. S., & Reschetilowski, W. (2017). Removal of perfluorinated surfactants from wastewater by adsorption and ion exchange — Influence of material properties, sorption mechanism and modeling. *Journal of Environmental Sciences*, *54*, 160-170. https://doi.org/https://doi.org/10.1016/j.jes.2016.06.011

Sengupta, A. K., & Clifford, D. (1986). Some unique characteristics of chromate ion exchange. *Reactive Polymers, Ion Exchangers, Sorbents*, *4*(2), 113-130. https://doi.org/https://doi.org/10.1016/0167-6989(86)90007-3

Shuang, C., Pan, F., Zhou, Q., Li, A., Li, P., & Yang, W. (2012). Magnetic Polyacrylic Anion Exchange Resin: Preparation, Characterization and Adsorption Behavior of Humic Acid. *Industrial & Engineering Chemistry Research*, *51*(11), 4380-4387. https://doi.org/10.1021/ie201488g

Sohn, S., & Kim, D. (2005). Modification of Langmuir isotherm in solution systems—definition and utilization of concentration dependent factor. *Chemosphere*, *58*(1), 115-123. https://doi.org/https://doi.org/10.1016/j.chemosphere.2004.08.091

Song, H., Zhou, Y., Li, A., & Mueller, S. (2012). Selective removal of nitrate from water by a macroporous strong basic anion exchange resin. *Desalination*, *296*, 53-60. https://doi.org/https://doi.org/10.1016/j.desal.2012.04.003

Sörengård, M., Franke, V., Tröger, R., & Ahrens, L. (2020). Losses of poly- and perfluoroalkyl substances to syringe filter materials. *Journal of Chromatography A*, *1609*, 460430. https://doi.org/https://doi.org/10.1016/j.chroma.2019.460430

Subramonian, S., & Clifford, D. (1988). Monovalent/divalent selectivity and the charge separation concept. *Reactive Polymers, Ion Exchangers, Sorbents*, *9*(2), 195-209. https://doi.org/https://doi.org/10.1016/0167-6989(88)90033-5

Tran, H. N. (2017). Comments on "Characterization and adsorption capacity of raw pomegranate peel biosorbent for copper removal". *Journal of Cleaner Production*, *144*, 553-558. https://doi.org/https://doi.org/10.1016/j.jclepro.2016.12.066

Tran, H. N., Wang, Y.-F., You, S.-J., & Chao, H.-P. (2017). Insights into the mechanism of cationic dye adsorption on activated charcoal: The importance of π–π interactions. *Process Safety and Environmental Protection*, *107*, 168-180. https://doi.org/https://doi.org/10.1016/j.psep.2017.02.010

Tran, H. N., You, S.-J., & Chao, H.-P. (2017a). Fast and efficient adsorption of methylene green 5 on activated carbon prepared from new chemical activation method. *Journal of Environmental Management*, *188*, 322-336. https://doi.org/https://doi.org/10.1016/j.jenvman.2016.12.003

Tran, H. N., You, S.-J., & Chao, H.-P. (2017b). Insight into adsorption mechanism of cationic dye onto agricultural residues-derived hydrochars: Negligible role of π-π interaction. *Korean Journal of Chemical Engineering*, *34*(6), 1708-1720. https://doi.org/10.1007/s11814-017-0056-7

Tran, H. N., You, S.-J., Hosseini-Bandegharaei, A., & Chao, H.-P. (2017). Mistakes and inconsistencies regarding adsorption of contaminants from aqueous solutions: A critical review. *Water Research*, *120*, 88-116. https://doi.org/https://doi.org/10.1016/j.watres.2017.04.014

USEPA. (2019). EPA's per-and polyfluoroalkyl substances (PFAS) action plan. *EPA 823-R-18-004*. https://www.epa.gov/sites/default/files/2019-02/documents/pfas_action_plan_021319_508compliant_1.pdf

Vchirawongkwin, V., & Rode, B. M. (2007). Solvation energy and vibrational spectrum of sulfate in water – An ab initio quantum mechanical simulation. *Chemical Physics Letters*, *443*(1), 152-157. https://doi.org/https://doi.org/10.1016/j.cplett.2007.06.040

Wang, W., Maimaiti, A., Shi, H., Wu, R., Wang, R., Li, Z., Qi, D., Yu, G., & Deng, S. (2019). Adsorption behavior and mechanism of emerging perfluoro-2-propoxypropanoic acid (GenX) on activated carbons and resins. *Chemical Engineering Journal*, *364*, 132-138. https://doi.org/https://doi.org/10.1016/j.cej.2019.01.153

Wawrzkiewicz, M. (2011). Comparison of gel anion exchangers of various basicity in direct dye removal from aqueous solutions and wastewaters. *Chemical Engineering Journal*, *173*(3), 773-781. https://doi.org/https://doi.org/10.1016/j.cej.2011.08.048

Wawrzkiewicz, M., & Hubicki, Z. (2011). Remazol Black B removal from aqueous solutions and wastewater using weakly basic anion exchange resins. *Central European Journal of Chemistry*, *9*(5), 867-876. https://doi.org/10.2478/s11532-011-0072-0

Woodard, S., Berry, J., & Newman, B. (2017). Ion exchange resin for PFAS removal and pilot test comparison to GAC [https://doi.org/10.1002/rem.21515]. *Remediation Journal*, *27*(3), 19-27. https://doi.org/https://doi.org/10.1002/rem.21515

Xiao, F., Davidsavor, K. J., Park, S., Nakayama, M., & Phillips, B. R. (2012). Batch and column study: Sorption of perfluorinated surfactants from water and cosolvent systems by Amberlite XAD resins. *Journal of Colloid and Interface Science*, *368*(1), 505-511. https://doi.org/https://doi.org/10.1016/j.jcis.2011.11.011

Yang, Y., Ding, Q., Yang, M., Wang, Y., Liu, N., & Zhang, X. (2018). Magnetic ion exchange resin for effective removal of perfluorooctanoate from water: study of a response surface methodology and adsorption performances. *Environmental Science and Pollution Research*, *25*(29), 29267-29278. https://doi.org/10.1007/s11356-018-2797-1

Yao, Y., Volchek, K., Brown, C. E., Robinson, A., & Obal, T. (2014). Comparative study on adsorption of perfluorooctane sulfonate (PFOS) and perfluorooctanoate (PFOA) by different adsorbents in water. *Water Science and Technology*, *70*(12), 1983-1991. https://doi.org/10.2166/wst.2014.445

Yu, Q., Deng, S., & Yu, G. (2008). Selective removal of perfluorooctane sulfonate from aqueous solution using chitosan-based molecularly imprinted polymer adsorbents. *Water Research*, *42*(12), 3089-3097. https://doi.org/https://doi.org/10.1016/j.watres.2008.02.024

Yu, Q., Zhang, R., Deng, S., Huang, J., & Yu, G. (2009). Sorption of perfluorooctane sulfonate and perfluorooctanoate on activated carbons and resin: Kinetic and isotherm study. *Water Research*, *43*(4), 1150-1158. https://doi.org/https://doi.org/10.1016/j.watres.2008.12.001

Zaggia, A., Conte, L., Falletti, L., Fant, M., & Chiorboli, A. (2016). Use of strong anion exchange resins for the removal of perfluoroalkylated substances from contaminated drinking water in batch and continuous pilot plants. *Water Research*, *91*, 137-146. https://doi.org/https://doi.org/10.1016/j.watres.2015.12.039

Zeng, C., Atkinson, A., Sharma, N., Ashani, H., Hjelmstad, A., Venkatesh, K., & Westerhoff, P. (2020). Removing per- and polyfluoroalkyl substances from groundwaters using activated carbon and ion exchange resin packed columns [https://doi.org/10.1002/aws2.1172]. *AWWA Water Science*, *2*(1), e1172. https://doi.org/https://doi.org/10.1002/aws2.1172

Zhang, H., Shields, A. J., Jadbabaei, N., Nelson, M., Pan, B., & Suri, R. P. S. (2014). Understanding and Modeling Removal of Anionic Organic Contaminants (AOCs)

by Anion Exchange Resins. *Environmental Science & Technology*, *48*(13), 7494-7502. https://doi.org/10.1021/es500914q

APPENDIX A

BATCH EXPERIMENTS

Table A1. Adsorption isotherm models and corresponding linear forms and plots used to obtain starting values for the nonlinear-optimization method.

Adsorption Isotherm	Nonlinear form	Linear form	Plot
Langmuir Type I (Hanes-Woolf)	$q_e = \frac{q_0 K_L C_e}{1 + bC_e}$	$\frac{C_e}{q_e} = \frac{1}{K_L q_0} + \frac{1}{q_0} C_e$	$\frac{C_e}{q_e}\ vs\ C_e$
Langmuir Type II (Lineweaver-Burke)		$\frac{1}{q_e} = \frac{1}{q_0} + \frac{1}{K_L q_0}\frac{1}{C_e}$	$\frac{1}{q_e}\ vs\ \frac{1}{C_e}$
Langmuir Type III (Eadie-Hoffsiee)		$q_e = q_0 - \frac{1}{K_L}\frac{q_e}{C_e}$	$q_e\ vs\ \frac{q_e}{C_e}$
Langmuir Type IV (Scatchard)		$\frac{q_e}{C_e} = q_0 - K_L q_e$	$\frac{q_e}{C_e}\ vs\ q_e$
Freundlich	$q_e = K_F C_e^{1/n}$	$\log(q_e) = \log(K_F) + \frac{1}{n}\log C_e$	$\log(q_e)\ vs\ \log(C_e)$
Dubinin-Astakhov	$q_e = q_0 \exp\left(-\left(\frac{\varepsilon}{E\sqrt{2}}\right)^{n_D}\right)$	$\ln(\ln(q_0) - \ln(q_e)) = -n_D \ln\left(E\sqrt{2}\right) + n_D \ln(\varepsilon)$	$\ln(\ln(q_e))\ vs\ \ln(\varepsilon)$
Dubinin-Radushkevich	$q_e = q_0 \exp\left(-\left(\frac{\varepsilon}{E\sqrt{2}}\right)^2\right)$	$\ln(q_e) = \ln(q_0) - \frac{1}{2E^2}\varepsilon^2$	$\ln(q_e)\ vs\ \varepsilon^2$

Redlich-Peterson[a]	$q_e = \frac{K_{RP} C_e}{1 + b_{RP} C_e^{\alpha}}$	$\ln(K_{RP}\frac{C_e}{q_e} - 1)$ $= \ln(b_{RP}) + \alpha \ln(C_e)$	$\ln(K_{RP}\frac{C_e}{q_e} - 1)\ vs\ \ln(C_e)$

Table A2. Estimated influence of resin properties on nitrate, sulfate, and 3-PPA selectivity.

Resin	IRA 458	A520E	IRA 67	IRA 96
Classification	SB/PA/G/Trimethy l	SB/PS/MP/Triethy l	WB/PA/G/Dimethy l	WB/PS/MP/Dimethy l
Nitrate[a]	3-4	1	3-4	2
Sulfate[a]	2	4	1	3
3-PPA[a]	3-4	1	3-4	2
Hydrophobic character[b]	3-4	1	3-4	2
Spacing of IX sites[b]	2	1	3-4	3-4

Strong-Base (SB), Weak-Base (WB), Polyacrylic (PA), Polystyrene (PS), Gel (G), Macroporous (MP).

[a] Summary of contaminant removal sequence based on Fig. 3.1 results at pH 7.
[b] Predominant resin properties
1 ranks the highest and 4 the lowest.

Table A3. Nonlinear and linear Langmuir isotherm and goodness-of-fit model parameters for the single-analyte adsorption of (a) nitrate and (b) sulfate on AER at pH 4, 7 and 10. Nonlinear parameter values were determined using the least-squares regression method in RStudio. Linear parameter values were determined plotting corresponding linear forms of the Langmuir equation.

(a) Nitrate

Resin/pH	Langmuir Equation	K_L (L/mmol)	q_0 (mmol/g)	Linear R^2	Nonlinear R^2	ARE (%)	SSE ($mmol^2/g^2$)	RMSE (mmol/g)
IRA 458/4	Linear Type I	0.29	9.29	0.8762	0.988	2.291	0.0938	0.0791
	Linear Type II	0.27	9.93	0.9985	0.9877	2.412	0.0963	0.0801
	Linear Type III	0.33	8.49	0.8309	0.9876	2.436	0.0973	0.0805
	Linear Type IV	0.27	9.89	0.8309	0.9877	2.399	0.0960	0.0800
	Nonlinear	0.30	9.08	-	0.9881	2.378	0.0934	0.0789
A520E/4	Linear Type I	4.28	2.48	0.9978	0.9964	3.390	0.0200	0.0366
	Linear Type II	5.41	2.23	0.9971	0.9801	4.082	0.1106	0.0859
	Linear Type III	4.83	2.37	0.9788	0.9933	3.296	0.0372	0.0498
	Linear Type IV	4.73	2.39	0.9788	0.9944	3.305	0.0313	0.0457
	Nonlinear	4.17	2.49	-	0.9968	3.469	0.018	0.0346
IRA 67/4	Linear Type I	0.15	16.05	0.7654	0.9941	2.394	0.0455	0.0551
	Linear Type II	0.09	25.65	0.9967	0.9869	2.602	0.1011	0.0821
	Linear Type III	0.20	12.42	0.6797	0.9946	2.533	0.0416	0.0527

	Linear Type IV	0.13	17.43	0.6797	0.9933	2.401	0.0518	0.0588
	Nonlinear	0.19	12.58	-	0.9952	2.525	0.037	0.0497
IRA 96/4	Linear Type I	1.07	4.65	0.9962	0.9984	1.267	0.0135	0.0300
	Linear Type II	1.03	4.78	0.9992	0.998	1.247	0.0169	0.0336
	Linear Type III	1.06	4.68	0.9917	0.9984	1.252	0.0138	0.0303
	Linear Type IV	1.05	4.71	0.9917	0.9983	1.251	0.0142	0.0308
	Nonlinear	1.09	4.62	-	0.9984	1.291	0.0133	0.0298
IRA 458/7	Linear Type I	0.45	5.96	0.8417	0.9715	3.746	0.1689	0.1061
	Linear Type II	0.41	6.41	0.9948	0.971	3.570	0.1719	0.1071
	Linear Type III	0.51	5.45	0.7792	0.9702	4.129	0.1764	0.1084
	Linear Type IV	0.40	6.56	0.7792	0.9704	3.576	0.1752	0.1081
	Nonlinear	0.46	5.93	-	0.9716	3.706	0.168	0.1058
A520E/7	Linear Type I	4.09	2.42	0.9976	0.994	3.868	0.0313	0.0457
	Linear Type II	4.99	2.20	0.9816	0.9798	5.332	0.1052	0.0837
	Linear Type III	4.59	2.31	0.9560	0.9906	4.423	0.0491	0.0572

	Linear Type IV	4.39	2.36	0.9560	0.9927	4.112	0.0381	0.0504
	Nonlinear	3.97	2.44	-	0.9942	4.051	0.0301	0.0448
IRA 67/7	Linear Type I	0.10	21.97	0.6817	0.9954	2.325	0.038	0.0504
	Linear Type II	0.05	38.6	0.9971	0.9908	2.547	0.0763	0.0713
	Linear Type III	0.15	15.01	0.6055	0.9947	2.414	0.0436	0.0539
	Linear Type IV	0.09	23.59	0.6055	0.9951	2.336	0.0408	0.0522
	Nonlinear	0.13	17.58	-	0.9959	2.250	0.0343	0.0478
IRA 96/7	Linear Type I	1.23	4.18	0.9691	0.985	3.579	0.1186	0.0889
	Linear Type II	0.99	4.81	0.9969	0.9744	2.934	0.2026	0.1162
	Linear Type III	1.16	4.33	0.9417	0.9845	3.259	0.1232	0.0906
	Linear Type IV	1.09	4.49	0.9417	0.9824	3.111	0.1394	0.0964
	Nonlinear	1.28	4.12	-	0.9856	3.668	0.1144	0.0873
IRA 458/10	Linear Type I	0.3	7.23	0.9667	0.9969	1.693	0.0169	0.0336
	Linear Type II	0.28	7.81	0.9987	0.9959	1.497	0.0225	0.0387
	Linear Type III	0.31	7.11	0.9458	0.9970	1.741	0.0165	0.0332

	Linear Type IV	0.29	7.43	0.9458	0.9967	1.613	0.0181	0.0348
	Nonlinear	0.32	6.89	-	0.9971	1.831	0.016	0.0327
A520E/10	Linear Type I	3.84	2.76	0.9983	0.9971	3.291	0.02	0.0365
	Linear Type II	5.02	2.42	0.9865	0.9717	5.953	0.1929	0.1134
	Linear Type III	4.37	2.61	0.9612	0.9926	3.899	0.0502	0.0578
	Linear Type IV	4.2	2.66	0.9612	0.9949	3.534	0.0348	0.0481
	Nonlinear	3.69	2.77	-	0.9975	3.415	0.0172	0.0338

(b) Sulfate

Resin/pH	Langmuir Equation	K_L (L/mmol)	q_0 (mmol/g)	Linear R^2	Nonlinear R^2	ARE (%)	SSE ($mmol^2/g^2$)	RMSE (mmol/g)
IRA 458/4	Linear Type I	38.47	1.96	0.9982	0.9351	18.285	0.3370	0.1499
	Linear Type II	20.79	2.83	0.7623	0.4503	31.188	2.8544	0.4362
	Linear Type III	59.22	1.73	0.5664	0.9138	22.458	0.4474	0.1727
	Linear Type IV	33.55	2.20	0.5664	0.8958	22.155	0.5408	0.1899
	Nonlinear	47.84	1.93	-	0.9479	18.871	0.2706	0.1343

A520E/4	Linear Type I	8.21	1.04	0.9917	0.9844	7.020	0.0153	0.0319
	Linear Type II	12.32	0.88	0.9939	0.9492	5.880	0.0496	0.0575
	Linear Type III	10.68	0.95	0.9443	0.9741	5.731	0.0253	0.0411
	Linear Type IV	10.09	0.97	0.9443	0.9787	5.905	0.0208	0.0372
	Nonlinear	8.05	1.03	-	0.9855	7.416	0.0141	0.0307
IRA 67/4	Linear Type I	45.57	2.25	0.9974	0.9064	23.280	0.6765	0.2124
	Linear Type II	28.13	2.93	0.6208	0.7067	30.424	2.1199	0.3759
	Linear Type III	88.81	1.86	0.4191	0.8287	33.614	1.2377	0.2872
	Linear Type IV	37.22	2.66	0.4191	0.8327	28.088	1.2090	0.2839
	Nonlinear	55.74	2.25	-	0.9192	23.425	0.5842	0.1974
IRA 96/4	Linear Type I	43.40	1.55	0.9990	0.9545	11.841	0.1293	0.0929
	Linear Type II	31.79	1.83	0.8801	0.8119	16.804	0.5342	0.1887
	Linear Type III	55.41	1.47	0.7516	0.9622	12.618	0.1075	0.0846

	Linear Type IV	41.64	1.63	0.7516	0.9447	13.159	0.1569	0.1023
	Nonlinear	53.32	1.52	-	0.9675	12.238	0.0923	0.0784
IRA 458/7	Linear Type I	39.12	1.96	0.9982	0.9369	17.402	0.3248	0.1472
	Linear Type II	21.99	2.80	0.8007	0.4290	30.195	2.9376	0.4425
	Linear Type III	58.55	1.75	0.6122	0.9293	20.138	0.3638	0.1557
	Linear Type IV	35.84	2.15	0.6122	0.9073	20.432	0.4769	0.1783
	Nonlinear	50.27	1.92	-	0.9527	17.819	0.2435	0.1274
A520E/7	Linear Type I	10.36	0.94	0.9803	0.9734	5.341	0.0234	0.0395
	Linear Type II	13.08	0.86	0.9950	0.9533	5.272	0.0412	0.0524
	Linear Type III	11.72	0.91	0.9455	0.9684	5.132	0.0278	0.0431
	Linear Type IV	11.08	0.93	0.9455	0.9715	5.219	0.0252	0.0410
	Nonlinear	9.72	0.96	-	0.9741	6.241	0.0228	0.0390
IRA 67/7	Linear Type I	56.51	2.16	0.9910	0.8912	25.857	0.7748	0.2273

	Linear Type II	30.71	2.83	0.6000	0.7170	29.806	2.0157	0.3666
	Linear Type III	98.34	1.83	0.3858	0.8001	35.298	1.4237	0.3081
	Linear Type IV	37.94	2.70	0.3858	0.7830	29.274	1.5455	0.3210
	Nonlinear	59.87	2.23	-	0.8993	25.536	0.7173	0.2187
IRA 96/7	Linear Type I	41.91	1.52	0.9985	0.9544	10.949	0.1227	0.0904
	Linear Type II	33.08	1.75	0.8889	0.8571	14.536	0.3844	0.1601
	Linear Type III	54.41	1.45	0.7667	0.9633	11.729	0.0988	0.0811
	Linear Type IV	41.72	1.59	0.7667	0.9503	11.763	0.1338	0.0944
	Nonlinear	52.01	1.50	-	0.9681	11.336	0.0859	0.0757
IRA 458/10	Linear Type I	44.60	1.65	0.9991	0.9397	15.296	0.2119	0.1188
	Linear Type II	24.27	2.27	0.8342	0.5014	26.432	1.7504	0.3416
	Linear Type III	57.36	1.55	0.6419	0.9370	17.513	0.2211	0.1214
	Linear Type IV	36.82	1.84	0.6419	0.8951	18.696	0.3681	0.1567

	Nonlinear	52.95	1.65	-	0.9505	15.624	0.1736	0.1076
A520E/10	Linear Type I	9.23	0.96	0.9864	0.9804	5.198	0.0172	0.0339
	Linear Type II	12.07	0.86	0.9937	0.9567	5.339	0.0380	0.0503
	Linear Type III	10.71	0.91	0.9485	0.9744	5.008	0.0225	0.0387
	Linear Type IV	10.16	0.94	0.9485	0.9776	4.948	0.0196	0.0362
	Nonlinear	8.73	0.97	-	0.9810	5.925	0.0166	0.0333

Table A4. Nonlinear Langmuir isotherm model parameters for the adsorption of (a) nitrate, (b) 3-phenylpropionic acid, and (c) sulfate on AER at different solution pH.

(a) Nitrate

Resin/pH	K_L (L/mmol)	q_0 (mmol/g)	R_L	ΔG^0 (kJ/mol)	Nonlinear R^2	ARE (%)	SSE ($mmol^2/g^2$)	RMSE (mmol/g)	χ^2 (mmol/g)
IRA 458/4	0.30	9.08	0.627	2.92	0.9881	2.38 %	0.093	0.079	0.038
A520E/4	4.17	2.49	0.108	-3.50	0.9968	3.47 %	0.018	0.035	0.024
IRA 67/4	0.19	12.58	0.724	4.02	0.9952	2.53 %	0.037	0.050	0.022
IRA 96/4	1.09	4.62	0.316	-0.20	0.9984	1.29 %	0.013	0.030	0.006

IRA 458/7	0.46	5.93	0.520	1.93	0.9716	3.71 %	0.168	0.106	0.080
A520E/7	3.97	2.44	0.110	-3.39	0.9942	4.05 %	0.030	0.045	0.038
IRA 67/7	0.13	17.58	0.792	5.05	0.9959	2.25 %	0.034	0.048	0.017
IRA 96/7	1.28	4.12	0.275	-0.61	0.9856	3.67 %	0.114	0.087	0.053
IRA 458/10	0.32	6.89	0.588	2.76	0.9971	1.83 %	0.016	0.033	0.009
A520E/10	3.69	2.77	0.112	-3.20	0.9975	3.42 %	0.017	0.034	0.031

(b) 3-phenylpropionic acid (3-PPA)

Resin/pH	K_L (L/mmol)	q_0 (mmol/g)	R_L	Nonlinear R^2	ARE (%)	SSE ($mmol^2/g^2$)	RMSE (mmol/g)	χ^2 (mmol/g)
IRA 458/4	-0.42	-0.28	11.694	0.9132	9.21	0.101	0.082	0.119
A520E/4	-0.32	-0.87	3.180	0.9932	4.07	0.007	0.022	0.022
IRA 67/4	-0.52	-0.04	-9.908	0.9431	22.88	0.099	0.081	0.239
IRA 96/4	-0.38	-0.72	5.362	0.9577	9.15	0.090	0.077	0.156
IRA 458/7	-0.30	-1.72	2.922	0.9884	3.31	0.040	0.051	0.027
A520E/7	0.31	4.24	0.602	0.9925	3.91	0.015	0.031	0.020
IRA 67/7	-0.41	-1.13	8.295	0.9616	12.60	0.221	0.122	0.247
IRA 96/7	-0.01	-82.12	1.030	0.8817	11.71	0.447	0.173	0.368
IRA 458/10	-0.19	-2.76	1.703	0.9911	3.09	0.016	0.033	0.017

A520E/10	0.60	2.57	0.436	0.9943	2.92	0.009	0.025	0.012

(c) Sulfate

Resin/pH	K_L (L/mmol)	q_0 (mmol/g)	R_L	ΔG^0 (kJ/mol)	Nonlinear R^2	ARE (%)	SSE ($mmol^2/g^2$)	RMSE (mmol/g)	χ^2 (mmol/g)
IRA 458/4	47.84	1.93	0.019	-9.50	0.9479	18.87	0.271	0.134	0.416
A520E/4	8.05	1.03	0.106	-5.12	0.9855	7.42	0.014	0.031	0.039
IRA 67/4	55.74	2.25	0.017	-9.88	0.9192	23.43	0.584	0.197	0.779
IRA 96/4	53.32	1.52	0.017	-9.77	0.9675	12.24	0.092	0.078	0.165
IRA 458/7	50.27	1.92	0.018	-9.62	0.9527	17.82	0.244	0.127	0.365
A520E/7	9.72	0.96	0.089	-5.59	0.9741	6.24	0.023	0.039	0.038
IRA 67/7	59.87	2.23	0.015	-10.05	0.8993	25.54	0.717	0.219	0.873
IRA 96/7	52.01	1.50	0.018	-9.70	0.9681	11.34	0.086	0.076	0.151
IRA 458/10	52.95	1.65	0.018	-9.75	0.9505	15.62	0.174	0.108	0.283
A520E/10	8.73	0.97	0.098	-5.32	0.9810	5.93	0.017	0.033	0.032

Table A5. Nonlinear Freundlich isotherm model parameters for the adsorption of (a) nitrate, (b) 3-phenylpropionic acid, and (c) sulfate on AER at different solution pH.

(a) Nitrate

Resin/pH	K_F ($mmol^{(1-1/nF}\ L^{1/nF}/g$)	$1/n_F$	Nonlinear R^2	ARE (%)	SSE ($mmol^2/g^2$)	RMSE (mmol/g)	χ^2 (mmol/g)
IRA 458/4	2.09	0.81	0.9858	3.71	0.111	0.086	0.052
A520E/4	2.02	0.41	0.9786	9.21	0.119	0.089	0.131
IRA 67/4	2.03	0.86	0.9921	3.45	0.061	0.064	0.037
IRA 96/4	2.36	0.61	0.9871	6.11	0.111	0.086	0.087
IRA 458/7	1.81	0.73	0.9682	5.86	0.189	0.112	0.102
A520E/7	1.93	0.40	0.9689	9.94	0.162	0.104	0.161
IRA 67/7	1.98	0.89	0.9947	2.95	0.044	0.054	0.025
IRA 96/7	2.25	0.56	0.9613	9.00	0.306	0.143	0.195
IRA 458/10	1.66	0.77	0.9931	3.51	0.038	0.050	0.027
A520E/10	2.16	0.41	0.9745	9.96	0.174	0.108	0.162

(b) 3-phenylpropionic acid (3-PPA)

Resin/pH	K_F ($mmol^{(1-1/nF}\ L^{1/nF}/g$)	$1/n_F$	Nonlinear R^2	ARE (%)	SSE ($mmol^2/g^2$)	RMSE (mmol/g)	χ^2 (mmol/g)
IRA 458/4	0.13	3.25	0.8949	13.24	0.122	0.090	0.202
A520E/4	0.41	1.67	0.9778	7.84	0.023	0.039	0.072
IRA 67/4	4.45E-05	16.25	0.9805	11.21	0.034	0.048	0.081
IRA 96/4	0.44	2.07	0.9182	13.36	0.174	0.108	0.335
IRA 458/7	0.74	1.67	0.9882	4.39	0.040	0.052	0.037
A520E/7	0.97	0.79	0.9940	3.10	0.012	0.028	0.017
IRA 67/7	0.76	2.28	0.9841	7.96	0.092	0.078	0.099
IRA 96/7	1.27	0.90	0.9363	10.44	0.240	0.127	0.202

IRA 458/10	0.65	1.36	0.9946	1.91	0.010	0.025	0.009
A520E/10	0.94	0.67	0.9973	2.07	0.004	0.017	0.006

(c) Sulfate

Resin/pH	K_F ($mmol^{(1-1/nF}\ L^{1/nF}/g$)	$1/n_F$	Nonlinear R^2	ARE (%)	SSE ($mmol^2/g^2$)	RMSE (mmol/g)	χ^2 (mmol/g)
IRA 458/4	2.32	0.26	0.8674	29.25	0.688	0.214	0.825
A520E/4	1.09	0.41	0.9914	6.51	0.008	0.024	0.029
IRA 67/4	2.71	0.25	0.8243	35.34	1.270	0.291	1.242
IRA 96/4	1.71	0.22	0.8779	21.52	0.347	0.152	0.506
IRA 458/7	2.30	0.26	0.8810	27.18	0.612	0.202	0.760
A520E/7	1.01	0.37	0.9527	10.12	0.042	0.053	0.078
IRA 67/7	2.61	0.24	0.7756	37.54	1.599	0.326	1.442
IRA 96/7	1.67	0.22	0.8806	20.56	0.321	0.146	0.471
IRA 458/10	1.89	0.23	0.8587	25.05	0.496	0.182	0.674
A520E/10	1.02	0.38	0.9633	9.19	0.032	0.046	0.064

Table A6. Nonlinear Dubinin-Radushkevich (DR) isotherm model parameters for the adsorption of (a) nitrate, (b) 3-phenylpropionic acid, and (c) sulfate on AER at different solution pH.

(a) Nitrate

Resin/pH	E (kJ/mol)	q_0 (g/g)	Nonlinear R^2	ARE (%)	SSE ($mmol^2/g^2$)	RMSE (mmol/g)	χ^2 (mmol/g)
IRA 458/4	4.72	0.395	0.9875	3.27	0.098	0.081	0.045

A520E/4	7.43	0.195	0.9974	2.89	0.014	0.031	0.014
IRA 67/4	4.45	0.440	0.9974	1.61	0.020	0.037	0.010
IRA 96/4	5.68	0.316	0.9980	1.55	0.017	0.034	0.008
IRA 458/7	4.92	0.317	0.9717	3.32	0.168	0.106	0.079
A520E/7	7.41	0.188	0.9924	4.46	0.040	0.051	0.037
IRA 67/7	4.32	0.466	0.9960	1.66	0.033	0.047	0.014
IRA 96/7	5.85	0.291	0.9824	4.38	0.139	0.096	0.067
IRA 458/10	4.67	0.324	0.9974	1.70	0.014	0.031	0.009
A520E/10	7.29	0.214	0.9962	3.10	0.026	0.042	0.021

(b) 3-phenylpropionic acid (3-PPA)

Resin/pH	E (kJ/mol)	q_0 (g/g)	Nonlinear R^2	ARE (%)	SSE ($mmol^2/g^2$)	RMSE (mmol/g)	χ^2 (mmol/g)
IRA 458/4	1.57	2.550	0.8808	14.85	0.138	0.096	0.265
A520E/4	2.39	0.561	0.9521	11.76	0.050	0.058	0.178
IRA 67/4	0.67	7.99E+05	0.9811	10.73	0.033	0.047	0.078
IRA 96/4	2.09	1.140	0.8834	16.38	0.248	0.129	0.562
IRA 458/7	2.37	1.036	0.9780	7.17	0.075	0.071	0.106
A520E/7	3.90	0.347	0.9839	5.49	0.032	0.046	0.052
IRA 67/7	2.02	2.442	0.9904	5.61	0.055	0.061	0.056
IRA 96/7	3.40	0.586	0.9669	6.66	0.125	0.091	0.093
IRA 458/10	2.61	0.620	0.9930	3.48	0.013	0.029	0.017
A520E/10	4.31	0.289	0.9877	4.73	0.019	0.036	0.031

(c) Sulfate

Resin/pH	E (kJ/mol)	q_0 (g/g)	Nonlinear R^2	ARE (%)	SSE ($mmol^2/g^2$)	RMSE (mmol/g)	χ^2 (mmol/g)
IRA 458/4	10.44	0.241	0.9081	24.28	0.477	0.178	0.645
A520E/4	7.70	0.129	0.9983	1.84	0.002	0.011	0.003
IRA 67/4	10.71	0.280	0.8730	30.49	0.918	0.247	1.010
IRA 96/4	11.23	0.179	0.9151	18.12	0.241	0.127	0.372
IRA 458/7	10.55	0.238	0.9170	22.64	0.427	0.169	0.593
A520E/7	8.05	0.119	0.9751	4.64	0.022	0.038	0.030
IRA 67/7	11.00	0.272	0.8345	32.77	1.179	0.280	1.164
IRA 96/7	11.25	0.175	0.9182	17.46	0.220	0.121	0.341
IRA 458/10	10.99	0.196	0.8969	21.69	0.362	0.155	0.530
A520E/10	7.87	0.121	0.9833	3.65	0.015	0.031	0.020

Table A7. Nonlinear Dubinin-Astakhov (DA) isotherm model parameters for the adsorption of (a) nitrate, (b) 3-phenylpropionic acid, and (c) sulfate on AER at different solution pH.

(a) Nitrate

Resin/pH	E (kJ/mol)	n_D	Nonlinear R^2	ARE (%)	SSE ($mmol^2/g^2$)	RMSE (mmol/g)	χ^2 (mmol/g)
IRA 458/4	5.73	2.97	0.9801	5.92	0.156	0.102	0.100
A520E/4	8.39	2.98	0.9967	3.15	0.019	0.035	0.019
IRA 67/4	5.40	2.97	0.9943	3.24	0.044	0.054	0.033
IRA 96/4	6.89	3.43	0.9900	5.39	0.086	0.076	0.075
IRA 458/7	5.46	2.46	0.9701	4.20	0.177	0.109	0.086
A520E/7	8.23	2.86	0.9947	3.89	0.027	0.043	0.030
IRA 67/7	5.34	3.11	0.9888	4.20	0.092	0.079	0.055
IRA 96/7	6.86	3.25	0.9873	3.70	0.100	0.082	0.048

IRA 458/10	5.24	2.50	0.9956	2.69	0.024	0.040	0.019
A520E/10	8.50	3.56	0.9866	7.06%	0.092	0.078	0.111

(b) 3-phenylpropionic acid (3-PPA)

Resin/pH	E (kJ/mol)	n_D	Nonlinear R^2	ARE (%)	SSE ($mmol^2/g^2$)	RMSE (mmol/g)	χ^2 (mmol/g)
IRA 458/4	2.37	3.36	0.8622	16.38	0.160	0.103	0.311
A520E/4	2.83	2.48	0.9387	13.12	0.064	0.066	0.187
IRA 67/4	2.58	15.91	0.9775	8.15	0.039	0.051	0.081
IRA 96/4	2.81	2.92	0.8507	18.41	0.318	0.146	0.563
IRA 458/7	2.92	2.72	0.9678	8.59	0.110	0.086	0.151
A520E/7	3.79	1.86	0.9859	5.04	0.028	0.043	0.039
IRA 67/7	3.06	4.12	0.9912	4.01	0.051	0.058	0.046
IRA 96/7	3.70	2.46	0.9740	4.94	0.098	0.081	0.063
IRA 458/10	2.61	2.00	0.9929	3.44	0.013	0.029	0.017
A520E/10	3.72	1.54	0.9942	2.59	0.009	0.025	0.010

(c) Sulfate

Resin/pH	E (kJ/mol)	n_D	Nonlinear R^2	ARE (%)	SSE ($mmol^2/g^2$)	RMSE (mmol/g)	χ^2 (mmol/g)
IRA 458/4	11.49	3.78	0.9402	20.08	0.310	0.144	0.453
A520E/4	8.11	2.26	0.9972	1.85	0.003	0.013	0.004
IRA 67/4	11.95	4.86	0.9201	23.66	0.578	0.196	0.757
IRA 96/4	11.69	3.47	0.9455	15.26	0.155	0.102	0.230
IRA 458/7	11.54	3.61	0.9436	19.07	0.290	0.139	0.418

A520E/7	8.10	2.06	0.9756	4.08	0.022	0.038	0.027
IRA 67/7	12.05	5.38	0.8995	24.53	0.716	0.218	0.840
IRA 96/7	11.61	3.09	0.9423	15.22	0.155	0.102	0.235
IRA 458/10	10.94	2.12	0.8985	21.19	0.356	0.154	0.515
A520E/10	8.00	2.11	0.9840	3.02%	0.014	0.031	0.018

Table A8. Nonlinear Redlich-Peterson (RP) isotherm model parameters for the adsorption of (a) nitrate, (b) 3-phenylpropionic acid, and (c) sulfate on AER at different solution pH.

(a) Nitrate

Resin/pH	K_{RP} (L/g)	b_{RP} $(L/mmol)^{\alpha}$	α	Nonlinear R^2	ARE (%)	SSE $(mmol^2/g^2)$	RMSE (mmol/g)	χ^2 (mmol/g)
IRA 458/4	2.76	0.30	1.00	0.9881	2.38	0.093	0.079	0.038
A520E/4	13.04	5.49	0.88	0.9991	1.16	0.005	0.018	0.003
IRA 67/4	2.45	0.19	1.00	0.9952	2.53	0.037	0.050	0.022
IRA 96/4	5.02	1.09	1.00	0.9984	1.29	0.013	0.030	0.006
IRA 458/7	2.70	0.46	1.00	0.9716	3.71	0.168	0.106	0.080
A520E/7	11.13	4.73	0.92	0.9952	3.77	0.025	0.041	0.025
IRA 67/7	2.25	0.13	1.00	0.9959	2.25	0.034	0.048	0.017
IRA 96/7	5.28	1.28	1.00	0.9856	3.67	0.114	0.087	0.053
IRA 458/10	2.24	0.32	1.00	0.9971	1.83	0.016	0.033	0.009
A520E/10	11.78	4.41	0.92	0.9984	2.05	0.011	0.027	0.014

(b) 3-phenylpropionic acid (3-PPA)

Resin/pH	K_{RP} (L/g)	b_{RP} (L/mmol)$^{\alpha}$	α	Nonlinear R^2	ARE (%)	SSE ($mmol^2/g^2$)	RMSE (mmol/g)	χ^2 (mmol/g)
IRA 458/4	0.12	-0.42	1.00	0.9132	9.21	0.101	0.082	0.119
A520E/4	0.28	-0.32	1.00	0.9932	4.07	0.007	0.022	0.022
IRA 67/4	0.002	-0.95	0.08	0.9463	22.15	0.093	0.079	0.226
IRA 96/4	0.28	-0.38	1.00	0.9577	9.15	0.090	0.077	0.156
IRA 458/7	0.17	-0.78	0.16	0.9896	3.10	0.036	0.049	0.025
A520E/7	3.75	2.84	0.29	0.9940	3.17	0.012	0.028	0.017
IRA 67/7	0.002	-1.00	0.002	0.9727	10.52	0.158	0.102	0.178
IRA 96/7	1.46	0.13	1.00	0.9431	10.27	0.215	0.120	0.190
IRA 458/10	0.002	-1.00	0.001	0.9939	2.20	0.011	0.027	0.010
A520E/10	3.56	2.75	0.47	0.9977	1.57	0.004	0.016	0.004

(c) Sulfate

Resin/pH	K_{RP} (L/g)	b_{RP} (L/mmol)$^{\alpha}$	α	Nonlinear R^2	ARE (%)	SSE ($mmol^2/g^2$)	RMSE (mmol/g)	χ^2 (mmol/g)
IRA 458/4	92.46	47.84	1.00	0.9479	18.87	0.271	0.134	0.416
A520E/4	17.13	15.71	0.74	0.9992	1.60	0.001	0.007	0.002
IRA 67/4	125.29	55.74	1.00	0.9192	23.43	0.584	0.197	0.779
IRA 96/4	81.28	53.32	1.00	0.9675	12.24	0.092	0.078	0.165
IRA 458/7	96.46	50.27	1.00	0.9527	17.82	0.243	0.127	0.365
A520E/7	12.20	12.36	0.88	0.9774	3.27	0.020	0.036	0.024

IRA 67/7	133.44	59.87	1.00	0.8993	25.54	0.717	0.219	0.873
IRA 96/7	77.83	52.01	1.00	0.9681	11.34	0.086	0.076	0.151
IRA 458/10	87.17	52.95	1.00	0.9505	15.62	0.174	0.108	0.283
A520E/10	11.45	11.40	0.87	0.9847	2.84	0.013	0.030	0.017

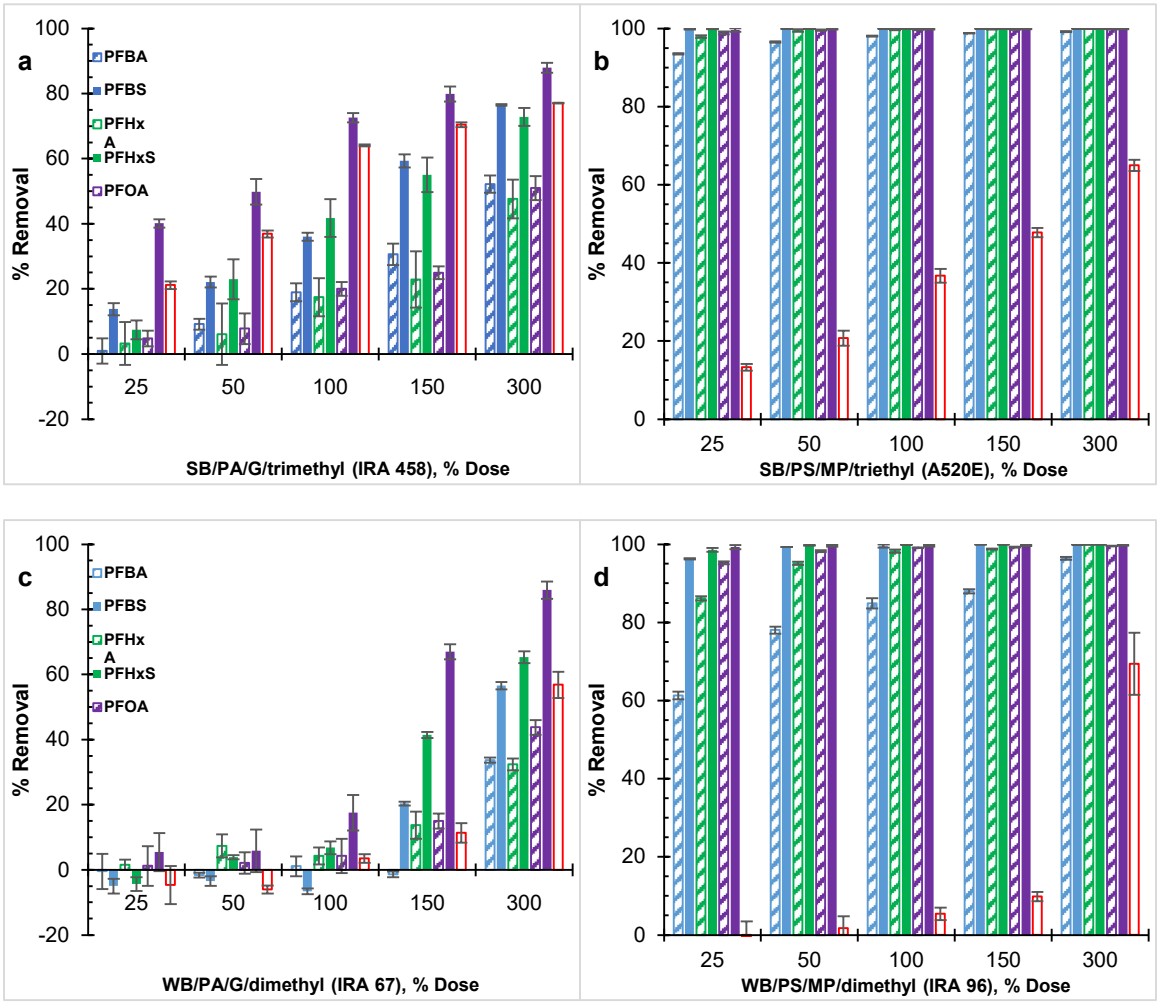

Fig. A1. Perfluoroalkyl acids (PFAAs) removal by (a,c) polyacrylic (PA), and (b,d) polystyrene (PS) AER at pH 10 in the presence of sodium bicarbonate ($C_0 \approx$ 2.14 meq/L). Initial concentration of each PFAS was $C_0 = 80$ µg/L ($\sum$PFAS = 480 µg/L). DIC is dissolved organic carbon.

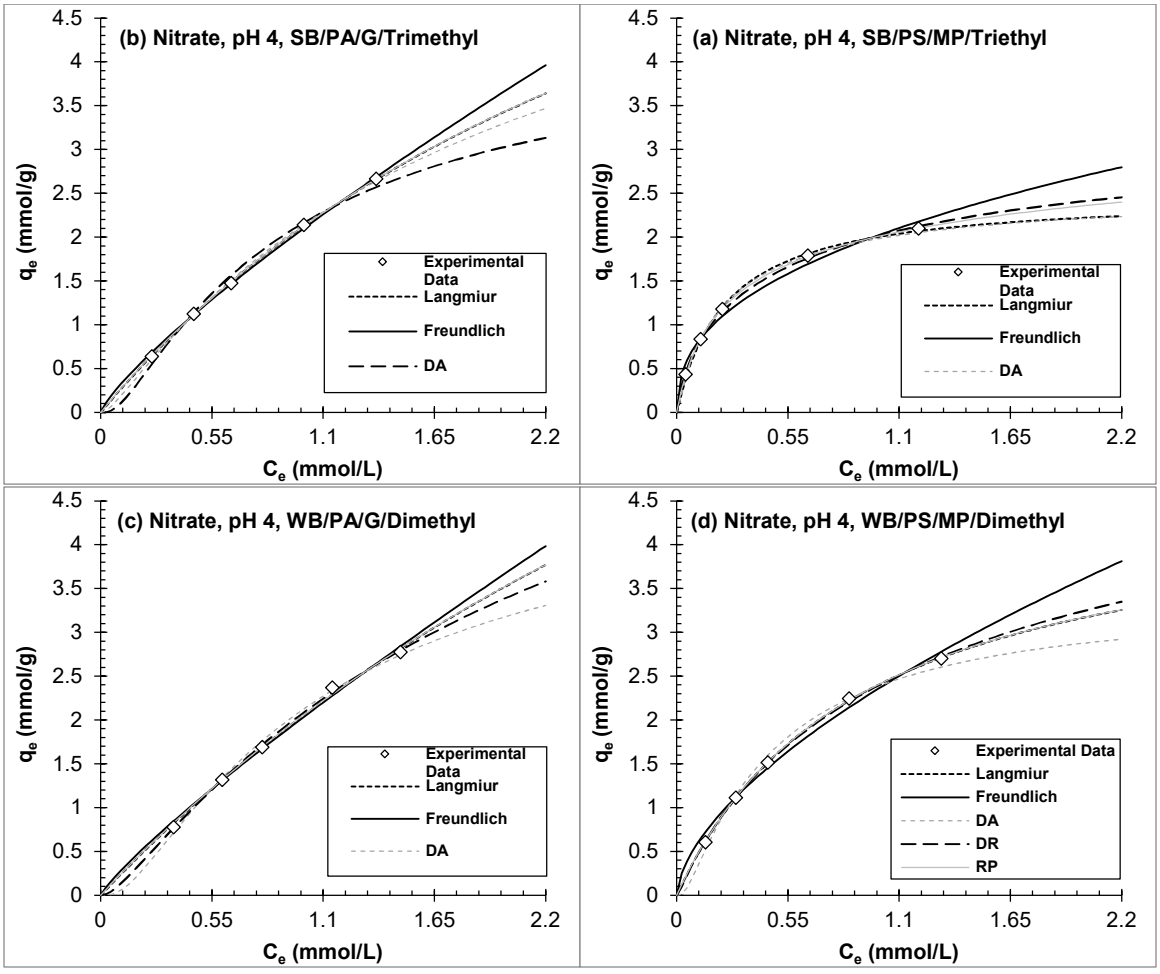

Fig. A2. Equilibrium adsorption isotherms of nitrate onto (a,c) polyacrylic and (b,d) polystyrene anion exchange resins at pH 4.

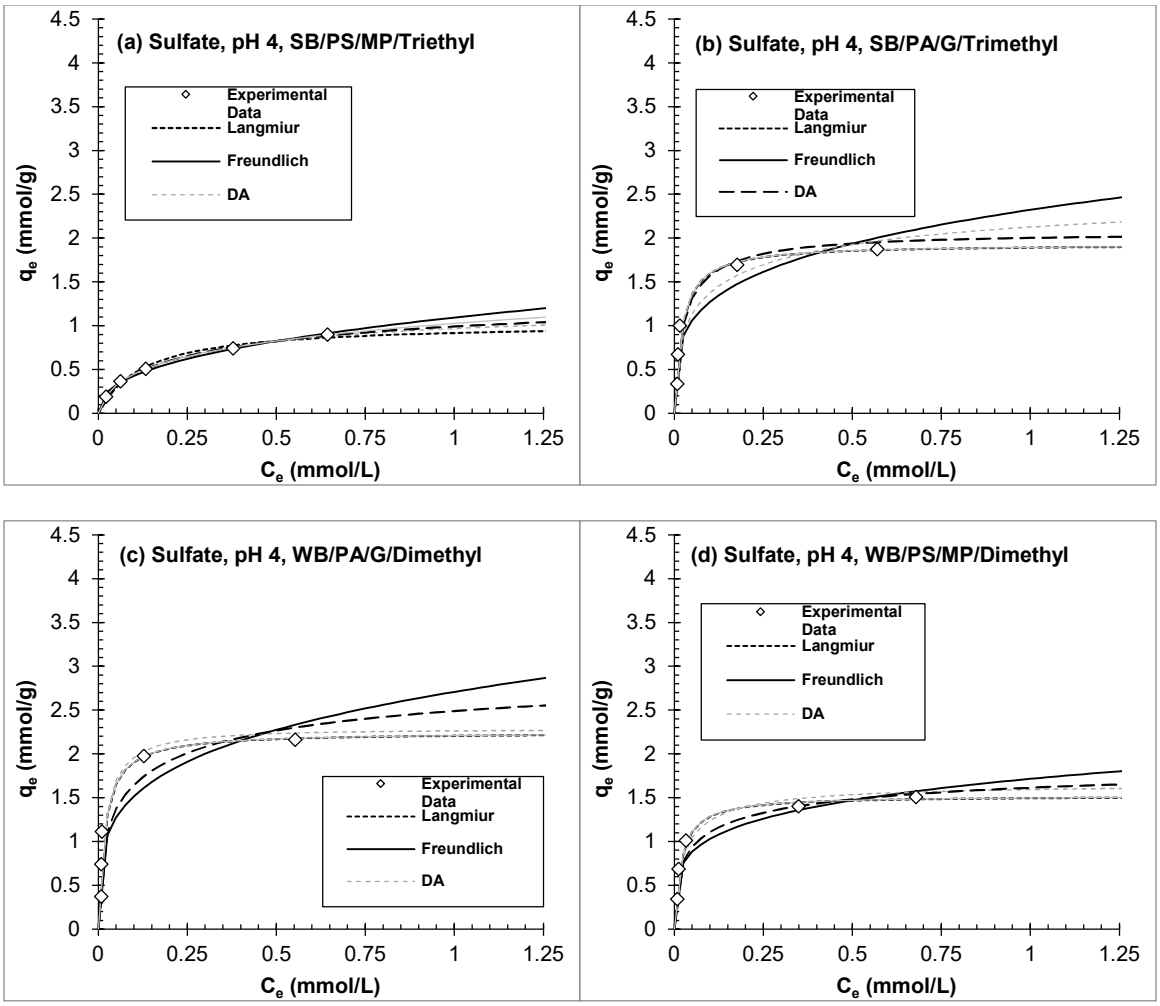

Fig. A3. Equilibrium adsorption isotherms of sulfate onto (a,c) polyacrylic and (b,d) polystyrene anion exchange resins at pH 4.

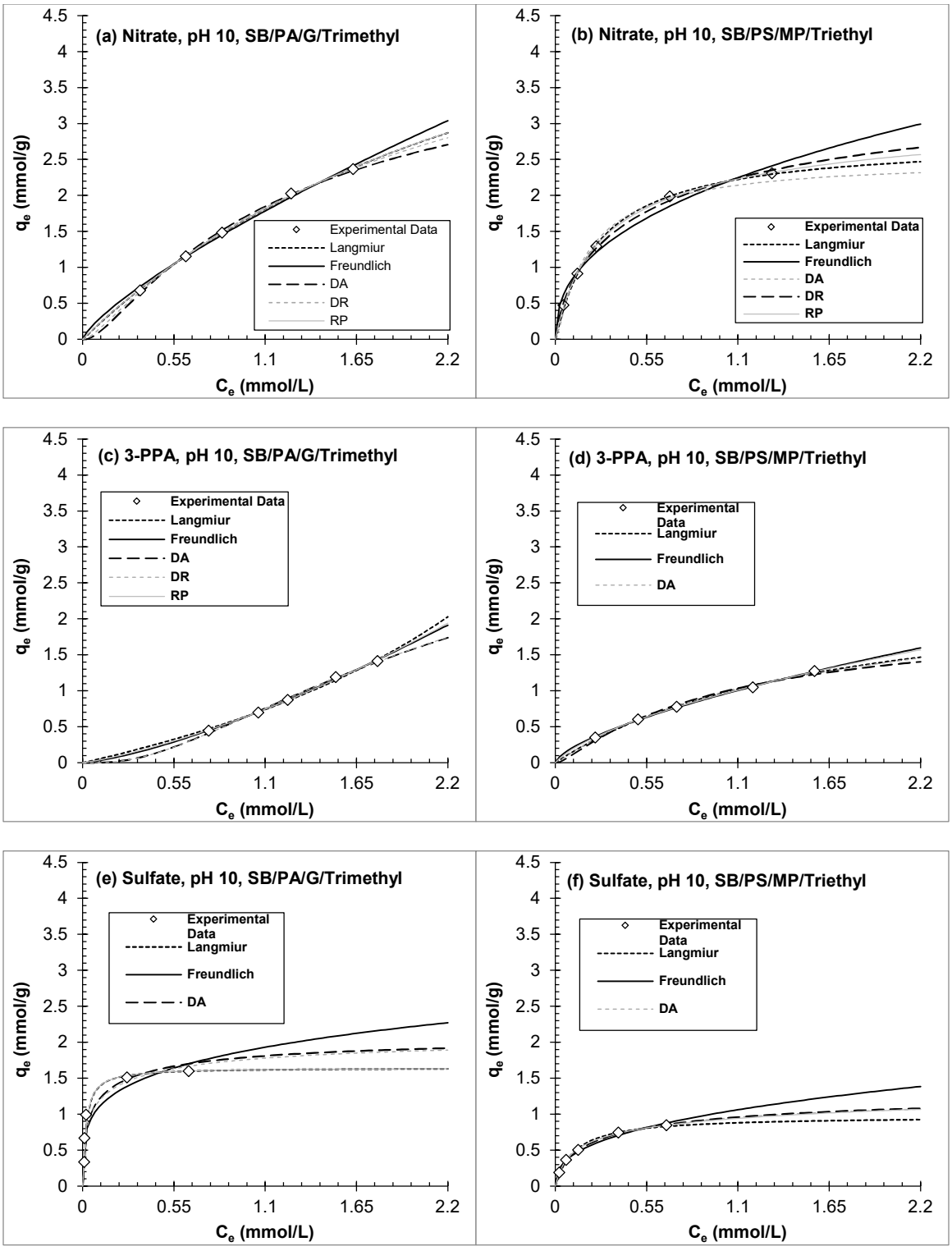

Fig. A4. Equilibrium adsorption isotherms of (a,b) nitrate, (c,d) 3-phenylpropionic acid

(3-PPA), and (e,f) sulfate onto polyacrylic (left panels) and polystyrene (right panels) strong-base anion exchange resins at pH 10.

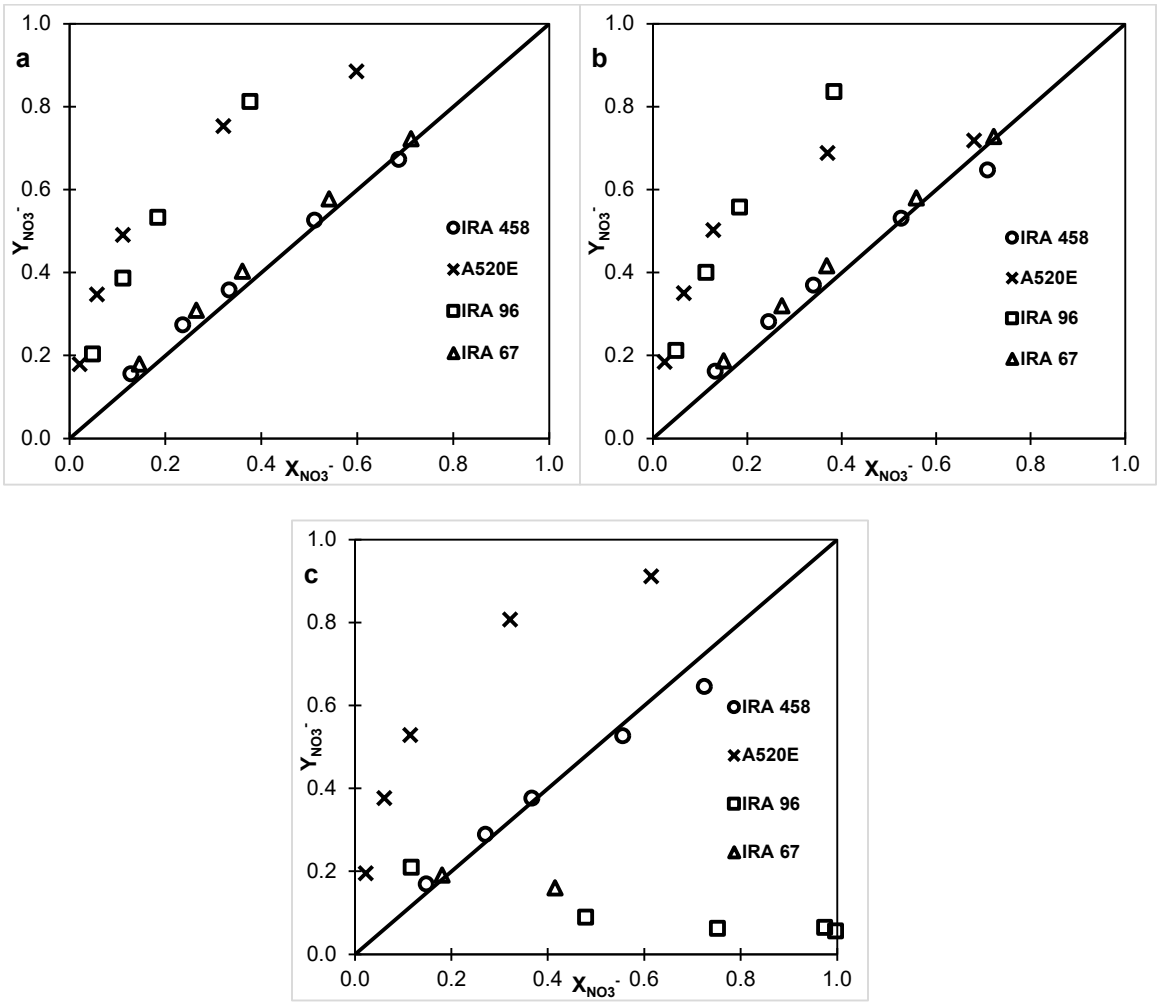

Fig. A5. Equilibrium exchange plots of nitrate at (a) pH 4, (b) pH 7 and (c) pH 10 with chloride-form anion exchange resins in single-solute systems.

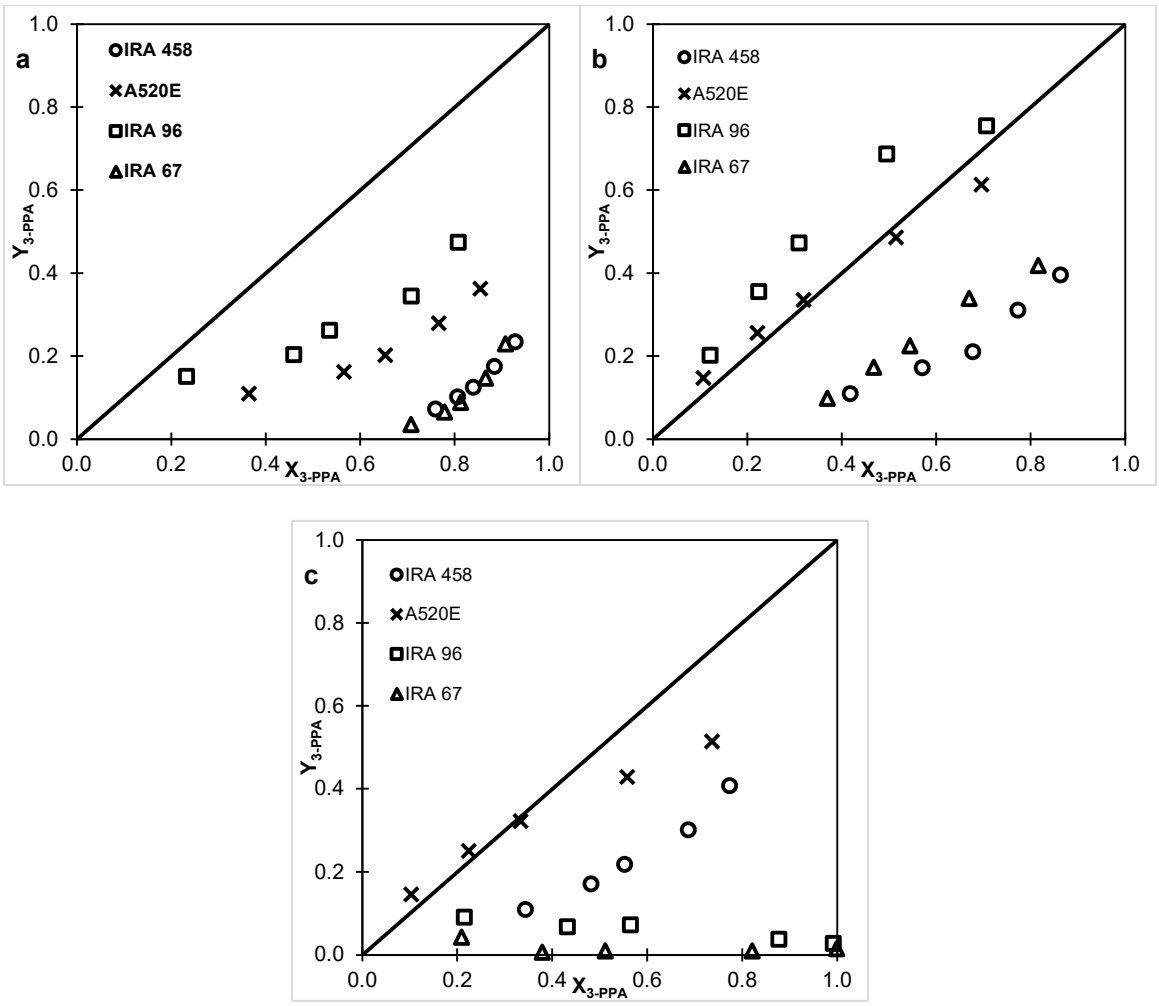

Fig. A6. Equilibrium exchange plots of 3-phenylpropionic acid at (a) pH 4, (b) pH 7, and (c) pH 10 with chloride-form anion exchange resins in single-solute systems.

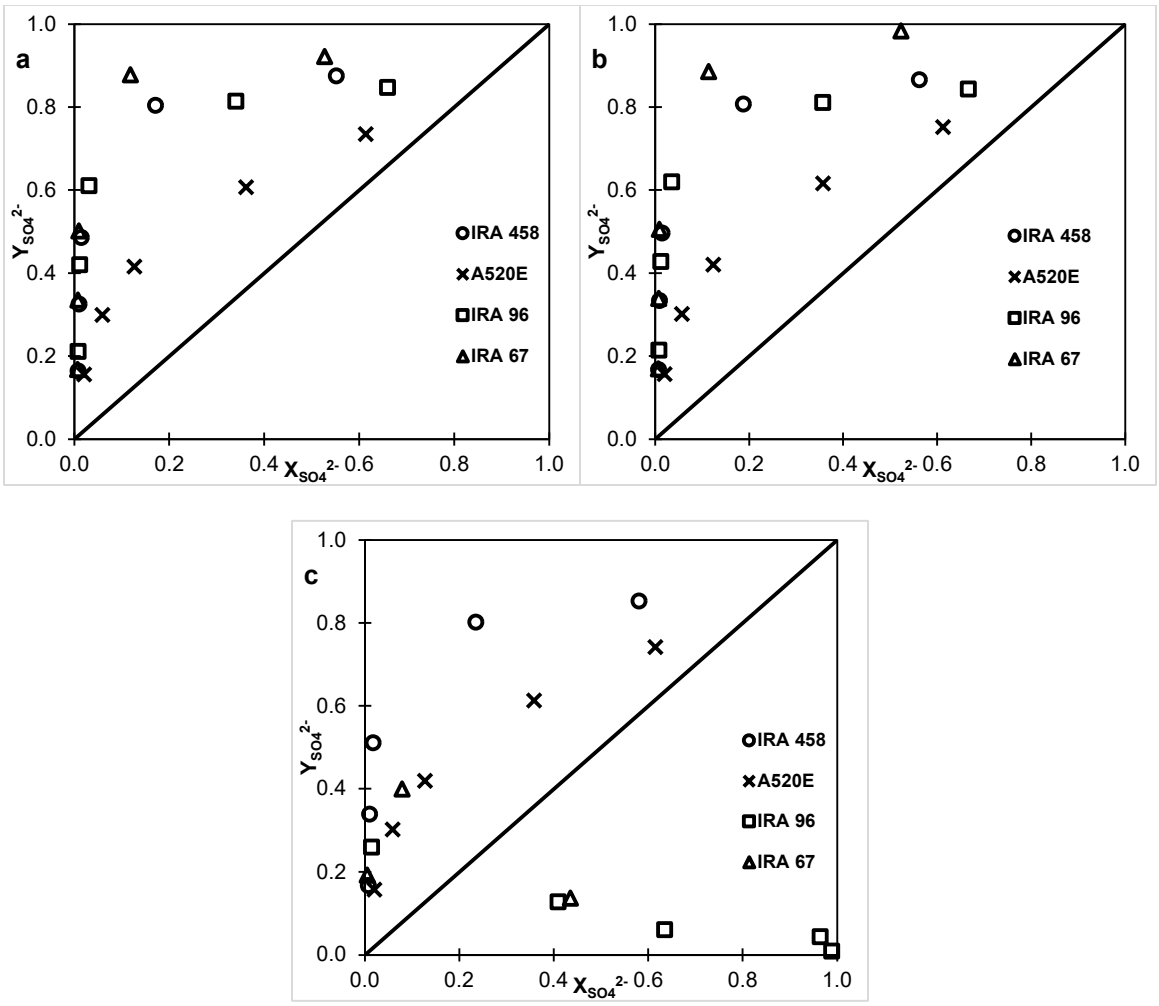

Fig. A7. Equilibrium exchange plots of sulfate at (a) pH 4, (b) pH 7 and (c) pH 10 with chloride-form anion exchange resins in single-solute systems.

APPENDIX B

PRELIMINARY STUDY

Table B1. Water quality data of PFAA-spiked groundwater used in ion-exchange column experiments.

AER	A860	A520E	IRA67	IRA96
pH (SU)		8.5 ± 0.2		8.2 ± 0.1
Alkalinity (mg/L as $CaCO_3$)		157		247
Nitrate (mg/L)		14.8		17.9
Sulfate (mg/L)		91.2		47.5
Chloride		283.9		106.1
Sodium (mg/L)		201.4		46.3
Potassium (mg/L)		5.3		1.9
Magnesium (mg/L)		27.3		60.6
Calcium (mg/L)		62.1		67.1
DOC (mg/L as C)		2.64		0.64
UV 254 (1/cm)		0.039		0.033
SUVA 254 (L/mg-m)		1.48		5.09
Total Nitrogen (mg/L N)		2.17		2.57
Conductivity (µS/cm)		Not measured		898.1
FPBA (µg/L)	443.2	443.2	529.0	490.5
PFBS (µg/L)	546.8	546.8	389.2	350.8
PFHxA (µg/L)	911.5	911.5	1056.1	948.7
PFHxS (µg/L)	795.6	795.6	843.7	897.9
PFOA (µg/L)	1517.9	1517.9	1877.8	1873.8
PFOS (µg/L)	1513.5	1513.5	1511.6	1476.6
ΣPFAAs (µg/L)	5728.5	5728.5	6207.5	6038.3

AER = Anion Exchange Resins, PFAAs = Perfluoroalkyl acids.

Experiments involving A860, A520E, and IRA 67 resins used the same groundwater source.

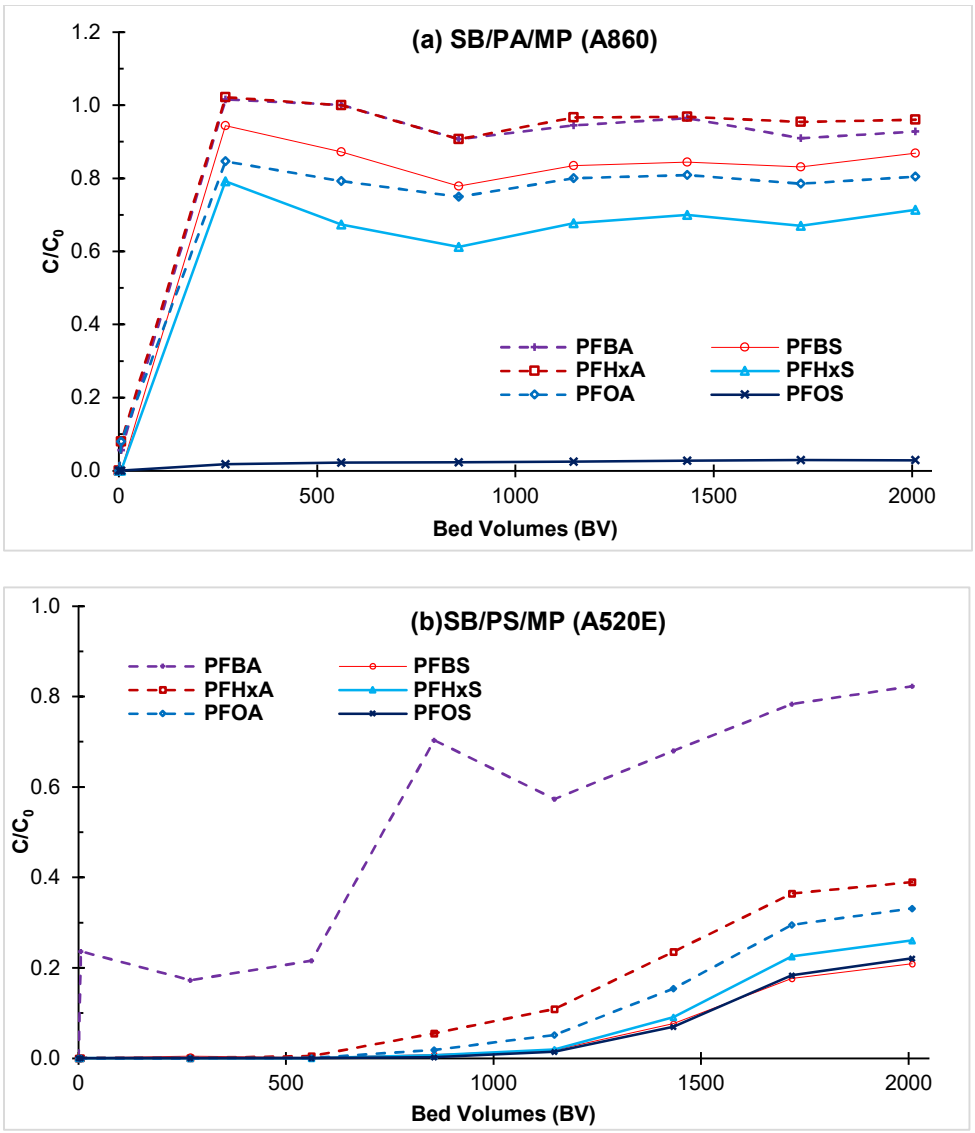

Fig. B1. Efficiency of strong-base (a) polyacrylic/macroporous and (b) polystyrene/macroporous anion exchange resins for PFAAs removal in impacted groundwater. Each data point represents the average of triplicate column experiments with same operating conditions. Initial concentrations of individual and total PFAAs given in Table B1.

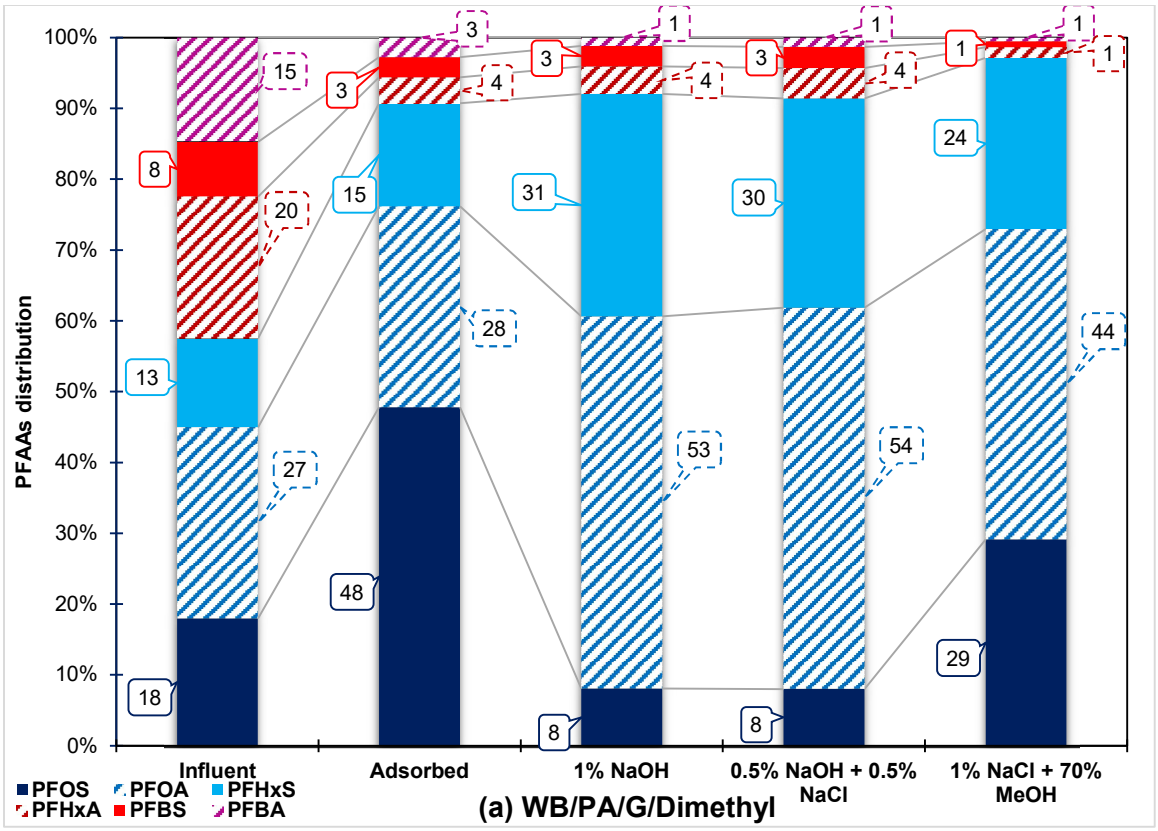
100%
90%
80%
70%
60%
50%
40%
30%
20%
10%
0%
PFAAs distribution
Influent
Adsorbed
1% NaOH
0.5% NaOH + 0.5% NaCl
1% NaCl + 70% MeOH
PFOS
PFOA
PFHxS
PFHxA
PFBS
PFBA
(a) WB/PA/G/Dimethyl

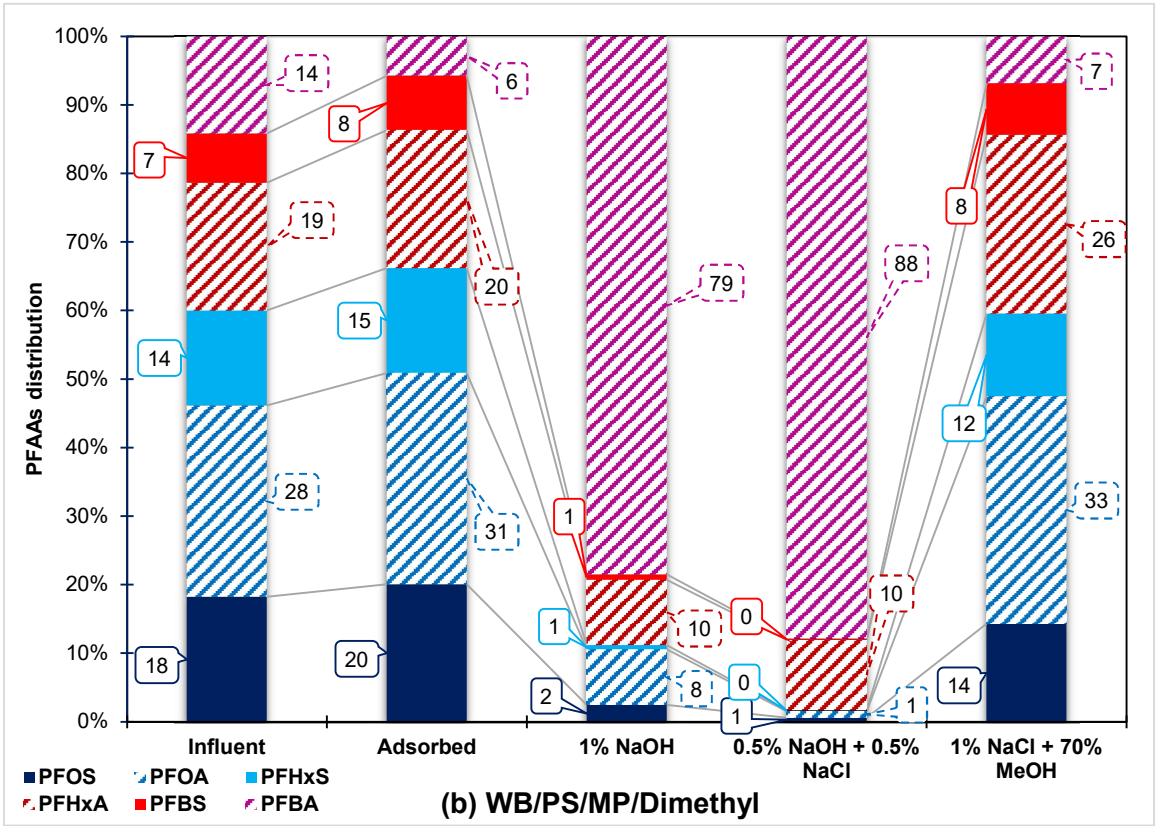
100%
90%
80%
70%
60%
50%
40%
30%
20%
10%
0%
PFAAs distribution
Influent
Adsorbed
1% NaOH
0.5% NaOH + 0.5% NaCl
1% NaCl + 70% MeOH
PFOS
PFOA
PFHxS
PFHxA
PFBS
PFBA
(b) WB/PS/MP/Dimethyl

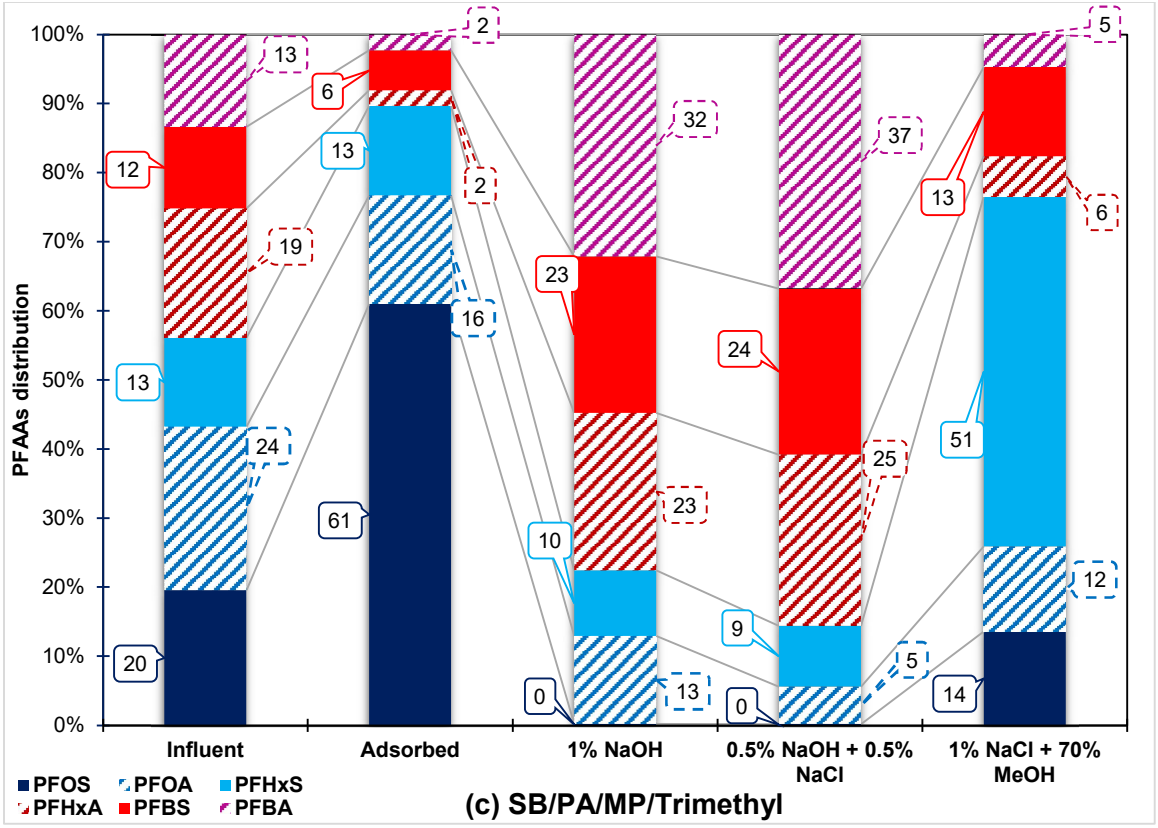
100%
90%
80%
70%
60%
50%
40%
30%
20%
10%
0%
PFAAs distribution
Influent
Adsorbed
1% NaOH
0.5% NaOH + 0.5% NaCl
1% NaCl + 70% MeOH
PFOS
PFOA
PFHxS
PFHxA
PFBS
PFBA
(c) SB/PA/MP/Trimethyl

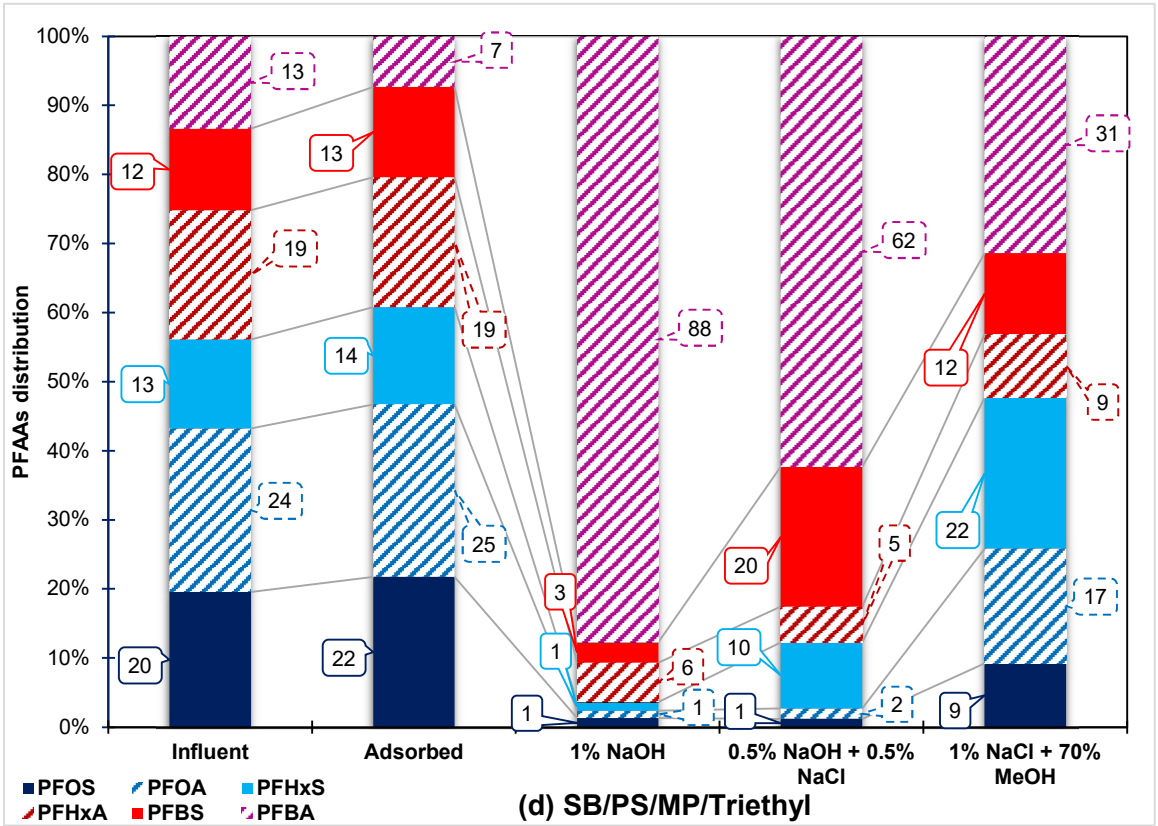
100%
90%
80%
70%
60%
50%
40%
30%
20%
10%
0%
PFAAs distribution
Influent
Adsorbed
1% NaOH
0.5% NaOH + 0.5% NaCl
1% NaCl + 70% MeOH
PFOS
PFOA
PFHxS
PFHxA
PFBS
PFBA
(d) SB/PS/MP/Triethyl

Fig. B2. The distribution on an equivalence basis of the six studied PFAAs in the influent phase, the resin phase and in three regeneration solutions for (a) IRA67 (WB/PA/G/dimethyl), (b) IRA96 (WB/PS/MP/dimethyl), (c) A860 (SB/PA/MP/trimethyl), and (d) A520E (SB/PS/MP/triethyl). Values expressed in precent (%) of total PFAAs concentration in each of the five phases. Influent and adsorbed values are average of triplicate column experiments.

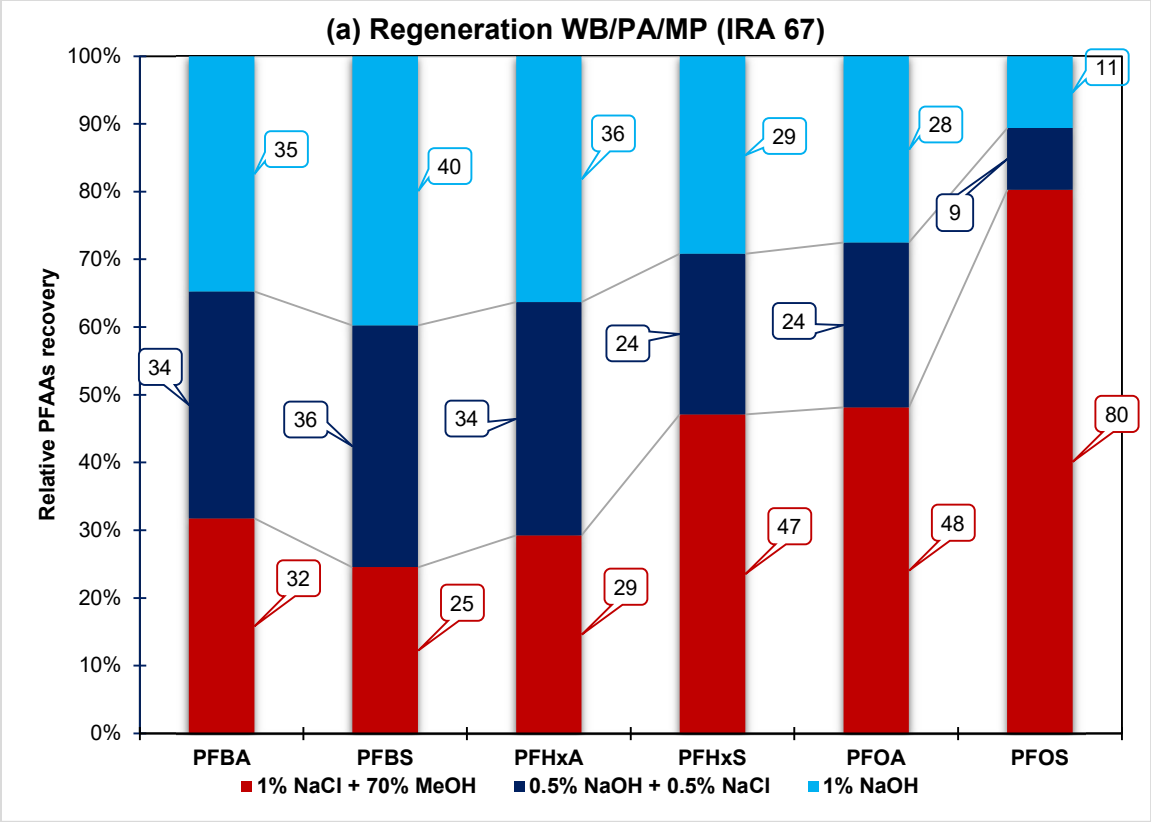
(a) Regeneration WB/PA/MP (IRA 67)
Relative PFAAs recovery
100%
90%
80%
70%
60%
50%
40%
30%
20%
10%
0%
35
40
36
29
28
11
9
34
36
34
24
24
80
32
25
29
47
48
PFBA
PFBS
PFHxA
PFHxS
PFOA
PFOS
1% NaCl + 70% MeOH
0.5% NaOH + 0.5% NaCl
1% NaOH

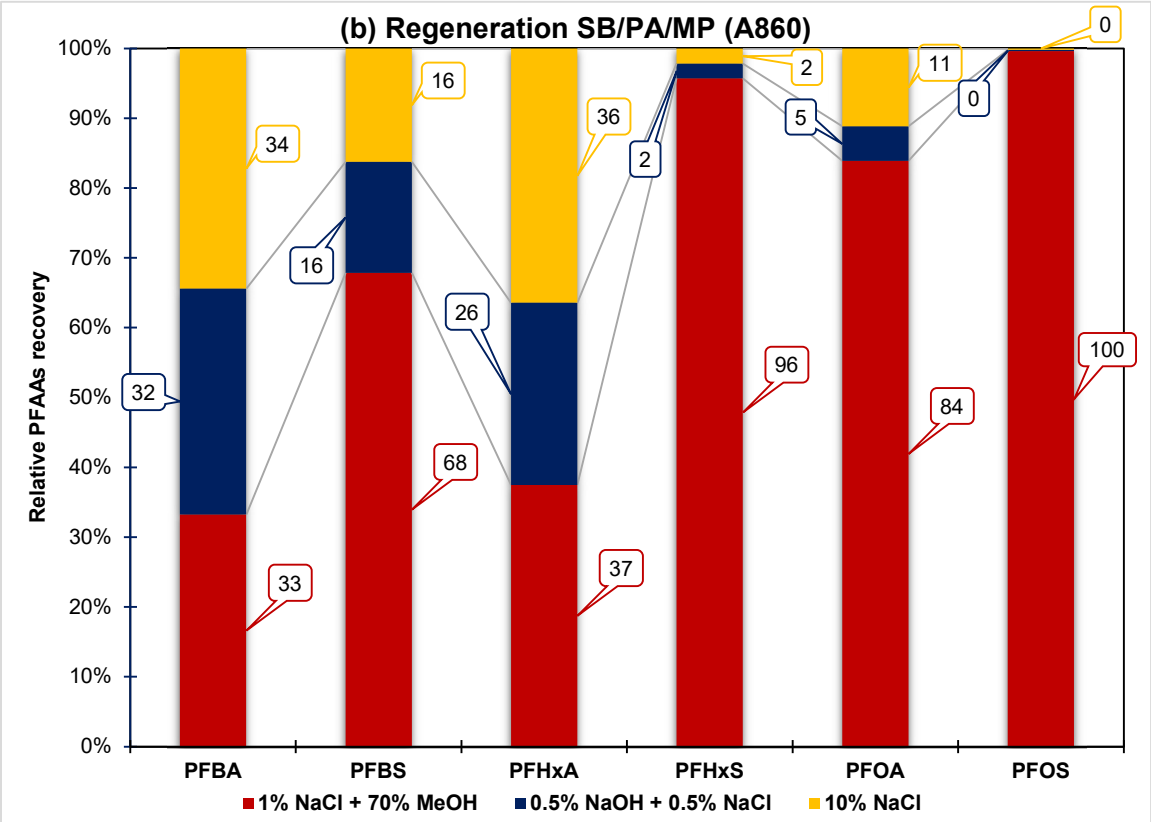
(b) Regeneration SB/PA/MP (A860)
Relative PFAAs recovery
100%
90%
80%
70%
60%
50%
40%
30%
20%
10%
0%
34
16
36
2
5
11
0
0
16
26
96
100
32
68
84
33
37
PFBA
PFBS
PFHxA
PFHxS
PFOA
PFOS
1% NaCl + 70% MeOH
0.5% NaOH + 0.5% NaCl
10% NaCl

Fig. B3. Comparative recovery efficiency of PFAA from (a) weak-base and (b) strong-base polyacrylic resins in three regeneration solutions. Values for each PFAA are the amount recovered in one regenerant normalized by the total amount recovered in all three regenerants.

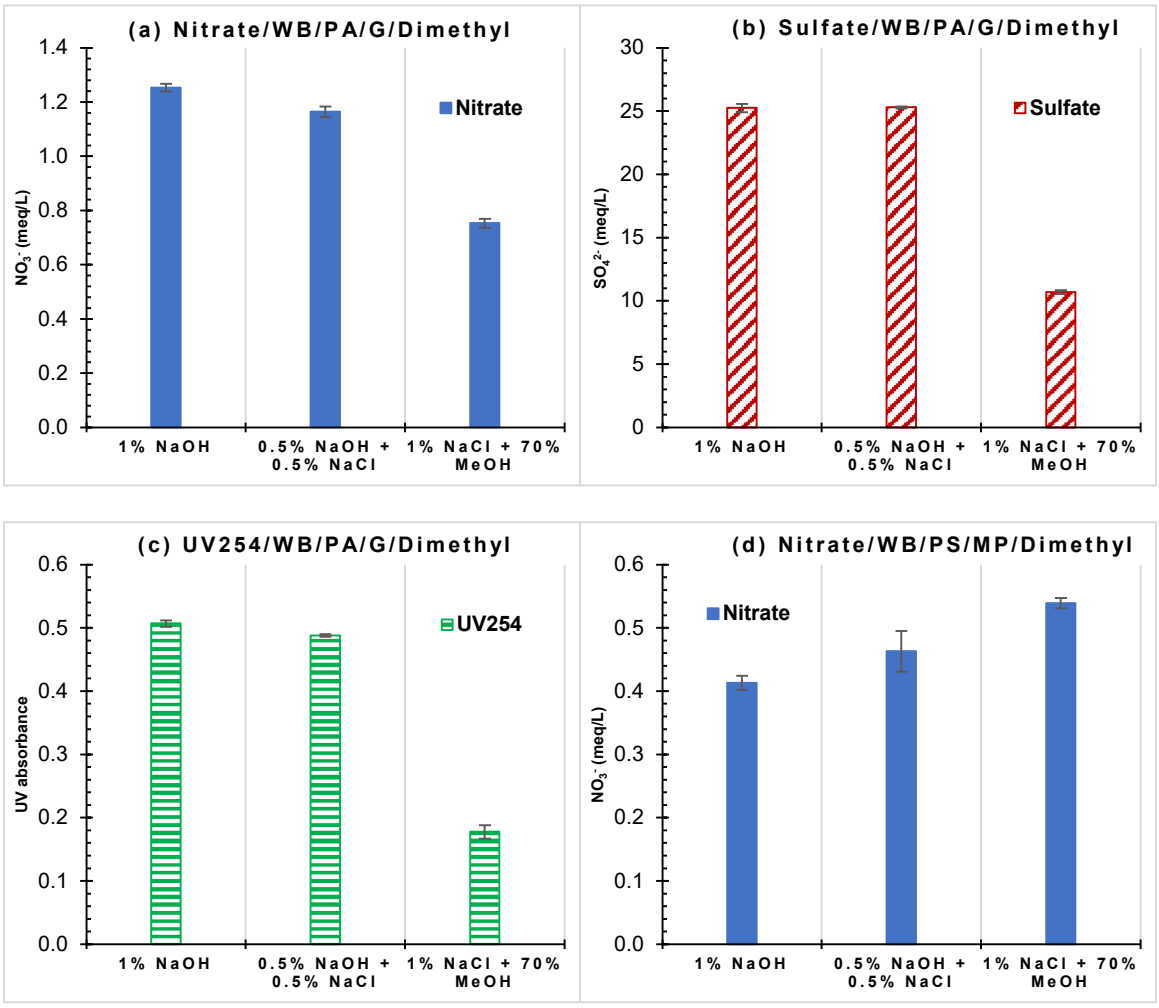

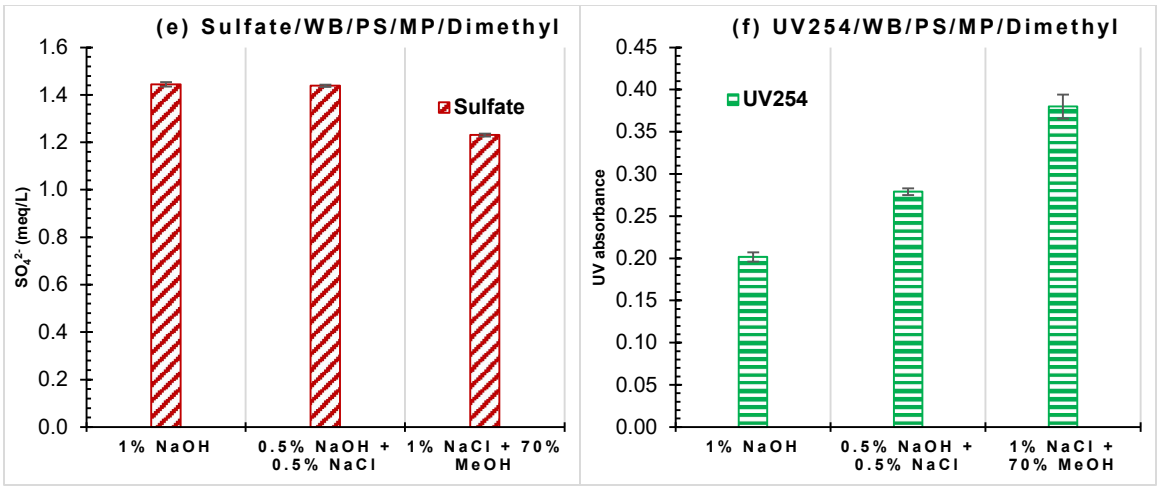

Fig. B4. Measurements of nitrate (meq/L), sulfate (meq/L), and UV254 (dimensionless) in the regeneration solutions after desorption from spent (a-c) IRA 67 (WB/PA/G/dimethyl) and (d-f) IRA 96 (WB/PS/MP/dimethyl) WB resins.